

UNITED STATES PATENT AND TRADEMARK OFFICE

BEFORE THE PATENT TRIAL AND APPEAL BOARD

AMAZON.COM, INC.,
Petitioner,

v.

JAWBONE INNOVATIONS, LLC,
Patent Owner.

IPR2023-00216
U.S. Patent No. 8,280,072

DECLARATION OF CAROL S. PETERSON
REGARDING *POWERS* AND *G&B*

<p><i>Amazon v. Jawbone</i> U.S. Patent 8,280,072 Amazon Ex. 1015</p>
--

I, Carol S. Peterson, state and declare as follows:

I. Introduction

1. I am currently a Research Librarian with the law firm of Knobbe, Martens, Olson & Bear, LLP, located at 2040 Main Street, 14th Floor, Irvine, CA 92614.

2. I am over eighteen years of age. I am competent to make this Declaration, and I make this Declaration based on my own personal knowledge as well as my knowledge of library science practices.

3. I earned a Master of Library Science from the University of California Los Angeles in 1979 and a Bachelors in English from the University of California, Davis in 1977. I have worked as a research librarian at Knobbe, Martens, Olson & Bear for approximately 40 years.

4. I understand that a petition for *inter partes* review of U.S. Patent No. 8,280,072 will be filed concurrently with this Declaration.

5. Exhibit 1003 of the concurrently filed petition is a true and correct copy of Thomas A. Powers & Volkmar Hamacher, Thomas A. Powers et al., *Three-Microphone Instrument Is Designed to Extend Benefits of Directionality*, 55 The Hearing Journal, no. 10, Oct. 2002, at 38-45 (“Powers”) that was downloaded from The Hearing Journal’s publisher’s website at <https://journals.lww.com/thehearingjournal/toc/2002/10000>.

6. I understand that Exhibit 1005 of the concurrently filed petition is a copy of excerpts from *Acoustic Signal Processing for Telecommunication* (Steven L. Gay & Jacob Benesty eds., 2000) (“*G&B*”).

7. Appendix J to this Declaration is a true and correct copy of excerpts from *G&B* obtained from the University of California Irvine Library. I have reviewed Exhibit 1005 of the concurrently filed petition and Appendix J to this Declaration, and based on this review, Exhibit 1005 is a true and accurate copy of a softcover version of *G&B* that contains the same disclosure as Appendix J.

II. Standard Library Practices Making Library Materials Publicly Available

8. I have personal knowledge of standard library practices for making materials available to the public.

9. I have knowledge of and experience with the Machine-Readable Cataloging (MARC) system, an industry-wide standard that libraries use to catalog materials. Since at least 1980, MARC has been the international standard for cataloging bibliographic data in libraries’ systems. Each MARC record contains fields that provide specific information about how cataloged items are held and made available to the public. MARC records can be accessed through many libraries’ electronic cataloging systems.

III. MARC Records

10. The MARC record system uses a specific three-digit numeric code (from 001-999) to identify each field in a catalog record. For example:

- a. field tag 008 provides bibliographic information and includes the six-digit date of when the item was cataloged in the “**YYMMDD**” format (*Date entered on file*), the four-digit year of the item’s publication date;
- b. field tag 022 provides the International Standard Serial Number (ISSN), which is a unique identification number assigned to serial publications;
- c. field tag 245 identifies the full title statement for the work;
- d. field tags 260 and 264 provide information on the publication, printing, distribution, issue, release, or production of a work;
- e. field tag 300 identifies the physical description, often including holdings information, for the work;
- f. field tag 310 provides the current publication frequency;
- g. field tag 321 provides the former publication frequency;
- h. field tag 338 identifies the format of the storage and housing of a carrier;

- i. field tag 362 indicates the numbering used for chronological cataloging of individual issues of the serial including information on when the serial began, which affects how issues of the serial are checked in, processed, and added to the library’s main collection; and
- j. field tags 9XX provide information on the local holdings information for the resource.

11. More information about the MARC record system can be found on the Library of Congress’s website at:

<https://www.loc.gov/marc/bibliographic/bd20x24x.html>.

12. After an item is received by a library, the standard practice for the library is to process, catalog, date stamp, and then shelve the item. The public may then access the item by searching the catalog and either requesting a print or electronic copy of the item. If a resource is available online or electronically, standard practice is to provide a link in the library’s online catalog through which the resource can be downloaded. Standard practice is to make the item available to the public within a few days or weeks of cataloging it.

IV. Serial Publications

13. A serial publication, often known as a “journal,” is a resource that is published in successive parts (“issues”) and has no predetermined conclusion. Each

issue is usually chronologically numbered and dated. The presence of enumeration, years of coverage, and/or other chronological information also indicates a serial publication.

14. There are significant differences between cataloging finite resources (e.g., books) and continuing resources (e.g., serial publications). For serial publications, the MARC record provides information about the serial as a whole, including the first or earliest available issue. It also provides information about the volumes and issues held by a library, including the dates a serial publication's issues were received by the library and the date they were made available to the public.

15. Serial publications contain unique identifying characteristics that are slightly different from non-serial publications such as textbooks. The issue date for a print serial publication, for example, generally appears on the front or back cover, the masthead page, title page (if any), table of contents page(s), or on the pages of the individual articles contained in the issue. More information regarding the unique aspects of cataloging serials can be found at:

<https://www.loc.gov/aba/pcc/conser/scctppt/Basic-2014/Basic-Trainee-Manual.pdf>.

V. Powers

16. As detailed below, I have reviewed the University of California Irvine Library and Yale Library records for the serial publication, *The Hearing Journal*, containing *Powers*.

A. University of California Irvine Library Records for *Powers*

17. Appendix A to this Declaration is a true and correct copy of the University of California Irvine Library’s public catalog record for *The Hearing Journal*, which contains *Powers*. Appendix A was downloaded from https://uci.primo.exlibrisgroup.com/discovery/fulldisplay?docid=alma9914860432006531&context=L&vid=01CDL_IRV_INST:UCI&lang=en.

18. Appendix A provides the public with availability and holdings information for accessing *The Hearing Journal*. Appendix A provides the following information:

Title: *The Hearing journal*;

Publication Date: 1983;

Publisher: “New York, NY: Lippencott Williams & Wilkins. Print began with v. 36, no. 1 (Jan. 1983)”;

Frequency: Monthly.

Appendix A also indicates that full access is available online beginning with the 1994 volume 47, issue 1.

19. Appendix B to this Declaration is a true and accurate copy of the University of California Irvine Library’s public catalog record for *Powers*, which was downloaded from

https://uci.primo.exlibrisgroup.com/discovery/fulldisplay?docid=cdi_gale_infotrac_misc_A93026282&context=PC&vid=01CDL_IRV_INST:UCI&lang=en.

Appendix B shows that full access to The Hearing Journal is available online beginning with the 1994 volume 47, issue 1 and that *Powers* is available online.

Appendix B further provides the following information for the public to access *Powers*:

Title: Three-microphone instrument is designed to extend benefits of directionality;

Publisher: Lippincott Williams & Wilkens, Inc;

Is Part of: The Hearing journal, 2002, Vol. 55 (10), p.38-45.

20. Appendix C to this Declaration is a true and accurate copy of the University of California Irvine Library’s record for the serial publication containing *Powers*, which was downloaded from

https://uci.primo.exlibrisgroup.com/discovery/sourceRecord?vid=01CDL_IRV_INST:UCI&docId=alma9914860432006531&recordOwner=01UCS_NETWORK.

21. The University of California Irvine Library’s MARC record (Appendix C) for serial publication “The Hearing Journal” containing *Powers* indicates that:

- a. The data elements of field tag 008 (060425c19839999nyumr-
pso-----0---a0eng--) provide the “date entered on file” for the
record, which includes the six-digit date entry “000207,”
indicating that the MARC record for The Hearing Journal was
created on April 25, 2006, with the character position “c”
followed by “19839999” indicating that The Hearing Journal is
a continuing resource (serial publication) that was first published
in 1983 and is currently published. This denotes that The
Hearing Journal was first cataloged by the University of
California Irvine Library on April 25, 2006.
- b. Field tag 022 provides The Hearing Journal’s ISSN (2333-6218).
- c. Field tag 245 denotes the title statement of the work as “The
Hearing Journal.”
- d. Field tag 264 indicates that the Hearing Journal is published by
Lippencott Williams & Wilkins.
- e. Field tag 310 indicates that The Hearing Journal is published
monthly.
- f. Field tag 338 indicates that The Hearing Journal is an online
resource.

g. Field tag 362 indicates that “Print began with v. 36, no. 1 (Jan. 1983).”

B. Yale Library Records for *Powers*

22. Appendix D to this Declaration is a true and correct copy of the Yale Library public catalog record for the serial publication “The Hearing Journal” containing *Powers*, which was downloaded from:

<https://orbis.library.yale.edu/vwebv/holdingsInfo?bibId=12026360>.

23. Appendix D provides the public with availability and holdings information for accessing The Hearing Journal, including *Powers*. Appendix D provides the following information:

Uniform Title: Hearing journal (Online);

Title: The Hearing journal [electronic resource];

ISSN: 2333-6218;

Published/Created: New York, NY : Lippencott Williams & Wilkins;

Location: Yale Internet Resource;

Frequency: Monthly;

Extent: “Print began with v. 36, no. 1 (Jan. 1983).”

24. Appendix E to this Declaration is a true and accurate copy of the Yale Library’s MARC record for The Hearing Journal, which was downloaded from:

<https://orbis.library.yale.edu/vwebv/staffView?bibId=12026360>.

25. The Yale Library’s record (Appendix E) for *Powers* indicates that:
- a. The data elements of field tag 008 (830301c19839999nyumr pso 0 a0eng d) provide the “date entered on file” for the record, which includes the six-digit date entry “830301,” indicating that the MARC record for The Hearing Journal was created, and The Hearing Journal was first cataloged by the Yale Library, on March 1, 1983, with the character position “c” followed by “19839999” indicating that The Hearing Journal is a continuing resource (serial publication) that was first published in 1983 and is currently published.
 - b. Field tag 022 provides The Hearing Journal’s ISSN (2333-6218).
 - c. Field tag 245 denotes the title statement of the work as “The Hearing Journal” and indicates it is an electronic resource.
 - d. Field tag 260 indicates that the Hearing Journal is published by Lippencott Williams & Wilkins.
 - e. Field tag 310 indicates that The Hearing Journal is published monthly.
 - f. Field tag 362 indicates that “Print began with v. 36, no. 1 (Jan. 1983).”

C. The Library Catalog and MARC Records are Consistent with Publication Information in *Powers*

26. The copy of *Powers* attached as Exhibit 1003 to the concurrently filed petition indicates that the work is titled “Three-microphone instrument is designed to extend benefits of directionality,” that it was written by Thomas A. Powers and Volkmar Hamacher, and that it published in Volume 55, No. 10 of The Hearing Journal in October 2002.

27. The library catalog and MARC records for The Hearing Journal and *Powers*, discussed above, are consistent with and confirm the bibliographic and publication information provided in the copy of *Powers* (Exhibit 1003).

28. Based on the evidence discussed above and my understanding of standard library practices, it is my opinion that *Powers* would have been publicly available no later than October 2002.

VI. G&B

29. As detailed below, I have reviewed the University of California Irvine and The Ohio State University Library MARC records for *G&B*.

D. University of California Irvine Library Records for *G&B*

30. Appendix F to this Declaration is a true and correct copy of the University of California Irvine Library’s public catalog record for *G&B*, which was downloaded from

https://uci.primo.exlibrisgroup.com/discovery/fulldisplay?docid=alma991023927229704701&context=L&vid=01CDL_IRV_INST:UCI&lang=en.

31. Appendix F provides the public with availability and holdings information for accessing *G&B*, including the location, scope of holdings, and call number for locating *G&B*. Appendix F provides the following information for the public to access *G&B*:

Main title: Acoustic signal processing for telecommunication / edited by

Steven L. Gay, Jacob Benesty;

Publication Date: 2000;

Publisher Boston: Kluwer Academic;

ISBNs: 0792378148 and 9780792378143.

Appendix F also indicates that a copy with call number TK5102.9 .A27 2000 held at the University of California Irvine Library is currently on loan until December 12, 2022, and that five other University of California schools have copies available.

32. Appendix G to this Declaration is a true and accurate copy of the University of California Irvine Library's MARC record for its copy of *G&B*, which was downloaded from

https://uci.primo.exlibrisgroup.com/discovery/sourceRecord?vid=01CDL_IRV_INST:UCI&docId=alma991023927229704701&recordOwner=01UCS_NETWORK.

33. The University of California Irvine Library MARC record (Appendix G) for *G&B* indicates that:

- a. The data elements of field tag 008 (000207s2000 maua b 001 0 eng) provide the “date entered on file” for the record, which includes the six-digit date entry “000207,” indicating that the MARC record for *G&B* was created on February 7, 2000, with the character position “s” followed by “2000” indicating that the item has a single known date of publication in 2000. This denotes that *G&B* was first cataloged by the University of California Irvine Library on February 7, 2000. Based on standard library practices, *G&B* would have been processed, cataloged, shelved, and made available to the public, on an ongoing, continuing basis, beginning a few days or weeks after February 7, 2000.
- b. Field tag 245 denotes the title statement of the work as “Acoustic signal processing for telecommunication” and indicates the work was authored or edited by Steven L. Gay and Jacob Benesty.
- c. Field tag 260 indicates that the work was first published or distributed in Boston by Kluwer Academic in 2000.

E. The Ohio State University Library Records for *G&B*

34. Appendix H to this Declaration is a true and correct copy of The Ohio State University Library’s public catalog record for *G&B*, which was downloaded from: <https://library.ohio-state.edu/record=b5220423>.

35. Appendix H provides the public with availability and holdings information for accessing *G&B*, including the location, scope of holdings, and call number for locating *G&B*. Appendix H provides the following information for the public to access *G&B*:

Title: Acoustic signal processing for telecommunication / edited by Steven L.

Gay, Jacob Benesty;

Imprint: Boston : Kluwer Academic, [2000];

ISBN: 0792378148.

Appendix H also indicates that a copy with call number TK5102.9 .A27 2000 is available at “18th Ave Library Basement Compact Shelving” and another copy with call number TK5102.9 .A27 2000 c.2 is available at the Book Depository.

36. Appendix I to this Declaration is a true and accurate copy of The Ohio State University Library’s MARC record for its copy of *G&B*, which was downloaded from: <https://library.ohio-state.edu/search~S7?/.b5220423/.b5220423/1%2C1%2C1%2CB/marc~b5220423>.

37. The Ohio State University Library MARC record (Appendix I) for *G&B* indicates that:

- a. The data elements of field tag 008 (000207t20002000maua 001 0 eng) provide the “date entered on file” for the record, which includes the six-digit date entry “000207,” indicating that the MARC record for *G&B* was created on February 7, 2000, with the character position “t” followed by “20002000” indicating that the item has a publication date of 2000 and a copyright date of 2000. This denotes that *G&B* was first cataloged by the University of California Irvine Library on February 7, 2000. Based on standard library practices, *G&B* would have been processed, cataloged, shelved, and made available to the public, on an ongoing, continuing basis, beginning a few days or weeks after February 7, 2000.
- b. Field tag 245 denotes the title statement of the work as Acoustic signal processing for telecommunication and indicates the work good to was authored or edited by Steven L. Gay and Jacob Benesty.

- c. Field tag 264 indicates that the work was first published, released, or issued in Boston by Kluwer Academic in 2000 with a copyright date of 2000.

F. The Library Catalog and MARC Records are Consistent with Publication Information in *G&B*

38. Appendix J to the concurrently filed petition indicates that the work is titled “Acoustic Signal Processing for Telecommunication,” and published in 2000. Appendix J also indicates that Acoustic Signal Processing for Telecommunication has an ISBN of 0-7923-7814-8, that the work was edited by Steven L. Gay and Jacob Benesty, and that it was published by Kluwer Academic Publishers. Furthermore, Appendix J bears a handwritten note on the front pages as well as a sticker on the outside spine of the work indicating it was published in 2000 and assigned call number TK 5102.9 A27 2000.

39. The library catalog and MARC records for *G&B*, discussed above, are consistent with and confirm the bibliographic and publication information provided in the University of California Irvine Library’s copy of *G&B* (Appendix J).

40. Based on the evidence discussed above and my understanding of standard library practices, it is my opinion that *G&B* would have been publicly available within a few days or weeks of February 7, 2000.

VII. Conclusion

I declare that all statements made herein of my knowledge are true, and that all statements made on information and belief are believed to be true, and that these statements were made with the knowledge that willful false statements and the like so made are punishable by fine or imprisonment, or both, under Section 1001 of Title 18 of the United States Code.

Executed on November 14, 2022 in Irvine, California.



Carol S. Peterson

APPENDIX A



JOURNAL

The Hearing journal.

1983

PEER REVIEWED

[Available Online >](#)



Send to

[TOP](#)

[SEND TO](#)

[SEARCH INSIDE](#)

[VIEW ONLINE](#)

[DETAILS](#)

[LINKS](#)



EXPORT TO EXCEL



EMAIL RECORD



PERMALINK



CITATION



PRINT



EASYBIB



ENDNOTE BASIC



EXPORT RIS

Search inside

Search for articles within this journal

Article title or keyword



View Online

Full access online

[Free E- Journals](#)



Available from 1994 volume: 47 issue: 1.

[Report a Problem](#)

Details

Title	The Hearing journal.
Other title	HJ
Publication Date	1983
Publisher	New York, NY : Lippencott Williams & Wilkins. Print began with v. 36, no. 1 (Jan. 1983).
Frequency	Monthly
Notes	Refereed/Peer-reviewed
Subject	Audiology -- Periodicals > Audiology > Periodicals > Electronic journals >
MESH subjects	Audiology >
Genre	Periodicals.
Related titles	Earlier title : Hearing aid journal >
Identifier	ISSN : 2333-6218



Language

English

Source

Library Catalog

Links

[Display Source Record](#)  



APPENDIX B



ARTICLE

Three-microphone instrument is designed to extend benefits of directionality

Powers, Thomas A ; Hamacher, Volkmar

The Hearing journal, 2002, Vol.55 (10), p.38-45

[Download PDF](#)[Available Online >](#)[TOP](#)[SEND TO](#)[VIEW ONLINE](#)[DETAILS](#)[CITATIONS](#)

Send to

EXPORT TO
EXCEL

EMAIL RECORD



PERMALINK



CITATION



PRINT



EASYBIB

ENDNOTE
BASIC

EXPORT RIS

View Online

Full access online

[Free E- Journals](#)

Available from 1994 volume: 47 issue: 1.

[Report a Problem](#)

Details

Creator[Powers, Thomas A >](#)[Hamacher, Volkmar >](#)**Title**

Three-microphone instrument is designed to extend benefits of directionality

Publisher

Lippincott Williams & Wilkins, Inc

Is Part Of

The Hearing journal, 2002, Vol.55 (10), p.38-45

Identifier

ISSN: 0745-7472

EISSN: 2333-6218

DOI: 10.1097/01.HJ.0000293844.13775.fb

Language

English

Source

Alma/SFX Local Collection



Citations

Find sources



citing this

or sources



cited in this

Related reading

recommended items that are related to the record

Influence of environmental factors on hearing aid microphone preference.

Laurel Olson

Journal of the American Academy of Audiology.2002, Vol. 13(6), p. 308-22

ARTICLE suggested by 

Speech understanding in background noise with the two-microphone adaptive beamformer BEAM™ in the nucleus Freedom™ cochlear implant system

A. Spriet

Ear and hearing.2007, Vol. 28(1), p. 62-72

ARTICLE suggested by 

Performance of directional microphone hearing aids in everyday life.

Laurel Olson

Journal of the American Academy of Audiology.2002, Vol. 13(6), p. 295-307

ARTICLE suggested by 

Evaluation of an adaptive, directional-microphone hearing aid.

Paula Henry

International journal of audiology.2002, Vol. 41(2), p. 100-12

ARTICLE suggested by 

Challenges and recent developments in hearing aids. Part I. Speech understanding in noise, microphone technologies and noise reduction algorithms.

King Chung

Trends in amplification.2004, Vol. 8(3), p. 83-124

ARTICLE suggested by 

MORE SUGGESTIONS



APPENDIX C

Leader -----nas--22005297i-4500
001 99110978977286280
005 20200404031311.2
006 m-----o--d-----
007 cr-un|||||
008 060425c1983999nyumr-pso-----0---a0eng--
010 ##\$a 2013207623
015 ##\$aGBB575713 \$2bnb
016 7#\$a016282912 \$2Uk
022 ##\$a2333-6218
035 ##\$a(DE-599)ZDB2202232-6
035 ##\$a(OCOLC)67618507
035 ##\$a(CKB)110978977286280
035 ##\$a(CONSER)--2013207623
037 ##\$bThe Hearing Journal, 333 Seventh Avenue, 19th Floor, New York, NY 10001
041 0#\$aeng \$beng
042 ##\$ansdp \$apcc
050 10\$aISSN RECORD
050 #4\$aRF300 \$b.N38
060 #4\$aW1 \$bHE6416
082 00\$a617 \$223
082 14\$a617 \$211
210 ##\$aHEARING JOURNAL
210 ##\$aHEAR J
210 0#\$aHearing j. \$b(Online)
222 #4\$aThe hearing journal (Online)
245 04\$aThe Hearing journal.
246 1#\$aHJ
264 #1\$aNew York, NY : \$bLippencott Williams & Wilkins.
310 ##\$aMonthly
336 ##\$atext \$btxt \$2rdacontent
337 ##\$acomputer \$bc \$2rdamedia
338 ##\$aonline resource \$bnc \$2rdacarrier
362 1#\$aPrint began with v. 36, no. 1 (Jan. 1983).
500 ##\$aRefereed/Peer-reviewed
588 ##\$aDescription based on: Volume 47, issue 1 (January 1994); title from banner (LWW website, viewed on February 5, 2014).
588 ##\$aLatest issue consulted: Volume 67, issue 2 (February 2014) (viewed February 5, 2014).
650 #0\$aAudiology \$vPeriodicals.
650 #7\$aAudiology. \$2fast \$0(OCOLC)fst00821108
650 #2\$aAudiology.
655 #7\$aPeriodicals. \$2fast \$0(OCOLC)fst01411641
655 #0\$aElectronic journals.
776 ##\$x0745-7472
780 00\$tHearing aid journal \$w(CKB)110985822450684 \$w(DLC)sn79003994
906 ##\$aJOURNAL



APPENDIX D

Quick Search :

[Search History](#)

Uniform Title: [Hearing journal \(Online\)](#)
Title: The Hearing journal [electronic resource].
ISSN: 2333-6218 0745-7472
Published/Created: New York, NY : Lippencott Williams & Wilkins.
Links: [Full text](#)

Actions

- [Add to My List](#)
- [Print](#)
- [E-mail](#)
- [Export](#)

This item

- [Full View](#)
- [Staff \(MARC\) View](#)

Yale Holdings

Location: Yale Internet Resource
[Information about Off Campus Access](#)

Call Number: None
Status: No information available
Notes: Online Resource

Frequency: Monthly
Extent: Print began with v. 36, no. 1 (Jan. 1983).
Local Notes: Access is available to the Yale community.
Notes: Description based on: Volume 47, issue 1 (January 1994); title from banner (LWW website, viewed on February 5, 2014).
 Latest issue consulted: Volume 67, issue 2 (February 2014) (viewed February 5, 2014).
Access and use: Access restricted by licensing agreement.
Variant and related titles: [Hearing j. \(Online\)](#)
 The Hearing journal
 HJ
Other formats: Print version: [Hearing journal](#)
Continues: [Hearing aid journal](#)
Format: Periodical
Subjects: [Audiology--Periodicals.](#)
Subjects (Medical): [Audiology.](#)

Link to this page: <https://hdl.handle.net/10079/bibid/12026360>

APPENDIX E

Quick Search :

[Search History](#)

- 000** 02198cas a22005177i 4500
001 12026360
005 20220128160346.0
006 m o d
007 cr n
008 830301c19839999nyumr pso 0 a0eng d
015 ___ |a GBB575713 |2 bnb
016 7_ |a 016282912 |2 Uk
022 ___ |a 2333-6218 |y 0745-7472
035 ___ |a (WaSeSS)ssj0004896
035 ___ |a ssj0004896
037 ___ |b The Hearing Journal, 333 Seventh Avenue, 19th Floor, New York, NY 10001
040 ___ |a OCLCS |b eng |c OCLCS |d OCLCS |d HUA |d OCLCQ |d OCLCE |d OCLCQ
|d OCLCF |d DLC |d COO |d OCLCO |d OCLCQ |d OCLCO |d TSC |d BUF |d REB |d OCLCO
|d EZC |d OCLCO |d NLE |d AU@ |d OCLCO |d UKMGB |d WYU |d VT2 |d OCLCO
|d OCLCA |d WaSeSS
041 0_ |a eng |b eng
042 ___ |a nsdp |a pcc
050 _4 |a RF300 |b .N38
060 _4 |a W1 |b HE6416
082 00 |a 617 |2 23
082 14 |a 617 |2 11
130 0_ |a Hearing journal (Online)
210 0_ |a Hearing j. |b (Online)
222 _4 |a The Hearing journal
245 14 |a The Hearing journal |h [electronic resource].
246 1_ |a HJ
260 ___ |a New York, NY : |b Lippencott Williams & Wilkins.
310 ___ |a Monthly
362 1_ |a Print began with v. 36, no. 1 (Jan. 1983).
506 ___ |a Access restricted by licensing agreement.
588 ___ |a Description based on: Volume 47, issue 1 (January 1994); title from banner (LWW website, viewed on February 5, 2014).
588 ___ |a Latest issue consulted: Volume 67, issue 2 (February 2014) (viewed February 5, 2014).
590 ___ |a Access is available to the Yale community.
650 _0 |a Audiology |v Periodicals.
650 _2 |a Audiology.
776 08 |i Print version: |t Hearing journal |x 0745-7472 |w (DLC)sc 83008167
|w (OCoLC)9267554
780 00 |t Hearing aid journal
856 40 |u http://WA4PY6YJ8T.search.serialssolutions.com/?
V=1.0&L=WA4PY6YJ8T&S=JCS&C=THEHEAJOU&T=marc&tab=JOURNALS |y Full text
866 ___ |a Freely Accessible Medical Journals: 1994 to present
866 ___ |a Freely Accessible Science Journals: 1994 to present
866 ___ |a Journals@Ovid LWW Total Access Collection 2022 with Neurology: 01/01/1994 to present
866 ___ |a Journals@Ovid - LWW Extended Archive Collection: 01/01/1994 to 12/31/2008
905 ___ |a journal
946 ___ |a DO NOT EDIT. DO NOT EXPORT.

Actions

- [Add to My List](#)
- [Print](#)
- [E-mail](#)
- [Export](#)

This item

- [Full View](#)
- [Staff \(MARC\) View](#)

APPENDIX F



BOOK

Acoustic signal processing for telecommunication / edited by Steven L. Gay, Jacob Benesty.

Gay, Steven L.; Benesty, Jacob.

©2000

Request through Interlibrary Loan (UC Affiliates) >

TOP

SEND TO

GET IT

DETAILS

VIRTUAL BROWSE

LINKS

Send to

EXPORT TO EXCEL

EMAIL RECORD

PERMALINK

CITATION

PRINT

EASYBIB

ENDNOTE BASIC

EXPORT RIS

Get It

Please sign in to check if there are any request options. Sign in

[← BACK TO LOCATIONS](#)

LOCATION ITEMS

Out of library **Science Library ; TK5102.9. A27 2000**
(1 copy, 0 available, 0 requests)

On loan until 12/12/2022 5:00:00 PM PST
Sign in for borrowing details

[Call Number Locator](#)
[Report a Problem](#)

OTHER UC LIBRARIES

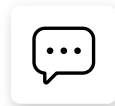
University of California Berkeley
[Available in institution](#)

University of California Los Angeles
[Available in institution](#)

University of California, Santa Barbara
[Available in institution](#)

University of California Davis
[Available in institution](#)

UC S... Di



Details

Title	Acoustic signal processing for telecommunication / edited by Steven L. Gay, Jacob Benesty.
Format	xxii, 333 pages : illustrations ; 25 cm.
Publication Date	©2000
Publisher	Boston : Kluwer Academic
Series	Kluwer international series in engineering and computer science ; SECS 551 > Kluwer international series in engineering and computer science ; SECS 551. >
Contents	An introduction to acoustic echo and noise control / Steven L. Gay, Jacob Benesty -- The fast affine projection algorithm / Steven L. Gay -- Subband acoustic echo cancellation using the FAP-RLS algorithm : fixed-point implementation issues / Mohamed Ghanassi, Benoit Champagne -- Real-time implementation of the exact block NLMS algorithm for acoustic echo control in hands-free telephone systems / Bernhard H. Nitsch -- Double-talk detection schemes for acoustic echo cancellation / Tomas Gänsler, Jacob Benesty, Steven L. Gay -- Multi-channel sound, acoustic echo cancellation, and multi-channel time-domain adaptive filtering / Jacob Benesty, Tomas Gänsler, Peter Eneroth -- Multi-channel frequency-domain adaptive filtering / Jacob Benesty, Dennis R. Morgan -- A real-time stereophonic acoustic subband echo canceler / Peter Eneroth [and others] -- Subband noise reduction methods for speech enhancement / Eric J. Diethorn -- Superdirectional microphone arrays / Gary W. Elko -- Microphone arrays for video camera steering / Yiteng (Arden) Huang, Jacob Benesty, Gary W. Elko -- Nonlinear, model-based microphone array speech enhancement / Michael S. Brandstein, Scott M. Griebel -- 3D audio and virtual acoustical environment synthesis / Jiashu Chen -- Virtual sound using loudspeakers : robust acoustic crosstalk cancellation / Darren B. Ward, Gary W. Elko -- An introduction to blind source separation of speech signals / Jacob Benesty.
Subject	Traitement du signal -- Techniques numériques > Algorithmes > Traitement adaptatif du signal > Bruit -- Lutte contre > algorithms > noise control > Computer algorithms > Algorithms > Signal processing -- Digital techniques > Speech processing systems > Adaptive signal processing > Noise control > Traitement du signal > Signal, Théorie du (télécommunications) > Télécommunications >
MESH subjects	Algorithms >
Contributor	Gay, Steven L. > Benesty, Jacob. >
Identifier	ISBN : 0792378148 ISBN : 9780792378143
Language	English
Source	Library Catalog





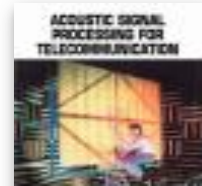
< Linear aspects of communications: discrete ...
©2001



Acoustic echo and noise control : a practical approach ...
©2004



Topics in acoustic echo and noise control : selected ...
©2006



Acoustic signal processing for telecommunication ...
©2000



Adaptive signal processing : applications to real-world ...
©2003



Links

[Display Source Record](#) >



APPENDIX G

leader 04803cam a22008774a 4500
001 9912449444506531
005 20220720213020.0
008 000207s2000 maua b 001 0 eng
010 ##\$a 00022051
015 ##\$aGBA034483 \$2bnb
016 7#\$aB0007256 \$2bccb
016 7#\$a008431036 \$2Uk
020 ##\$a0792378148
020 ##\$a9780792378143
035 ##\$a(CU-S)b41403812-01ucs_sdi
035 ##\$a(OCOLC)43434615
035 ##\$a(OCOLC)ocm43434615
040 ##\$aDLC \$beng \$cDLC \$dC#P \$dUKM \$dPMC \$dOHX \$dLVB \$dBAKER \$dNLGGC \$dBCTA \$dYDXCP \$dIG# \$dZWZ \$dOCLCF \$dOCLCQ \$dOCLCA \$dSNN \$dUKMGB \$dOCLCQ \$
042 ##\$apcc
049 ##\$aMAIN
050 00\$aTK5102.9 \$b.A27 2000
072 #7\$aTK \$2lcco
082 00\$a621.382/2 \$221
084 ##\$aRQ 81 \$2blsrissc
245 00\$aAcoustic signal processing for telecommunication / \$cedited by Steven L. Gay, Jacob Benesty.
260 ##\$aBoston : \$bKluwer Academic, \$c02000.
300 ##\$axxii, 333 pages : \$billustrations ; \$c25 cm.
336 ##\$atext \$btxt \$2rdacontent
337 ##\$aunmediated \$bn \$2rdamedia
338 ##\$avolume \$bnc \$2rdacarrier
490 1#\$aKluwer international series in engineering and computer science ; \$vSECS 551
504 ##\$aIncludes bibliographical references and index.
505 0#\$aAn introduction to acoustic echo and noise control / Steven L. Gay, Jacob Benesty -- The fast affine projection algorithm / Steven L. Gay
650 #0\$aSignal processing \$xDigital techniques.
650 #0\$aAlgorithms.
650 #0\$aAdaptive signal processing.
650 #0\$aNoise control.
650 #0\$aComputer algorithms.
650 #2\$aAlgorithms
650 #6\$aTraitement du signal \$xTechniques numériques.
650 #6\$aAlgorithms.
650 #6\$aTraitement adaptatif du signal.
650 #6\$aBruit \$xLutte contre.
650 #7\$aalgorithms. \$2aat
650 #7\$aanoise control. \$2aat
650 #7\$aComputer algorithms. \$2fast \$0(OCOLC)fst00872010
650 #7\$aAdaptive signal processing. \$2fast \$0(OCOLC)fst00796495
650 #7\$aAlgorithms. \$2fast \$0(OCOLC)fst00805020
650 #7\$aNoise control. \$2fast \$0(OCOLC)fst01038383
650 #7\$aSignal processing \$xDigital techniques. \$2fast \$0(OCOLC)fst01118285
650 #7\$aSignal processing \$xDigital techniques. \$2nli
650 #7\$aSpeech processing systems. \$2nli
650 #7\$aAdaptive signal processing. \$2nli
650 #7\$aNoise control. \$2nli
650 #7\$aTraitement du signal. \$2ram
650 #7\$aSignal, Théorie du (télécommunications) \$2ram
650 #7\$aTélécommunications. \$2ram
700 1#\$aGay, Steven L.
700 1#\$aBenesty, Jacob.
830 #0\$aKluwer international series in engineering and computer science ; \$vSECS 551.
908 ##\$aWorldCat Daily Updates 2022-06-05 \$bWorldCat record variable field(s) change: 650
908 ##\$aWorldCat Daily Updates 2022-07-20 \$bWorldCat record variable field(s) change: 040, 650
938 ##\$aBaker & Taylor \$bBKT \$c149.00 \$d149.00 \$i0792378148 \$n0003482018 \$sactive
938 ##\$aBaker and Taylor \$bBTCP \$n00022051
938 ##\$aOtto Harrassowitz \$bHARR \$nhar005126492
938 ##\$aIngram \$bINGR \$n9780792378143
938 ##\$aYBP Library Services \$bYANK \$n1664010
962 ##\$aET \$9LOCAL
996 ##\$a991023927229704701 \$9LOCAL
996 ##\$a.b27232785 \$9LOCAL



APPENDIX H

[The Ohio State University Libraries](#)

Library Catalog

Catalog home	Request this item	Save for export	MARC display	Another search	OhioLINK catalog	ILL request	
RECORD NO	▼	b5220423			Search Full Catalog	▼	Search

[Permanent link to this record](#)

Title **Acoustic signal processing for telecommunication / edited by Steven L. Gay, Jacob Benesty**

Imprint Boston : Kluwer Academic, [2000]
©2000

LOCATION	CALL NO.	YEAR	STATUS	NOTE
18th Ave Library Basement Compact Shelving	TK5102.9 .A27 2000		AVAILABLE	
Book Depository	TK5102.9 .A27 2000 c.2		AVAILABLE	

Description xxii, 333 pages : illustrations ; 25 cm
text
unmediated
volume

Note Includes bibliographical references and index

ISBN [0792378148](#)

OCLC/Control # [43434615](#)

Series [Kluwer international series in engineering and computer science ; SECS 551.](#)

Subject [Signal processing -- Digital techniques.](#)
[Algorithms.](#)
[Adaptive signal processing.](#)
[Noise control.](#)

Add'l Author [Gay, Steven L.](#)
[Benesty, Jacob.](#)

List of Figures

List of Tables

Preface

Contributing Authors

1 An Introduction to Acoustic Echo and Noise Control / [Steven L. Gay](#), [Jacob Benesty](#) 1


Pt. I Mono-Channel Acoustic Echo Cancellation

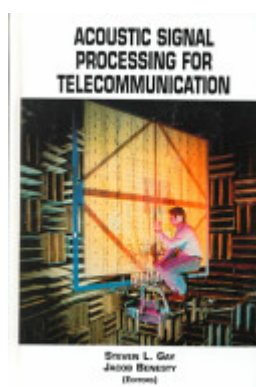
2 The Fast Affine Projection Algorithm / [Steven L. Gay](#) 23

3 Subband Acoustic Echo Cancellation Using the FAP-RLS Algorithm: Fixed-Point Implementation Issues / [Mohamed Ghanassi](#), [Benoit Champagne](#) 47

	4	Real-Time Implementation of the Exact Block NLMS Algorithm for Acoustic Echo Control in Hands-Free Telephone Systems / Bernhard H. Nitsch	67
	5	Double-Talk Detection Schemes for Acoustic Echo Cancellation / Tomas Gansler , Jacob Benesty , Steven L. Gay	81
Pt. II		Multi-Channel Acoustic Echo Cancellation	
	6	Multi-Channel Sound, Acoustic Echo Cancellation, and Multi-Channel Time-Domain Adaptive Filtering / Jacob Benesty , Tomas Gansler , Peter Eneroth	101
	7	Multi-Channel Frequency-Domain Adaptive Filtering / Jacob Benesty , Dennis R. Morgan	121
	8	A Real-time Stereophonic Acoustic Subband Echo Canceller [et al.] / Peter Eneroth , Steven L. Gay , Tomas Gansler	135
Pt. III		Noise Reduction Techniques with a Single Microphone	
	9	Subband Noise Reduction Methods for Speech Enhancement / Eric J. Diethorn	155
Pt. IV		Microphone Arrays	
	10	Superdirectional Microphone Arrays / Gary W. Elko	181
	11	Microphone Arrays for Video Camera Steering / Yiteng (Arden) Huang , Jacob Benesty , Gary W. Elko	239
	12	Nonlinear, Model-Based Microphone Array Speech Enhancement / Michael S. Brandstein , Scott M. Griebel	261
Pt. V		Virtual Sound	
	13	3D Audio and Virtual Acoustical Environment Synthesis / Jiashu Chen	283
	14	Virtual Sound Using Loudspeakers: Robust Acoustic Crosstalk Cancellation / Darren B. Ward , Gary W. Elko	303
Pt. VI		Blind Source Separation	
	15	An Introduction to Blind Source Separation of Speech Signals / Jacob Benesty	321
		Index	331

Additional Info:

 Book (Print)



[The Ohio State University Libraries](#)

© The Ohio State University - University Libraries

1858 Neil Avenue Mall | Columbus, Ohio 43210 | 614-292-OSUL (6785)

[Request an alternate format of this page](#) | [Accessibility](#) | [Privacy Policy](#) | [Contact Us](#)



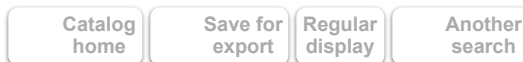
[Copyright Information](#) | [Details and Exceptions](#)



APPENDIX I

[The Ohio State University Libraries](#)

[Library Catalog](#)



```

LEADER 00000cam a22004214a 4500
001 43434615
003 OCoLC
005 20210625233037.0
008 000207t20002000maua b 001 0 eng
010 00022051
020 0792378148
035 .b52204236
040 DLC|cDLC|dC#P|dwaOLN|dUtOrBLW
042 pcc
049 OSU&
050 00 TK5102.9|b.A27 2000
050 00 TK5102.9|b.A27 2000
082 00 621.382/2|221
245 00 Acoustic signal processing for telecommunication /|cedited
    by Steven L. Gay, Jacob Benesty
264 1 Boston :|bKluwer Academic,|c[2000]
264 4 |c02000
300 xxii, 333 pages :|billustrations ;|c25 cm
336 text|btxt|2rdacontent
337 unmediated|bn|2rdamedia
338 volume|bnc|2rdacarrier
490 1 The Kluwer international series in engineering and
    computer science ;|vSECS 551
504 Includes bibliographical references and index
650 0 Signal processing|xDigital techniques.|0http://id.loc.gov/
    authorities/subjects/sh85122398
650 0 Algorithms.|0http://id.loc.gov/authorities/subjects/
    sh85003487
650 0 Adaptive signal processing.|0http://id.loc.gov/authorities
    /subjects/sh85000805
650 0 Noise control.|0http://id.loc.gov/authorities/subjects/
    sh85092183
700 1 Gay, Steven L.|0http://id.loc.gov/authorities/names/
    n00001624
700 1 Benesty, Jacob.|0http://id.loc.gov/authorities/names/
    n00001625
830 0 Kluwer international series in engineering and computer
    science ;|vSECS 551.|0http://id.loc.gov/authorities/names/
    n84749953
910 RDA ENRICHED|aMARS
910 MARS
910 YBP
910 &8c000612
970 01 |tList of Figures
970 01 |tList of Tables
970 01 |tPreface
970 01 |tContributing Authors
970 12 |l1|tAn Introduction to Acoustic Echo and Noise Control
    |cSteven L. Gay|fGay, Steven L.|cJacob Benesty|fBenesty,
    Jacob.|p1
970 11 |lPt. I|tMono-Channel Acoustic Echo Cancellation

```


- 970 12 |12|tThe Fast Affine Projection Algorithm|cSteven L. Gay
|fGay, Steven L.|p23
- 970 12 |13|tSubband Acoustic Echo Cancellation Using the FAP-RLS
Algorithm: Fixed-Point Implementation Issues|cMohamed
Ghanassi|fGhanassi, Mohamed|cBenoit Champagne|fChampagne,
Benoit|p47
- 970 12 |14|tReal-Time Implementation of the Exact Block NLMS
Algorithm for Acoustic Echo Control in Hands-Free
Telephone Systems|cBernhard H. Nitsch|fNitsch, Bernhard H.
|p67
- 970 12 |15|tDouble-Talk Detection Schemes for Acoustic Echo
Cancellation|cTomas Gansler|fGansler, Tomas|cJacob Benesty
|fBenesty, Jacob.|cSteven L. Gay|fGay, Steven L.|p81
- 970 11 |1Pt. II|tMulti-Channel Acoustic Echo Cancellation
- 970 12 |16|tMulti-Channel Sound, Acoustic Echo Cancellation, and
Multi-Channel Time-Domain Adaptive Filtering|cJacob
Benesty|fBenesty, Jacob.|cTomas Gansler|fGansler, Tomas
|cPeter Eneroth|fEneroth, Peter|p101
- 970 12 |17|tMulti-Channel Frequency-Domain Adaptive Filtering
|cJacob Benesty|fBenesty, Jacob.|cDennis R. Morgan|fMorgan,
Dennis R.|p121
- 970 12 |18|tA Real-time Stereophonic Acoustic Subband Echo
Canceler|cPeter Eneroth|fEneroth, Peter|cSteven L. Gay
|fGay, Steven L.|cTomas Gansler|fGansler, Tomas|d[et al.]
|p135
- 970 11 |1Pt. III|tNoise Reduction Techniques with a Single
Microphone
- 970 12 |19|tSubband Noise Reduction Methods for Speech
Enhancement|cEric J. Diethorn|fDiethorn, Eric J.|p155
- 970 11 |1Pt. IV|tMicrophone Arrays
- 970 12 |110|tSuperdirectional Microphone Arrays|cGary W. Elko
|fElko, Gary W.|p181
- 970 12 |111|tMicrophone Arrays for Video Camera Steering|cYiteng
(Arden) Huang|fHuang, Yiteng, 1972-|cJacob Benesty
|fBenesty, Jacob.|cGary W. Elko|fElko, Gary W.|p239
- 970 12 |112|tNonlinear, Model-Based Microphone Array Speech
Enhancement|cMichael S. Brandstein|fBrandstein, Michael S.
|cScott M. Griebel|fGriebel, Scott M.|p261
- 970 11 |1Pt. V|tVirtual Sound
- 970 12 |113|t3D Audio and Virtual Acoustical Environment
Synthesis|cJiashu Chen|fChen, Jiashu|p283
- 970 12 |114|tVirtual Sound Using Loudspeakers: Robust Acoustic
Crosstalk Cancellation|cDarren B. Ward|fWard, Darren B.
|cGary W. Elko|fElko, Gary W.|p303
- 970 11 |1Pt. VI|tBlind Source Separation
- 970 12 |115|tAn Introduction to Blind Source Separation of Speech
Signals|cJacob Benesty|fBenesty, Jacob.|p321
- 970 01 |tIndex|p331
- 971 |d20000614

LOCATION	CALL NO.	YEAR	STATUS	NOTE
18th Ave Library Basement Compact Shelving	TK5102.9 .A27 2000		AVAILABLE	
Book Depository	TK5102.9 .A27 2000 c.2		AVAILABLE	

[The Ohio State University Libraries](#)

© The Ohio State University - University Libraries

1858 Neil Avenue Mall | Columbus, Ohio 43210 | 614-292-OSUL (6785)

[Request an alternate format of this page](#) | [Accessibility](#) | [Privacy Policy](#) | [Contact Us](#)



[Copyright Information](#) | [Details and Exceptions](#)



APPENDIX J

RIES
IENCE

ACOUSTIC SIGNAL PROCESSING FOR TELECOMMUNICATION

SLBAR
TK
5102.9
A27
2000

Edited by
STEVEN L. GAY
Bell Laboratories, Lucent Technologies

JACOB BENESTY
Bell Laboratories, Lucent Technologies

6210 32785



Kluwer Academic Publishers
Boston/Dordrecht/London

The current revolution in electronic switching and transport technologies promises a dramatic increase in the intimacy and satisfaction that users will experience over imminent telecommunications networks. Improvement in communications, a corresponding a room is largely empty. The sense of presence that is due to the psycho-acoustic cues they sense from the human binaural hearing system evolved over millennia. Modern acoustic signal processing is just now beginning to be able to deliver that same experience to users remotely located from each other. This includes the ability to communicate in full duplex with wider bandwidths and multiple audio streams (e.g. stereo, 3D audio). It also involves locating and separating audio sources, suppressing noise, and using sound to automatically steer video cameras.

Acoustic Signal Processing for Telecommunication presents digital signal processing techniques for telecommunications acoustics that are both cutting edge and practical. Each chapter presents material that has not appeared in book form before and yet is easily realizable in today's technology. To this end, both new theory and implementation techniques are presented. Topics include, new adaptive filtering algorithms, multi-channel acoustic echo cancellation, noise control, virtual sound, sound source localization for camera tracking, source separation, and microphone arrays.



UC IRVINE LIBRARIES
3 1970 02062 4810

ISBN 0-7923-7814-8



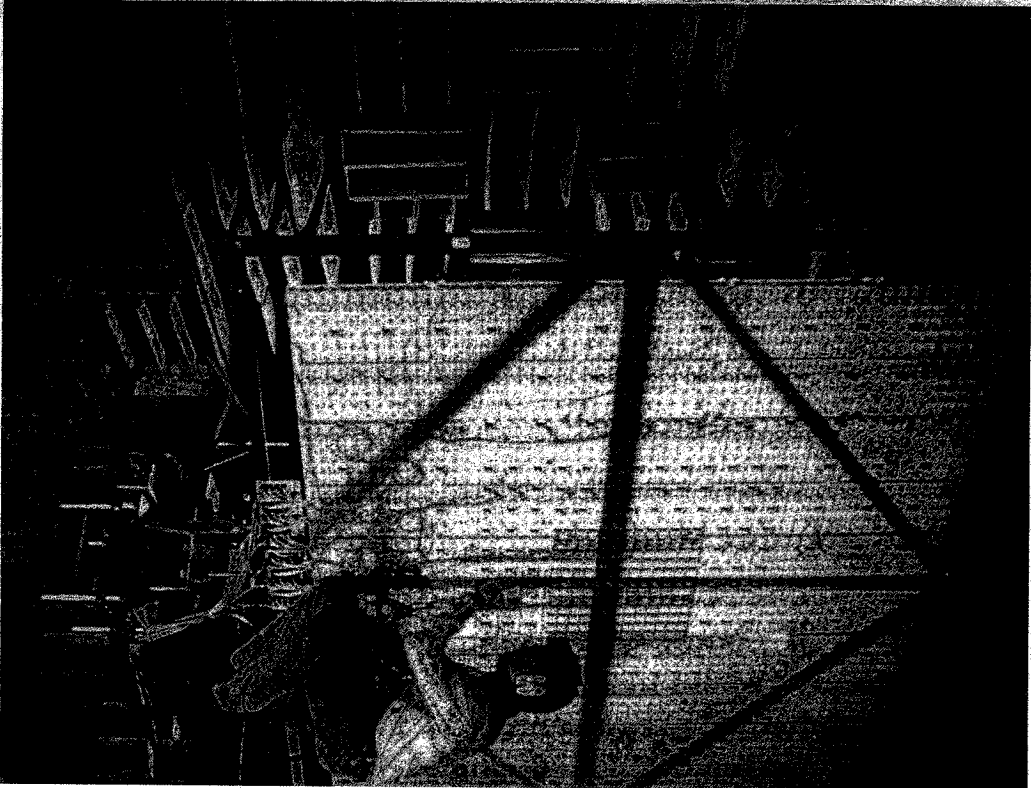
SECS 551
O-7923-7814-8

**GAY
BENESTY**

**ACOUSTIC SIGNAL PROCESSING
FOR TELECOMMUNICATION**

TK
5102.9
A27
2000

**ACOUSTIC SIGNAL
PROCESSING FOR
TELECOMMUNICATION**



**STEVEN L. GAY
JACOB BENESTY
(EDITORS)**

Distributors for North, Central and South America:

Kluwer Academic Publishers
101 Philip Drive
Assinippi Park
Norwell, Massachusetts 02061 USA
Telephone (781) 871-6600
Fax (781) 871-6528
E-Mail <kluwer@wkap.com>

Distributors for all other countries:

Kluwer Academic Publishers Group
Distribution Centre
Post Office Box 322
3300 AH Dordrecht, THE NETHERLANDS
Telephone 31 78 6392 392
Fax 31 78 6546 474
E-Mail services@wkap.nl>



Electronic Services <<http://www.wkap.nl>>

Library of Congress Cataloging-in-Publication

Acoustic signal processing for telecommunication / edited by Steven L. Gay, Jacob Benesty.
p. cm. -- (Kluwer international series in engineering and computer science ; SECS 551)
Includes bibliographical references and index.
ISBN 0-7923-7814-8
1. Signal processing--Digital techniques. 2. Algorithms. 3. Adaptive signal processing.
4. Noise control. I. Gay, Steven L. II. Benesty, Jacob. III. Series.

TK5102.9. A27 2000
621.382'2--dc21

00-022051

Copyright © 2000 by Kluwer Academic Publishers.

All rights reserved. No part of this publication may be reproduced, stored in a retrieval system or transmitted in any form or by any means, mechanical, photo-copying, recording, or otherwise, without the prior written permission of the publisher, Kluwer Academic Publishers, 101 Philip Drive, Assinippi Park, Norwell, Massachusetts 02061

Printed on acid-free paper.

Printed in the United States of America

Contents

List of Figures	xi
List of Tables	xviii
Preface	xix
Contributing Authors	xxi
1	
An Introduction to Acoustic Echo and Noise Control	1
<i>Steven L. Gay Jacob Benesty</i>	
1. Human Perception of Echoes	1
2. The Network Echo Problem	3
3. The Acoustic Echo Problem	6
4. Adaptive Filters for Echo Cancellation	8
4.1 The LMS and NLMS Algorithms	9
4.2 Least Squares and Recursive Least Squares Algorithms	12
5. Noise Reduction	17
6. Conclusions	18
Part I Mono-Channel Acoustic Echo Cancellation	
2	
The Fast Affine Projection Algorithm	23
<i>Steven L. Gay</i>	
1. Introduction	23
2. The Affine Projection Algorithm	24
2.1 Projections Onto an Affine Subspace	26
2.2 Convergence and Regularization	29
2.3 The Connection Between APA and Recursive Least Squares	29
3. Fast Affine Projections	31
3.1 Fast Residual Echo Vector Calculation	31
3.2 Fast Adaptive Coefficient Vector Calculation	33

Gay, Jacob Benesty.
r science ; SECS 551)

signal processing.

00-022051

ed in a retrieval system or
ding, or otherwise, without
lishers, 101 Philip Drive,

vi *Acoustic Signal Processing*

3.3	Fast Normalized Residual Echo Vector Calculation	36
3.4	The FAP Algorithm	37
4.	Simulations	39
5.	Numerical Considerations	40
6.	Conclusions	40
	Appendix: Sliding Windowed Fast Recursive Least Squares	42
3		
	Subband Acoustic Echo Cancellation Using the FAP-RLS Algorithm: Fixed-Point Implementation Issues	47
	<i>Mohamed Ghanassi Benoit Champagne</i>	
1.	Introduction	47
2.	Overview of FAP-Based Subband AEC System	49
	2.1 FAP-RLS Algorithm	50
	2.2 Uniform DFT Filter Banks	53
3.	Scope of Fixed-Point Study	54
4.	Fixed-Point Implementation of FAP-RLS	55
	4.1 Update of Inverse Data Covariance Matrix	56
	4.2 Update of Correlation Vector	58
	4.3 Filtering and Adaptation	58
	4.4 Algorithm Precision	60
5.	Fixed-Point WOA Implementation	60
	5.1 DFT or FFT?	60
	5.2 Analysis Bank	62
	5.3 Synthesis Bank	62
6.	Evaluation of Complete Algorithm	63
7.	Conclusion	63
4		
	Real-Time Implementation of the Exact Block NLMS Algorithm for Acous- tic Echo Control in Hands-Free Telephone Systems	67
	<i>Bernhard H. Nitsch</i>	
1.	Introduction	67
2.	Block Processing	68
3.	The Exact Block NLMS Algorithm	69
4.	Reduction of the Signal Delay	71
5.	The PEFBNLMS Algorithm	73
6.	Performance	74
7.	Real-Time Implementation	77
8.	Conclusions	80
5		
	Double-Talk Detection Schemes for Acoustic Echo Cancellation	81
	<i>Tomas Gänsler Jacob Benesty Steven L. Gay</i>	
1.	Introduction	81
2.	Basics of AEC and DTD	84
	2.1 AEC Notations	84
	2.2 The Generic DTD	84
	2.3 A Suggestion to Performance Evaluation of DTDs	85
3.	Double-Talk Detection Algorithms	86
	3.1 Geigel Algorithm	86

ion 36
 37
 39
 40
 40
 42

 ithm: 47

 47
 49
 50
 53
 54
 55
 56
 58
 58
 60
 60
 60
 62
 62
 63
 63

 acous- 67

 67
 68
 69
 71
 73
 74
 77
 80

 81

 81
 84
 84
 84
 85
 86
 86

 s 86

3.2	Cross-Correlation Method	86
3.3	Normalized Cross-Correlation Method	87
3.4	Coherence Method	88
3.5	Normalized Cross-correlation Matrix	90
3.6	Two-Path Model	92
3.7	DTD Combinations with Robust Statistics	93
4.	Discussion	95
Part II Multi-Channel Acoustic Echo Cancellation		
6	Multi-Channel Sound, Acoustic Echo Cancellation, and Multi-Channel Time-Domain Adaptive Filtering	101
	<i>Jacob Benesty Tomas Gänsler Peter Eneroth</i>	
1.	Introduction	101
2.	Multi-Channel Identification and the Nonuniqueness Problem	104
3.	Some Different Solutions for Decorrelation	106
4.	The Hybrid Mono/Stereo Acoustic Echo Canceler	108
5.	Multi-Channel Time-Domain Adaptive Filters	110
5.1	The Classical and Factorized Multi-Channel RLS	110
5.2	The Multi-Channel Fast RLS	112
5.3	The Multi-Channel LMS Algorithm	113
5.4	The Multi-Channel APA	116
6.	Discussion	118
7	Multi-Channel Frequency-Domain Adaptive Filtering	121
	<i>Jacob Benesty Dennis R. Morgan</i>	
1.	Introduction	121
2.	Mono-Channel Frequency-Domain Adaptive Filtering Revisited	122
3.	Generalization to the Multi-Channel Case	127
4.	Application to Acoustic Echo Cancellation and Simulations	129
5.	Conclusions	131
8	A Real-time Stereophonic Acoustic Subband Echo Canceler	135
	<i>Peter Eneroth Steven L. Gay Tomas Gänsler Jacob Benesty</i>	
1.	Introduction	136
2.	Acoustic Echo Canceler Components	137
2.1	Adaptive Algorithm	137
2.2	Filterbank Design	139
2.3	Residual Echo Suppression	145
2.4	Computational Complexity	146
2.5	Implementation Aspects	147
3.	Simulations	148
Part III Noise Reduction Techniques with a Single Microphone		
9	Subband Noise Reduction Methods for Speech Enhancement	155
	<i>Eric J. Diethorn</i>	

1.	Introduction	155
2.	Wiener Filtering	158
3.	Speech Enhancement by Short-Time Spectral Modification	159
3.1	Short-Time Fourier Analysis and Synthesis	159
3.2	Short-Time Wiener Filter	160
3.3	Power Subtraction	161
3.4	Magnitude Subtraction	162
3.5	Parametric Wiener Filtering	163
3.6	Review and Discussion	164
4.	Averaging Techniques for Envelope Estimation	169
4.1	Moving Average	169
4.2	Single-Pole Recursion	170
4.3	Two-Sided Single-Pole Recursion	170
4.4	Nonlinear Data Processing	171
5.	Example Implementation	172
5.1	Subband Filter Bank Architecture	172
5.2	A-Posteriori-SNR Voice Activity Detector	173
5.3	Example	175
6.	Conclusion	175
Part IV Microphone Arrays		
10	Superdirectional Microphone Arrays	181
<i>Gary W. Elko</i>		
1.	Introduction	181
2.	Differential Microphone Arrays	182
3.	Array Directional Gain	192
4.	Optimal Arrays for Spherically Isotropic Fields	193
4.1	Maximum Gain for Omnidirectional Microphones	193
4.2	Maximum Directivity Index for Differential Microphones	195
4.3	Maximum Front-to-Back Ratio	197
4.4	Minimum Peak Directional Response	200
4.5	Beamwidth	201
5.	Design Examples	201
5.1	First-Order Designs	202
5.2	Second-Order Designs	207
5.3	Third-Order Designs	216
5.4	Higher-Order designs	221
6.	Optimal Arrays for Cylindrically Isotropic Fields	222
6.1	Maximum Gain for Omnidirectional Microphones	222
6.2	Optimal Weights for Maximum Directional Gain	224
6.3	Solution for Optimal Weights for Maximum Front-to-Back Ratio for Cylindrical Noise	225
7.	Sensitivity to Microphone Mismatch and Noise	230
8.	Conclusions	233
Appendix: Directivity Factor and Room Acoustics		236
11	Microphone Arrays for Video Camera Steering	239

tion
 155
 158
 159
 159
 160
 161
 162
 163
 164
 169
 169
 170
 170
 171
 172
 172
 173
 175
 175
 181
 181
 182
 192
 193
 193
 195
 197
 200
 201
 201
 202
 207
 216
 221
 222
 222
 224
 225
 230
 233
 236
 239

<i>Yiteng (Arden) Huang Jacob Benesty Gary W. Elko</i>		
1.	Introduction	239
2.	Time Delay Estimation	241
2.1	Acoustic Models for the TDE Problem	242
2.2	The GCC Method	243
2.3	Adaptive Eigenvalue Decomposition Algorithm	244
3.	Source Localization	247
3.1	Source Localization Problem	247
3.2	Ideal Maximum Likelihood Locator	248
3.3	Triangulation Locator	250
3.4	The Spherical Equations	250
3.5	CLS and Spherical Intersection (SX) Methods	251
3.6	Spherical Interpolation (SI) Locator	252
3.7	One Step Least Squares (OSLS) Locator	253
4.	System Implementation	255
5.	Summary	257
12		
Nonlinear, Model-Based Microphone Array Speech Enhancement		261
<i>Michael S. Brandstein Scott M. Griebel</i>		
1.	Introduction	261
2.	Speech Enhancement Methods	263
3.	Nonlinear, Model-Based Processing	264
4.	A Multi-Channel Speech Enhancement Algorithm	265
4.1	Algorithm Details	266
4.2	Simulations	274
5.	Conclusion	275
Part V Virtual Sound		
13		
3D Audio and Virtual Acoustical Environment Synthesis		283
<i>Jiashu Chen</i>		
1.	Introduction	283
2.	Sound Localization Cues and Synthetic 3D Audio	284
2.1	Interaural Cues for Sound Localization	285
2.2	Head-Related Transfer Function (HRTF)	286
2.3	Synthetic 3D Audio	287
2.4	Modeling the Measured HRTFs	288
3.	Spatial Feature Extraction and Regularization (SFER) Model for HRTFs	290
3.1	SFER Model for Head-Related Impulse Response	290
3.2	TDSFER Model for Multiple 3D Sound Source Positioning	292
4.	Computing Architectures Using TDSFER Model	295
4.1	Multiple Sources with Multiple Reflections	295
4.2	Single Source with Multiple Reflections	298
5.	Specific Issues for VAES Implementation	299
6.	Conclusions	299
14		
Virtual Sound Using Loudspeakers: Robust Acoustic Crosstalk Cancellation		303

x *Acoustic Signal Processing*

Darren B. Ward Gary W. Elko

1.	Introduction	303
2.	Acoustic Crosstalk Cancellation	305
	2.1 Problem Statement	305
	2.2 Selection of the Design Matrix	306
3.	Robustness Analysis	307
	3.1 Robustness Measure	307
	3.2 Analysis of the Design Matrix	307
	3.3 Example of Ear Responses	308
	3.4 Spatial Responses	310
4.	Effect of Loudspeaker Position	313
	4.1 A Robust CCS	315
5.	Discussion and Conclusions	316

Part VI *Blind Source Separation*

15

An Introduction to Blind Source Separation of Speech Signals	321
--	-----

Jacob Benesty

1.	Introduction	321
2.	The Information Maximization Principle	322
3.	Different Stochastic Gradient Ascent Rules Based on ME	324
	3.1 The Infomax Stochastic Gradient Ascent Learning Rule	324
	3.2 The Natural Gradient Algorithm	325
	3.3 A Normalized Natural Gradient Algorithm	325
4.	Simulations	326
5.	Conclusions	328

Index

331

List of Figures

303
305
305
306
307
307
307
308
310
313
315
316

321

321

322

324

324

325

325

326

328

331

1.1	A simplified long distance connection.	4
1.2	A simplified network echo canceler.	5
1.3	Speakerphone with suppression and echo cancellation.	8
2.1	(a) Projection onto a linear subspace. (b) Relaxed projection onto a linear subspace.	26
2.2	(a) Projection onto an affine subspace. (b) Relaxed projection onto an affine subspace.	27
2.3	Comparison of coefficient error for FAP, FTF, and NLMS with speech as excitation.	38
2.4	Comparison of FAP for different orders of projection, N , with speech as excitation.	39
3.1	Block diagram of generic subband AEC system.	50
3.2	Quantization error power (QEP) in $[\mathbf{R}^{-1}(k)]_{11}$ versus time index k in 16-bit implementation of inverse data covariance matrix update for $\delta = 10\sigma_x^2$ and $50\sigma_x^2$.	57
3.3	Quantization error power (QEP) in $[\mathbf{R}^{-1}(k)]_{11}$ versus time index k in 16-bit and 32/16-bit implementations of inverse data covariance matrix update ($\delta = 12\sigma_x^2$).	58
3.4	Quantization error power (QEP) in $[\mathbf{r}(k)]_1$ versus time index k in 16-bit implementation of (3.6).	59
3.5	Short-time power of error signal $e(k)$ versus time in FAP-RLS for different precision b in bits.	61
3.6	Short-term power of residual echo in fixed-point implementation of subband FAP-RLS.	64
4.1	Reduction of the signal delay.	72
4.2	Block diagram of the PEFBNLMS algorithm.	75
4.3	Block diagram of the PEFBNLMS algorithm.	76

4.4	Complexity of the PEFBNLMS algorithm compared to the time-domain NLMS algorithm.	76
4.5	Typical convergence curves of the PEFBNLMS algorithm.	79
5.1	Block diagram of a basic AEC setup.	82
5.2	Estimated coherence using the multiple window method.	89
5.3	Two-path adaptive filtering.	93
5.4	Disturbances that enters the adaptive algorithm.	94
6.1	Schematic diagram of stereophonic acoustic echo cancellation.	104
6.2	Hybrid mono/stereo acoustic echo canceler.	109
7.1	Schematic diagram of stereophonic acoustic echo cancellation with nonlinear transformations of the two input signals.	130
7.2	Performance of the two-channel NLMS.	131
7.3	Performance of the two-channel FRLS.	131
7.4	Performance of the proposed algorithm (unconstrained version).	132
7.5	Same as in Fig. 7.4 with $\lambda_f = 0.9$.	132
8.1	A stereophonic echo canceler.	136
8.2	A subband stereophonic acoustic echo canceler.	138
8.3	State representation of the synthesis filterbank.	142
8.4	An example of a filterbank designed by solving (8.28).	143
8.5	Suppression and comfort noise fill.	146
8.6	Magnitude coherence between the right and left channel in the transmission room.	148
8.7	Mean square error convergence of the SAEC.	150
8.8	Mean square error convergence of the SAEC. Comparison between two-channel FRLS (solid line), NLMS (dashed line), and a SAEC with FRLS in the lower subbands and NLMS in the higher subbands (dotted line).	150
9.1	Gain functions for different methods of noise reduction.	165
9.2	Schroeder's noise reduction system.	165
9.3	Noise reduction system based on <i>a posteriori</i> SNR voice activity detection.	172
9.4	Speech time series for the noise reduction example.	176
9.5	Spectrograms corresponding to speech time series in Fig. 9.3.	176
9.6	Noisy and noise-reduced power spectrums corresponding to the time series in Fig. 9.3.	177
10.1	Finite-difference amplitude bias error in dB for a plane-wave propagating along the microphone axis.	185
10.2	Diagram of first-order microphone composed of two zero-order (omnidirectional) microphones.	186

ed to	76	10.3 Directivity plots for first-order arrays (a) $\alpha_1 = 0.55$, (b) $\alpha_1 = 0.20$.	188
gorithm.	79	10.4 Three dimensional representation of directivity in Fig. 10.3(b).	188
	82	10.5 Construction of differential arrays as first-order differential combinations up to third-order.	189
ethod.	89	10.6 Directivity index of first-order microphone versus the first-order differential parameter α_1 .	202
	93	10.7 Front-to-back ratio of first-order microphone versus the first-order differential parameter α_1 .	204
	94	10.8 3 dB beamwidth of first-order microphone versus the first-order differential parameter α_1 .	205
ancellation.	104	10.9 Various first-order directional responses, (a) dipole, (b) cardioid, (c) hypercardioid, (d) supercardioid.	206
	109	10.10 Contour plot of the directivity index DI in dB for second-order array versus α_1 and α_2 .	208
can-	130	10.11 Contour plot of the front-to-back ratio in dB for second-order arrays versus α_1 and α_2 .	208
nput	131	10.12 Various second-order directional responses, (a) dipole, (b) cardioid, (c) hypercardioid, (d) supercardioid.	209
	131	10.13 Second-order Olson-Sessler-West cardioid directional response.	210
ed version).	132	10.14 Various second-order equi-sidelobe designs, (a) Korenbaum design, (b) -15 dB sidelobes, (c) -30 dB sidelobes, (d) minimum rear half-plane peak response.	211
	132	10.15 Directivity index (solid) and front-to-back ratio (dotted) for equi-sidelobe second-order array designs versus sidelobe level.	214
	136	10.16 Directional responses for equi-sidelobe second-order differential arrays for, (a) maximum directivity index, and, (b) maximum front-to-back ratio.	214
	138	10.17 Maximum second-order differential directivity index DI for first-order differential microphones defined by (10.97).	215
3).	142	10.18 Maximum second-order differential front-to-back ratio for first-order differential microphones defined by (10.97).	216
	143	10.19 Various third-order directional responses, (a) dipole, (b) cardioid, (c) hypercardioid, (d) supercardioid.	217
	146	10.20 Third-order Olson-Sessler-West cardioid directional response.	218
nel	148	10.21 Equi-sidelobe third-order differential microphone for (a) -20 dB and (b) -30 dB sidelobes.	221
	150	10.22 Directivity index and front-to-back ratio for equi-sidelobe third-order differential array designs versus sidelobe level.	221
ari-	150		
ashed	165		
nd	165		
	172		
	176		
Fig. 9.3.	176		
d-	177		
e-	185		
o-	186		

10.23	Directivity responses for equi-sidelobe third-order differential arrays for (a) maximum directivity index and (b) maximum front-to-back ratio.	222
10.24	Maximum gain of an array of N omnidirectional microphones for spherical and cylindrical isotropic noise fields.	224
10.25	Optimum directivity patterns for differential arrays in a cylindrically isotropic noise field for (a) first, (b) second, (c) third, and (d) fourth-order	226
10.26	Directivity patterns for maximum front-to-back power ratio for differential arrays in a cylindrically isotropic noise field for (a) first, (b) second, (c) third, and (d) fourth-order	228
10.27	Sensitivity as a function of wavelength element-spacing product for, (a) various first-order differential microphones, and, (b) first, second, and third-order dipoles.	232
11.1	Acoustic models for time delay estimation problems. (a) Ideal free-field model. (b) Real reverberant model.	243
11.2	An adaptive filter for eigenvalue decomposition algorithm.	246
11.3	Spatial diagram illustrating notation defined in the source localization problem.	248
11.4	Schematic block diagram of the real-time system infrastructure.	256
11.5	Three-dimensional microphone array for passive acoustic source localization.	257
12.1	Outline of the proposed algorithm.	267
12.2	Clean speech and wavelet extrema reconstructions after 5 and 25 iterations.	269
12.3	Clustering results and coherence envelope.	270
12.4	LPC residual of clean speech, after beamforming, and after wavelet clustering technique.	271
12.5	Comparison 1: clean, reverberant, beamformed, and WVT extrema reconstructed speech.	272
12.6	Comparison 2: clean, reverberant, beamformed, and WVT extrema reconstructed speech.	273
12.7	Long-term coherence window.	274
12.8	Room setup - ● represents microphones, ○ represents the speech source.	275
12.9	Comparison of clean, reverberant, beamformed, and the proposed algorithm (reverberation-only case).	276
12.10	Comparison of clean, reverberant, beamformed, and the proposed algorithm (reverberation plus noise case).	277

r differ-
and (b) 222

micro-
se fields. 224

ys in a
second, 226

power
otropic
nd (d) 228

acing
phones, 232

ns. (a) 243

l. 246

gorithm. 248

source 256

nfrastructure. 257

icous- 267

after 269

270

, and 271

.WVT 272

WVT 273

274

s the 275

l the 276

l the 277

12.11 Bark spectral distortion results. 278

13.1 Interaural difference of a B&K HATS in horizontal plane. 285

13.2 HRTF variations in median plane for a KEMAR manikin. 286

13.3 Simple implementation of 3D sound. 287

13.4 Covariance analysis. 292

13.5 Computation efficiency improvement ratio of TDSFER model over direct convolution. 296

13.6 SFER computing model for multiple sound sources with multiple reflections. 297

14.1 Schematic diagram of a crosstalk cancellation system. 305

14.2 Conditioning of acoustic TF matrix versus frequency. 309

14.3 Example of ear responses. 310

14.4 Block diagram for spatial responses. 311

14.5 Spatial response at 2 kHz for the left program signal p_L . 312

14.6 Loudspeaker positions versus frequency. 315

14.7 Block diagram of a robust CCS. 316

15.1 Instantaneous mixing, unmixing, and nonlinear transformation. 322

15.2 Performance of different learning rules with four speech signal sources. 327

15.3 Performance of different learning rules with ten speech signal sources. 328

List of Tables

1.1	Subjective reaction to echo delay.	2
1.2	Subjective effect of 15 dB echo return loss.	3
3.1	FAP-RLS algorithm (complex version).	52
4.1	Complexity of the PEFBNLMS algorithm compared to the time-domain NLMS algorithm.	77
4.2	Maximum reachable filter length C_{max} in the real-time implementation.	79
8.1	Calculation complexity comparison given as number of real valued mult/add per fullband sample period.	147
10.1	Table of maximum array gain Q , and corresponding eigenvector for differential arrays from first to fourth-order for spherically isotropic noise fields.	197
10.2	Table of maximum F ratio and corresponding eigenvector for differential arrays from first to fourth-order for spherically isotropic noise fields.	199
10.3	Table of first-order differential, second-order differential, and third-order differential designs.	203
10.4	Table of maximum eigenvalue and corresponding eigenvector for differential arrays from first to fourth-order, for cylindrically isotropic noise fields.	225
10.5	Table of maximum eigenvalue corresponding to the maximum front-to-back ratio and corresponding eigenvector for differential arrays from first to fourth-order, for cylindrically isotropic noise fields.	227
10.6	Table of maximum directional gain and front-to-back power ratio for differential arrays from first to fourth-order, for cylindrically and spherically isotropic noise fields.	229

13.1 Comparison of number of instructions for HRIR filtering
between direct convolution and TDSFER model.

Preface

The overriding goal of acoustic signal processing for telecommunication systems is to promote the feeling of "telepresence" among users. That is, make users feel they are in the actual physical presence of each other even though they may be separated into many groups over large distances. Unfortunately, there are many obstacles which prevent system designers from easily attaining this goal. These include the user's acoustic environments, the physical and architectural aspects of modern telecommunication systems, and even the human auditory perceptual system itself.

Telepresence implies the use of hands-free communication which give rise to problems that are almost nonexistent when handsets are used. These difficulties have motivated a considerable body of research in signal processing algorithms. Technologies such as noise reduction and dereverberation algorithms using one or more microphones (Parts III and IV), camera tracking (Chapter 11), echo control algorithms (Parts I and II), virtual sound (Part V), and blind source separation (Part VI) have arisen to stabilize audio connections, eliminate echo, and improve audio transmission and rendering.

Researchers are now endeavoring to enhance the telepresence experience by using multi-channel audio streams between locations to increase spatial realism, signal separation, and talker localization and identification, by taking advantage of our binaural hearing system. While stereo and surround-sound are common examples of one-way free space multi-channel audio, realizing these technologies in the full duplex telecommunications realm has raised a set of new fundamental problems that have only recently been addressed in a satisfactory manner. Furthermore, multi-channel duplex communications enabled by multi-channel echo cancellation and control algorithms will allow participants of point-to-point and even multi-point teleconferences to instinctively know who is talking and from where, simply by using the normal auditory cues that have evolved in humans over millennia.

Acoustic signal processing also plays an important role in enhancing the visual aspect of multi-media telecommunication. Algorithms which localize and identify the nature of sound sources allow cameras to be steered automatically to the active participants of a teleconference, allowing participants to concentrate on the issues at hand rather than cumbersome camera manipulation.

Our strategy for selecting the chapters for this book has been to present digital signal processing techniques for telecommunications acoustics that are both cutting edge and practical. Each chapter presents material that has not appeared in book form before and yet is easily realizable in today's technology. To this end, those chapters that do not explicitly discuss implementation are followed by those that discuss implementation aspects on the same subject. The end result is a book that, we hope, is interesting to both researchers and developers.

STEVEN L. GAY

JACOB BENESTY

Contributing Authors

hancing the vi-
ch localize and
utomatically to
; to concentrate
tion.

een to present
oustics that are
ial that has not
y's technology.
ementation are
; same subject.
esearchers and

STEVEN L. GAY

JACOB BENESTY

Jacob Benesty

Bell Laboratories, Lucent Technologies

Michael S. Brandstein

Division of Engineering and Applied Sciences, Harvard University

Benoit Champagne

Department of Electrical and Computer Engineering, McGill University

Jiashu Chen

Lucent Technologies

Eric J. Diethorn

Microelectronics and Communications Technologies, Lucent Technologies

Gary W. Elko

Bell Laboratories, Lucent Technologies

Peter Eneroth

Department of Applied Electronics, Lund University

Steven L. Gay

Bell Laboratories, Lucent Technologies

Mohamed Ghanassi

EXFO Fiber Optic Test Equipment

Chapter 10

SUPERDIRECTIONAL MICROPHONE ARRAYS

Gary W. Elko

Bell Labs, Lucent Technologies

gwe@bell-labs.com

Abstract Noise and reverberation can seriously degrade both the microphone reception and the loudspeaker transmission of speech signals in hands-free telecommunication. Directional loudspeakers and microphone arrays can be effective in combating these problems. This chapter covers the design and implementation of differential arrays that are small compared to the acoustic wavelength. Differential arrays are therefore also superdirectional arrays since their directivity is higher than that of a uniformly summed array with the same geometry. Aside from the small size, another beneficial feature of these differential arrays is that their directivity is independent of frequency. Derivations are included for several optimal differential arrays that may be useful for teleconferencing and speech pickup in noisy and reverberant environments. Novel expressions and design details covering multiple-order hypercardioid and supercardioid-type differential arrays are given. Also, the design of Dolph-Chebyshev equi-sidelobe differential arrays is covered for the general multiple-order case. The results shown here should be useful in designing and selecting directional microphones for a variety of applications.

Keywords: Acoustic Arrays, Beamforming, Directional Microphones, Differential Microphones, Room Acoustics

1. INTRODUCTION

Noise and reverberation can seriously degrade both the microphone reception and the loudspeaker transmission of speech signals in hands-free telecommunication. The use of small directional microphones and loudspeakers can be effective in combating these problems. First-order differential microphones have been in existence now for more than 50 years. Due to their directional and close-talking properties, they have proven essential for the reduction of feedback in public address systems. In telephone applications, such as speakerphone teleconferencing, directional microphones are very useful but at present are sel-

dom utilized. Since small differential arrays can offer significant improvement in typical teleconferencing configurations, it is expected that they will become more prevalent in years to come.

Work on various differential microphone arrays has been ongoing in the Acoustics Research Department at Bell Labs for many years. The intent of the present work is to fill in some of the missing information and to develop some of the necessary analytical expressions in differential microphone array design. Included are several new results of potential importance to a designer of such microphone systems. Various design configurations of multiple-order differential arrays, that are optimal under various criteria, are discussed.

Generally, designs and applications of differential microphones are illustrated. Since transduction and transmission of acoustic waves are generally reciprocal processes the results are also applicable to loudspeakers. However, the loudspeaker implementation is difficult because of the large volume velocities required to approximate ideal differential microphones. The reasons are twofold: first, the source must be small compared to the acoustic wavelength; second, the real-part of the radiation impedance becomes very small for differential operation. Another additional factor that must be carefully accounted for in differential loudspeaker array design is the mutual radiation impedance between array elements.

2. DIFFERENTIAL MICROPHONE ARRAYS

The term *first-order* differential applies to any array whose sensitivity is proportional to the first spatial derivative of the acoustic pressure field. The term *nth-order* differential is used for arrays that have a response proportional to a linear combination of the spatial derivatives up to, and including *n*. The classification *superdirectional* is applied to an array whose directivity factor (to be defined later) is higher than that of an array of the same geometry with uniform amplitude weighting. The systems that are discussed in this chapter, respond to finite-differences of the acoustic pressure that closely approximate the pressure differentials for general order. Thus, the interelement spacing of the array microphones is much smaller than the acoustic wavelength and the arrays are therefore superdirectional. Typically, these arrays combine the outputs of closely-spaced microphones in an alternating sign fashion. These differential arrays are therefore also commonly referred to as *pattern-differencing* arrays.

Before we discuss the various implementations of *nth-order* finite-difference systems, we develop expressions for the *nth-order* spatial acoustic pressure derivative in a direction \mathbf{r} (the bold-type indicates a vector quantity). Since realizable differential arrays approximate the true acoustic pressure differentials, the equations for the general order differentials provide significant insight into the operation of these systems. To begin, we examine the case for a propagat-

ing acou
plane-v

where
transp
where.
 \mathbf{r} is the
the pos
taking
 \mathbf{r} yield

The pl
the m
square
Using
patter
of a d
octave
differ

The n

where
that f
fund
weig
in lat
appr
A
zero
tion
deriv
leng

ing acoustic plane-wave. The acoustic pressure field for a propagating acoustic plane-wave can be written as,

$$p(k, \mathbf{r}, t) = P_o e^{j(\omega t - \mathbf{k}^T \mathbf{r})} = P_o e^{j(\omega t - kr \cos \theta)}, \quad (10.1)$$

where P_o is the plane-wave amplitude, ω is the angular frequency, T is the transpose operator, \mathbf{k} is the acoustic wavevector ($\|\mathbf{k}\| = k = \omega/c = 2\pi/\lambda$ where λ is the acoustic wavelength), c is the speed of sound, and $r = \|\mathbf{r}\|$ where \mathbf{r} is the position vector relative to the selected origin, and θ is the angle between the position vector \mathbf{r} and the wavevector \mathbf{k} . Dropping the time dependence and taking the n^{th} -order spatial derivative along the direction of the position vector \mathbf{r} yields,

$$\frac{d^n}{dr^n} p(k, r) = P_o (-jk \cos \theta)^n e^{-jkr \cos \theta}. \quad (10.2)$$

The plane-wave solution is valid for the response to sources that are "far" from the microphone array. By "far" we mean distances that are many times the square of the relevant source dimension divided by the acoustic wavelength. Using (10.2) we can conclude that the n^{th} -order differential has a bidirectional pattern with the shape of $(\cos \theta)^n$. We can also see that the frequency response of a differential microphone is a high-pass system with a slope of $6n$ dB per octave. If we relax the far-field assumption and examine the response of the differential system to a point source located at the coordinate origin, then

$$p(k, r) = P_o \frac{e^{-j(kr \cos \theta)}}{r}. \quad (10.3)$$

The n^{th} -order spatial derivative in the direction r is

$$\frac{d^n}{dr^n} p(k, r, \theta) = P_o \frac{n!}{r^{n+1}} e^{-jkr \cos \theta} (-1)^n \sum_{m=0}^n \frac{(jkr \cos \theta)^m}{m!}, \quad (10.4)$$

where r is the distance to the source. The interesting thing to notice in (10.4) is that for $kr \cos \theta$ small, the microphone is independent of frequency. Another fundamental property is that the general n^{th} -order differential response is a weighted sum of bidirectional terms of the form $\cos^m \theta$. We use this property in later sections. First, though, we consider the effects of the finite-difference approximation of the spatial derivative.

After expanding the acoustic pressure field into a Taylor series, we must keep zero and first-order terms to express the first derivative. The resulting equation is nothing other than the finite-difference approximation to the first-order derivative. As long as the spacing is small compared to the acoustic wavelength, the higher-order terms (namely, the higher-order derivatives) become

insignificant over a desired frequency range. Likewise, the second and third-order derivatives can be incorporated by retaining the second and third-order terms in the expansion. The resulting approximation can be expressed as the exact spatial derivative multiplied by a bias error term. For the first-order case in a plane-wave acoustic field [(10.2)], the pressure derivative is

$$\frac{dp(k, r, \theta)}{dr} = -jkP_o \cos \theta e^{-jkr \cos \theta}. \quad (10.5)$$

The finite-difference approximation for the first-order system is defined as

$$\begin{aligned} \frac{\Delta p(k, r, \theta)}{\Delta r} &\equiv \frac{p(k, r + d/2, \theta) - p(k, r - d/2, \theta)}{d} \\ &= \frac{-j2P_o \sin(kd/2 \cos \theta) e^{-jkr \cos \theta}}{d}, \end{aligned} \quad (10.6)$$

where d the distance between the two microphones. If we now define the amplitude bias error ϵ_1 as

$$\epsilon_1 = \frac{\Delta p / \Delta r}{dp/dr}, \quad (10.7)$$

then on-axis ($\theta = 0$),

$$\epsilon_1 = \frac{\sin kd/2}{kd/2} = \frac{\sin \pi d/\lambda}{\pi d/\lambda}. \quad (10.8)$$

Figure 10.1 shows the amplitude bias error ϵ_1 between the true pressure differential and the approximation by the two closely-spaced omnidirectional (zero-order) microphones. The bias error is plotted as a nondimensional function of microphone spacing divided by the acoustic wavelength (d/λ). From Fig. 10.1, it can be seen that for less than 1 dB error, that the element spacing must be less than 1/4 of the acoustic wavelength. Similar equations can be written for higher-order arrays. The bias function for these systems is low-pass in nature if the frequency range is limited to the small kd range.

In general, to realize an array that is sensitive to the n^{th} derivative of the incident acoustic pressure field, we require m p^{th} -order microphones, where, $m + p - 1 = n$. For example, a first-order differential microphone requires two zero-order microphones. The linearized Euler's equation for an ideal (no viscosity) fluid states that

$$-\nabla p = \rho \frac{\partial \mathbf{v}}{\partial t}, \quad (10.9)$$

where ρ is the fluid density and \mathbf{v} is the acoustic particle velocity. The time derivative of the particle velocity is proportional to the pressure-gradient. For

Figure
the mi

an ax
the p
dipol
on b
ferer
parti
easy
der
whe
orde
F
elen

whe
fere
for
sma

As
nen

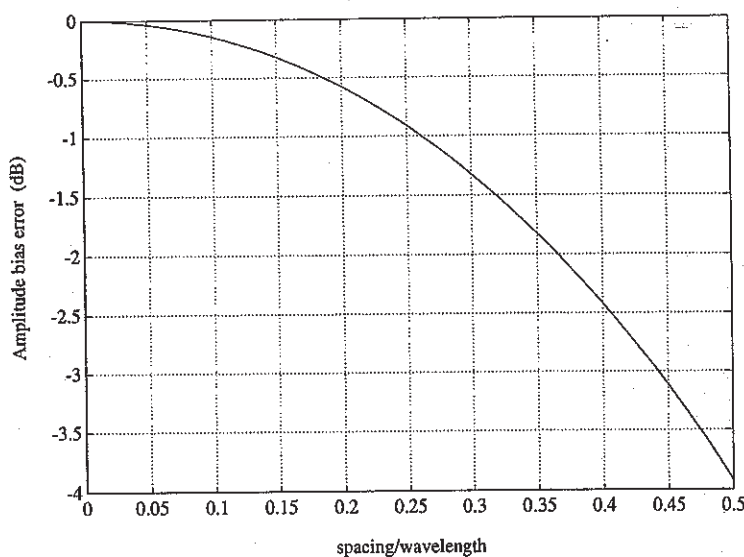


Figure 10.1 Finite-difference amplitude bias error in dB for a plane-wave propagating along the microphone axis, as a function of element spacing divided by the acoustic wavelength.

an axial component of a sinusoidal velocity vector, the output is proportional to the pressure differential along that axis. More typically, a first-order differential dipole microphone is designed as a diaphragm that is open to the sound field on both sides. The motion of the diaphragm is dependent on the net force difference (pressure-difference) across the diaphragm and is therefore an acoustic particle velocity microphone. Thus, by proper design of a microphone, it is easy to construct a first-order acoustic microphone. The design of higher order microphones can be formed by combinations of lower-order microphones where the sum of all of component microphone orders is equal to the desired order differential microphone.

For a plane-wave with amplitude P_o and wavenumber k incident on a two-element array, as shown in Fig. 10.2, the output can be written as

$$E_1(k, \theta) = P_o (1 - e^{-jkd \cos \theta}), \tag{10.10}$$

where d is the interelement spacing and the subscript indicates a first-order differential array. Note again that the explicit time dependence factor is neglected for the sake of compactness. If it is now assumed that the spacing is much smaller than the acoustic wavelength, we can write

$$E_1(k, \theta) \approx P_o kd \cos \theta. \tag{10.11}$$

As expected, the first-order array has the factor $\cos \theta$ that resolves the component of the acoustic particle velocity along the microphone axis.

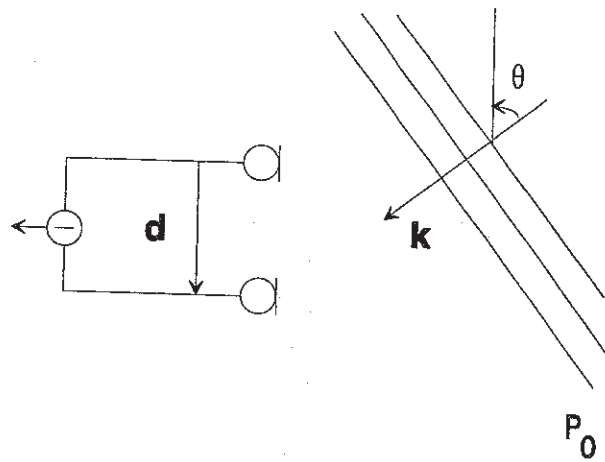


Figure 10.2 Diagram of first-order microphone composed of two zero-order (omnidirectional) microphones.

We now examine the case where a delay is introduced between these two zero-order microphones. For a plane-wave incident on this new array, we can write

$$E_1(\omega, \theta) = P_0 \left(1 - e^{-j\omega(\tau + d \cos \theta/c)} \right), \quad (10.12)$$

where τ is equal to the delay applied to the signal from one microphone and we have made the substitution $k = \omega/c$. If we again assume a small spacing ($kd \ll \pi$ and $\omega\tau \ll \pi$),

$$E_1(\omega, \theta) \approx P_0 \omega (\tau + d/c \cos \theta). \quad (10.13)$$

One thing to notice about (10.13), is that the first-order array has a first-order high-pass frequency dependence. The term in the parentheses in (10.13) contains the array directional response. In the design of differential arrays, the array directivity function is the quantity that is of interest. To simplify further analysis for the directivity of the first-order array, let us define a_0 , a_1 , and α_1 , such that

$$\alpha_1 = a_0 = \frac{\tau}{\tau + d/c} \quad (10.14)$$

and

$$1 - \alpha_1 = a_1 = \frac{d/c}{\tau + d/c}. \quad (10.15)$$

Then

$$a_0 + a_1 = 1. \quad (10.16)$$

Thus, the normalized directional response is

$$E_{N_1}(\theta) = a_0 + a_1 \cos \theta = \alpha_1 + (1 - \alpha_1) \cos \theta, \quad (10.17)$$

where the subscript N denotes the normalized response of a first-order system, i.e., $E_{N_1}(0) = 1$. The normalization of the array response has effectively factored out the term that defines the normalized directional response of the microphone array. The most interesting thing to notice in (10.17) is that the first-order differential array directivity function is *independent* of frequency within the region where the assumption of small spacing compared to the acoustic wavelength holds. Note that we have substituted the dependent variable α_1 which is itself a function of the variables d and τ .

The magnitude of (10.17) is the parametric expression for the "limaçon of Pascal" algebraic curve. The two terms in (10.17) can be seen to be the sum of a zero-order microphone (first-term) and a first-order microphone (second term), which is the general form of the first-order array. Early unidirectional microphones were actually constructed by summing the outputs of an omnidirectional pressure microphone and a velocity ribbon microphone (pressure-differential microphone) [12]. One implicit property of (10.17) is that for $0 \leq \alpha_1 \leq 1$ there is a maximum at $\theta = 0$ and a minimum at an angle between $\pi/2$ and π . For values of $\alpha_1 > 1/2$ the response has a minimum at 180° , although there is no zero in the response. An example of the response for this case is shown in Fig. 10.3(a). When $\alpha_1 = 1/2$, the parametric algebraic equation has a specific form which is called a cardioid. The cardioid pattern has a zero response at $\theta = 180^\circ$. For values of $\alpha_1 < 1/2$ there is no longer a minimum at $\theta = 180^\circ$, although there is a zero-response (null) at $90^\circ < \theta < 180^\circ$. Figure 10.3(b) shows a directivity response corresponding to this case. For the first-order system, the solitary null is located at

$$\theta_1 = \cos^{-1}\left(-\frac{a_0}{a_1}\right) = \cos^{-1}\left(\frac{-\alpha_1}{1 - \alpha_1}\right). \quad (10.18)$$

The directivities shown by Fig. 10.3 are actually a representation of a plane slice through the center line of the true three-dimensional directivity plot. The arrays discussed in this chapter are rotationally symmetric around their axes. Figure 10.4 shows a three-dimensional representation of the directivity pattern shown in Fig. 10.3(b).

The realization of a general first-order differential response is accomplished by adjusting the time delay between the two zero-order microphones that comprise the first-order system model. From (10.14) and (10.15), the value of τ determines the ratio of a_1/a_0 . The value of τ is proportional to d/c , the propagation time for an acoustic wave to axially travel between the zero-order

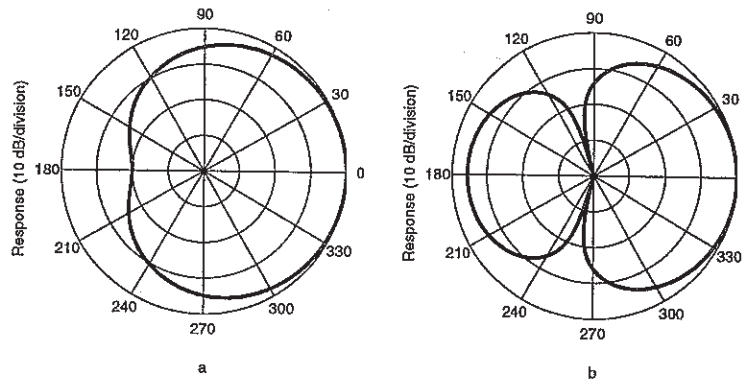


Figure 10.3 Directivity plots for first-order arrays (a) $\alpha_1 = 0.55$, (b) $\alpha_1 = 0.20$.

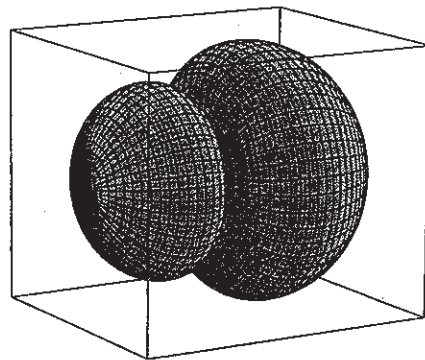


Figure 10.4 Three dimensional representation of directivity in Fig. 10.3(b). Note that the viewing angle is from the rear-half plane at an angle of approximately 225° . The viewing angle was chosen so that the rear-lobe of the array would not be obscured by the mainlobe.

microphones. This interelement propagation time is

$$\tau = \frac{d a_0}{c a_1} = \frac{d \alpha_1}{c(1 - \alpha_1)} \tag{10.19}$$

From (10.19) and (10.18), the pattern zero is at

$$\theta_1 = \cos^{-1} \left(-\frac{c \tau}{d} \right) \tag{10.20}$$

The n^{th} order array can be written as the sum of the n^{th} spatial derivative of the sound field plus lower-order terms. The n^{th} -order array can also be written as

Figure 10. third-order

the prod

where th
delays.
respons
represent
shows h
extensio
values c
and (10
If ag
imated

Equatic
done in
 $\alpha_i = \tau_i$

If the p
the res

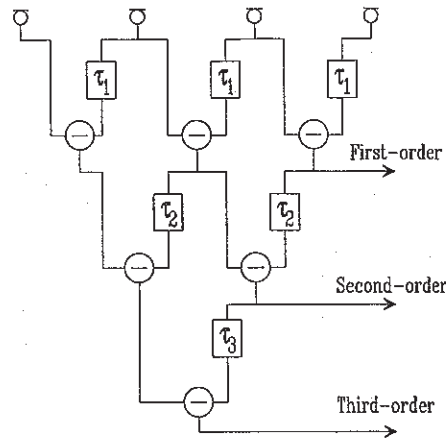


Figure 10.5 Construction of differential arrays as first-order differential combinations up to third-order.

the product of n first-order response terms as

$$E_n(\omega, \theta) = P_o \prod_{i=1}^n [1 - e^{-j\omega(\tau_i + d_i/c \cos \theta)}], \quad (10.21)$$

where the d_i relate to the microphone spacings, and the τ_i relate to chosen time delays. There is a design implementation advantage in expressing the array response in terms of the products of first-order terms since it is now simple to represent higher-order systems as cascaded systems of lower order. Figure 10.5 shows how a differential array can be constructed for orders up to three. The extension of the design technique to higher orders is straightforward. The values of τ_i can be determined by using the relationships developed in (10.14) and (10.19). The ordering of the τ_i is not important.

If again we assume that $kd_i \ll \pi$ and $\omega\tau_i \ll \pi$, then (10.21) can be approximated as

$$E_n(\omega, \theta) \approx P_o \omega^n \prod_{i=1}^n (\tau_i + d_i/c \cos \theta). \quad (10.22)$$

Equation (10.22) can be simplified by making the same substitution as was done in (10.14) and (10.15) for the arguments in the product term. If we set $\alpha_i = \tau_i/(\tau_i + d_i/c)$, then

$$E_n(\omega, \theta) \approx P_o \omega^n \prod_{i=1}^n [\alpha_i + (1 - \alpha_i) \cos \theta]. \quad (10.23)$$

If the product in (10.23) is expanded, a power series in $\cos \theta$ can be written for the response of the n^{th} -order array to an incident plane-wave with frequency ω .

The result is

$$E_n(\omega, \theta) = P_o A \omega^n (a_0 + a_1 \cos \theta + a_2 \cos^2 \theta + \dots + a_n \cos^n \theta), \quad (10.24)$$

where the constant A is an overall gain factor and we have suppressed the explicit dependence of the directivity function E on the variables d_i and τ_i for compactness. The only frequency dependent term in (10.24) is the term ω^n . The frequency response of an n^{th} -order differential array can therefore be easily compensated by a lowpass filter whose frequency response is proportional to ω^{-n} . By choosing the structure that places only a delay behind each element in a differential array, the coefficients in the power series in (10.24) are independent of frequency, resulting in an array whose beampattern is independent of frequency. To simplify the following exposition on the directional properties of differential arrays, we will assume that the amplitude factor can be neglected. Also, since the directional pattern described by the power series in $\cos \theta$ can have any general scaling, we will typically describe the normalized directional response as only a function of θ , such that

$$E_{N_n}(\theta) = a_0 + a_1 \cos \theta + a_2 \cos^2 \theta + \dots + a_n \cos^n \theta, \quad (10.25)$$

where the subscript N denotes a normalized response at $\theta = 0^\circ$ [as in (10.17)] which implies

$$\sum_{i=0}^n a_i = 1. \quad (10.26)$$

In general therefore, the n^{th} -order differential microphone has at most, n nulls (zeros). This follows directly from (10.25) and the fundamental theorem of algebra. Equation (10.25) can also be written in "canonic" form as the product of first-order terms

$$E_{N_n}(\theta) = \prod_{i=1}^n [\alpha_i + (1 - \alpha_i) \cos \theta]. \quad (10.27)$$

Note that we have dropped the frequency dependent variable ω in (10.25) and (10.27) since we have argued that the frequency response for small interelement spacing is simply proportional to ω^n . The terms a_i in (10.25) can take on any desired value by adjusting the delays used in defining the desired differential microphone array. For the second-order array

$$E_{N_2}(\theta) = a_0 + a_1 \cos \theta + a_2 \cos^2 \theta. \quad (10.28)$$

Equation (10.28) can also be factored into two first-order terms and written as

$$E_{N_2}(\theta) = [\alpha_1 + (1 - \alpha_1) \cos \theta][\alpha_2 + (1 - \alpha_2) \cos \theta], \quad (10.29)$$

where

or

As shown in order, values $0 \leq \theta \leq \pi$ appear nulls in angles

where result value that thing into t can b Since cause term order front micr dipo. It For a third

where

$$\begin{aligned} a_0 &= \alpha_1 \alpha_2 \\ a_1 &= \alpha_1(1 - \alpha_2) + \alpha_2(1 - \alpha_1) \\ a_2 &= (1 - \alpha_1)(1 - \alpha_2), \end{aligned} \tag{10.30}$$

or

$$\begin{aligned} \alpha_1 &= a_0 + a_1/2 \pm \sqrt{(a_0 + a_1/2)^2 - a_0} \\ \alpha_2 &= a_0 + a_1/2 \mp \sqrt{(a_0 + a_1/2)^2 - a_0}. \end{aligned} \tag{10.31}$$

As shown, the general form of the second-order system is the sum of second-order, first-order and zero-order terms. If certain constraints are placed on the values of a_0 and a_1 , it can be seen that there are two nulls (zeros) in the interval $0 \leq \theta < \pi$. The array response pattern is symmetric about $\theta = 0$. The appearance of four nulls in the interval $2\pi \leq \theta < 0$ are actually the same two nulls in the interval $0 \leq \theta < \pi$. These zeros can be explicitly found at the angles θ_1 and θ_2 :

$$\theta_1 = \cos^{-1} \left(\frac{-\alpha_1}{1 - \alpha_1} \right), \tag{10.32}$$

$$\theta_2 = \cos^{-1} \left(\frac{-\alpha_2}{1 - \alpha_2} \right), \tag{10.33}$$

where now α_1 and α_2 can take on either positive or negative values. If the resulting beampattern is constrained to have a maximum at $\theta = 0^\circ$, then the values of α_1 and α_2 can only take on certain values; we have ruled out designs that have a higher sensitivity at any angle other than $\theta = 0^\circ$. The interesting thing to note is that negative values of α_1 or α_2 correspond to a null moving into the front half-plane. Negative values of α_1 for the first-order microphone can be shown to have a rear-lobe sensitivity that exceeds the sensitivity at 0° . Since (10.29) is the product of two first-order terms, emphasis of the rear-lobe, caused by a negative value of α_2 , can be counteracted by the zero from the term containing α_1 . As a result, a beam-pattern can be found for the second-order microphone that has maximum sensitivity at $\theta = 0^\circ$ and a null in the front-half plane. This result also implies that the beamwidth of a second-order microphone with a negative value of α_2 is narrower than that of the second-order dipole.

It is straightforward to extend the previous results to the third-order case. For completeness, the equation governing the directional characteristics for the third-order array is

$$E_{N_3}(\theta) = a_0 + a_1 \cos \theta + a_2 \cos^2 \theta + a_3 \cos^3 \theta. \tag{10.34}$$

If certain constraints are placed on the coefficients in (10.34), it can be factored into three real roots:

$$E_{N_3}(\theta) = [\alpha_1 + (1 - \alpha_1) \cos \theta][\alpha_2 + (1 - \alpha_2) \cos \theta][\alpha_3 + (1 - \alpha_3) \cos \theta]. \quad (10.35)$$

The third-order microphone has the possibility of three zeros that can be placed at desired locations in the directivity pattern. Solving this cubic equation yields expressions for α_1 , α_2 , and α_3 in terms of a_0 , a_1 , a_2 , and a_3 . However, these expressions are long and algebraically cumbersome and, as such, not repeated here.

3. ARRAY DIRECTIONAL GAIN

In order to "best" reject the noise in an acoustic field, we need to optimize the way we combine multiple microphones. Specifically we need to consider the directional gain, i.e. the gain of the microphone array in a noise field over that of a simple omnidirectional microphone. A common quantity used is the Directivity Factor Q , or equivalently, the Directivity Index DI [$10 \log_{10}(Q)$].

The directivity factor is defined as

$$Q(\omega, \theta_0, \phi_0) = \frac{|E(\omega, \theta_0, \phi_0)|^2}{\frac{1}{4\pi} \int_0^{2\pi} \int_0^\pi |E(\omega, \theta, \phi)|^2 u(\omega, \theta, \phi) \sin \theta d\theta d\phi}, \quad (10.36)$$

where the angles θ and ϕ are the standard spherical coordinate angles, θ_0 and ϕ_0 are the angles at which the directivity factor is being measured, $E(\omega, \theta, \phi)$ is the pressure response of the array, and $u(\omega, \theta, \phi)$ is the distribution of the noise power. The function u is normalized such that

$$\frac{1}{4\pi} \int_0^{2\pi} \int_0^\pi u(\omega, \theta, \phi) \sin \theta d\theta d\phi = 1. \quad (10.37)$$

The directivity factor Q can be written as the ratio of two Hermitian quadratic forms [3] as

$$Q = \frac{\mathbf{w}^H \mathbf{A} \mathbf{w}}{\mathbf{w}^H \mathbf{B} \mathbf{w}}, \quad (10.38)$$

where

$$\mathbf{A} = \mathbf{S}_0 \mathbf{S}_0^H, \quad (10.39)$$

\mathbf{w} is the complex weighting applied to the microphones and \mathcal{H} is the complex conjugate transpose. The elements of the matrix \mathbf{B} are defined as

$$b_{mn} = \frac{1}{4\pi} \int_0^{2\pi} \int_0^\pi u(\omega, \theta, \phi) \exp [j\mathbf{k} \cdot (\mathbf{r}_m - \mathbf{r}_n)] \sin \theta d\phi d\theta, \quad (10.40)$$

and the elements of the vector \mathbf{S}_0 are defined as

$$s_{0n} = \exp(j\mathbf{k}_0 \cdot \mathbf{r}_n). \quad (10.41)$$

Note that for clarity we have left off the explicit functional dependencies of the above equations on the angular frequency ω . The solution for the maximum of Q , which is a Rayleigh quotient, is obtained by finding the maximum generalized eigenvector of the homogeneous equation

$$\mathbf{A}\mathbf{w} = \lambda_M \mathbf{B}\mathbf{w}. \quad (10.42)$$

The maximum eigenvalue of (10.42) is given by

$$\lambda_M = \mathbf{S}_0^H \mathbf{B}^{-1} \mathbf{S}_0. \quad (10.43)$$

The corresponding eigenvector contains the weights for combining the elements to obtain the maximum directional gain

$$\mathbf{w}_{opt} = \mathbf{B}^{-1} \mathbf{S}_0. \quad (10.44)$$

In general, the optimal weights \mathbf{w}_{opt} are a function of frequency, array geometry, element directivity and the spatial distribution of the noise field.

4. OPTIMAL ARRAYS FOR SPHERICALLY ISOTROPIC FIELDS

Acoustic reverberation in rooms has historically been modeled as spherically isotropic noise. A spherically isotropic noise field can be constructed by combining uncorrelated noises propagating in all directions with equal power. In room acoustics this noise field is referred to as a "diffuse" sound field and has been the model used for many investigations into the distribution of reverberant sound pressure fields. Since it is of interest to design microphone systems that optimally reject reverberant sound fields, the first optimization of array gain will assume a "diffuse" sound field.

4.1 MAXIMUM GAIN FOR OMNIDIRECTIONAL MICROPHONES

The literature on the maximization of the directional gain for an arbitrary array is quite extensive [17, 18, 13, 4, 16, 8]. Uzkov [17] showed that for uniformly spaced omnidirectional microphones that the directional gain reaches N^2 as the spacing between the elements goes to zero. The maximum value of directional gain is obtained when the array is steered to end-fire. Weston [18] has shown the same result by an alternative method. Parsons [13] has extended the proof to include nonuniformly spaced arrays that are much smaller than

the acoustic wavelength. The proof given here also relies on the assumption that the elements are closely-spaced compared to the acoustic wavelength. The approach taken here is similar to that of Chu [4], Tai [16], and Harrington [8], who expanded the radiated/received field in terms of spherical wave functions. Chu did not look explicitly at the limiting case. Harrington did examine the limiting case of vanishing spacing, but his analysis involved approximations that are not necessary in the following analysis.

For a spherically isotropic field and omnidirectional microphones,

$$u(\omega, \theta, \phi) = 1. \quad (10.45)$$

In general, the directivity of N closely-spaced microphones can be expanded in terms of spherical wave functions. Now let us express the farfield pressure response $E(\theta, \phi)$ as a summation of orthogonal polynomials,

$$E(\theta, \phi) = \sum_{n=0}^{N-1} \sum_{m=0}^n h_{nm} P_n^m[\cos(\theta - \theta_z)] \cos m(\phi - \phi_z), \quad (10.46)$$

where we have limited the sum to be equal to the number of degrees of freedom in the N -element microphone case, where the P_n^m are the associated Legendre functions, and θ_z and ϕ_z are possible rotations of the coordinate system. Now define

$$G_{nm}(\theta, \phi) = P_n^m[\cos(\theta - \theta_z)] \cos m(\phi - \phi_z). \quad (10.47)$$

The normalization of the function G_{nm} is

$$\begin{aligned} N_{nm} &= \int_0^{2\pi} \cos^2 m\phi \int_{-1}^1 [P_n^m(\eta)]^2 d\eta d\phi, \\ &= \frac{4\pi(n+m)!}{\varepsilon_m(2n+1)(n-m)!}, \end{aligned} \quad (10.48)$$

where ε_m is the Neumann factor, which equals 1 for $m = 0$ and 2 for $m \geq 1$. By using the orthogonal Legendre function expansion, we can write

$$Q(\theta_o, \phi_o) = \frac{\left[\sum_{n=0}^{N-1} \sum_{m=0}^n h_{nm} G_{nm}(\theta_o, \phi_o) \right]^2}{\frac{1}{4\pi} \sum_{n=0}^{N-1} \sum_{m=0}^n h_{nm}^2 N_{nm}}. \quad (10.49)$$

To find the maximum of (10.49), we set the derivative of Q with respect to h_{nm} for all n and m to zero. The resulting maximum occurs when

$$\begin{aligned}
 Q_{max} &= \sum_{n=0}^{N-1} \sum_{m=0}^n \frac{[G_{nm}(\theta_o, \phi_o)]^2}{\frac{1}{4\pi} N_{nm}} \\
 &= \sum_{n=0}^{N-1} \sum_{m=0}^n \frac{[P_n^m(\cos(\theta_o - \theta_z)) \cos m(\phi_o - \phi_z)]^2}{\frac{1}{4\pi} N_{nm}} \\
 &\leq \sum_{n=0}^{N-1} \sum_{m=0}^n \frac{[P_n^m(\cos(\theta_o - \theta_z))]^2}{\frac{1}{4\pi} N_{nm}}.
 \end{aligned}
 \tag{10.50}$$

The inequality in (10.50) infers that the maximum must occur when $\phi_o = \phi_z$. From the addition theorem of Legendre polynomials,

$$P_n(\cos \psi) = \sum_{m=0}^n \varepsilon_m \frac{(n-m)!}{(n+m)!} P_n^m(\cos \theta_o) P_n^m(\cos \theta_z) \cos(m(\phi_o - \phi_z)),
 \tag{10.51}$$

where ψ is the angle subtended by two points on a sphere and is expressed in terms of spherical coordinates as

$$\cos \psi = \cos \theta_o \cos \theta_z + \sin \theta_o \sin \theta_z \cos(\phi_o - \phi_z).
 \tag{10.52}$$

Equation (10.51) maximizes for all n , when $\psi = 0$. Therefore (10.50) maximizes when $\theta_o = \theta_z$. Since

$$P_n^m(1) = \begin{cases} 1 & m = 0 \\ 0 & \text{if } m > 0 \end{cases}
 \tag{10.53}$$

(10.50) can be reduced to

$$\begin{aligned}
 Q_{max} &= \sum_{n=0}^{N-1} (2n+1), \\
 &= N^2.
 \end{aligned}
 \tag{10.54}$$

Thus, the maximum directivity factor Q for N closely-spaced omnidirectional microphones is N^2 .

4.2 MAXIMUM DIRECTIVITY INDEX FOR DIFFERENTIAL MICROPHONES

As was shown in Section 2, there are an infinite number of possibilities for differential array designs. What we are interested in are the special cases that

are optimal in some respect. For microphones that are axisymmetric, as is the case for all of the microphones that are covered, (10.36) can be written in a simpler form:

$$Q(\omega) = \frac{2}{\int_0^\pi |E_N(\omega, \theta, \phi)|^2 \sin \theta d\theta}, \quad (10.55)$$

where it has also been assumed that the directions θ_0, ϕ_0 are in the direction of maximum sensitivity and that the array sensitivity function is normalized: $|E_N(\omega, \theta_0, \phi_0)| = 1$. If we now insert the formula from (10.25) and carry out the integration, we find the directivity factor

$$Q(a_0, \dots, a_n) = \left[\sum_{i=0}^n \sum_{\substack{j=0 \\ i+j \text{ even}}}^n \frac{a_i a_j}{1+i+j} \right]^{-1}. \quad (10.56)$$

The directivity factor for a general n^{th} -order differential array (no normalization assumption) can be written as

$$Q(a_0, \dots, a_n) = \left[\sum_{i=0}^n a_i \right]^2 \left[\sum_{i=0}^n \sum_{\substack{j=0 \\ i+j \text{ even}}}^n \frac{a_i a_j}{1+i+j} \right]^{-1} = \frac{\mathbf{a}^T \mathbf{B} \mathbf{a}}{\mathbf{a}^T \mathbf{H} \mathbf{a}}, \quad (10.57)$$

where \mathbf{H} is a Hankel matrix given by

$$H_{i,j} = \begin{cases} \frac{1}{1+i+j} & \text{if } i+j \text{ even} \\ 0 & \text{otherwise} \end{cases}$$

where

$$\mathbf{a}^T = \{a_0, a_1, \dots, a_n\} \quad (10.58)$$

and

$$\mathbf{B} = \mathbf{b} \mathbf{b}^T, \quad (10.59)$$

where

$$\mathbf{b}^T = \{ \overbrace{1, 1, \dots, 1}^{n+1} \}. \quad (10.60)$$

Table 10.1 Table of maximum array gain Q , and corresponding eigenvector for differential arrays from first to fourth-order for spherically isotropic noise fields.

microphone order	maximum eigenvalue	corresponding eigenvector
1	4	[1/4 3/4]
2	9	[-1/6 1/3 5/6]
3	16	[-3/32 -15/32 15/32 35/32]
4	25	[0.075 -0.300 -1.050 0.700 1.575]

From (10.57) we can see that the directivity factor Q is a Rayleigh quotient for two hermitian forms. The maximum of the Rayleigh quotient is reached at a value equal to the largest generalized eigenvalue of the equivalent generalized eigenvalue problem,

$$\mathbf{B}\mathbf{x} = \lambda\mathbf{H}\mathbf{x} \tag{10.61}$$

where, λ is the general eigenvalue and \mathbf{x} is the corresponding general eigenvector. The eigenvector corresponding to the largest eigenvalue will contain the coefficients a_i which maximize the directivity factor Q . Since \mathbf{B} equals a dyadic product there is only one eigenvector $\mathbf{x} = \mathbf{H}^{-1}\mathbf{b}$ with the eigenvalue $\mathbf{b}^T\mathbf{H}^{-1}\mathbf{b}$. Thus,

$$\max_a Q = \lambda_m = \mathbf{b}^T\mathbf{H}^{-1}\mathbf{b}. \tag{10.62}$$

Table 10.1 gives the maximum array gain (largest eigenvalue), Q , for differential orders up to fourth-order. Note that the largest eigenvector has been scaled such that the microphone output is unity at $\theta = 0^\circ$. The directivity index is a considerably useful measure in quantifying the directional properties of microphones and loudspeakers. The directivity index provides a rough estimate of the relative gain in signal-to-reverberation for a directional microphone in a reverberant environment. However, the directivity index is meaningless with respect to the performance of directional microphones in non-diffuse fields. A more detailed discussion on the relevance of the microphone directivity index with respect to room acoustics is given in Appendix A.

4.3 MAXIMUM FRONT-TO-BACK RATIO

Another possible measure of the "merit" of an array is the front-to-back rejection ratio, i.e., the gain of the microphone for signals propagating to the

front of the microphone relative to signals propagating to the rear. One such quantity was suggested by Marshall and Harry [11] which will be referred to here as " F ," for the front-to-back ratio. The ratio F is defined as

$$F(\omega) = \frac{\int_0^{2\pi} \int_0^{\pi/2} |E(\omega, \theta, \phi)|^2 \sin \theta d\theta d\phi}{\int_0^{2\pi} \int_{\pi/2}^{\pi} |E(\omega, \theta, \phi)|^2 \sin \theta d\theta d\phi}, \quad (10.63)$$

where the angles θ and ϕ are the spherical coordinate angles and $E(\omega, \theta, \phi)$ is the far-field pressure response. For axisymmetric microphones (10.63) can be written in a simpler form by uniform integration over ϕ ,

$$F(\omega) = \frac{\int_0^{\pi/2} |E_N(\omega, \theta, \phi)|^2 \sin \theta d\theta}{\int_{\pi/2}^{\pi} |E_N(\omega, \theta, \phi)|^2 \sin \theta d\theta}. \quad (10.64)$$

Carrying out the integration of (10.64) and using the form of (10.25) yields,

$$F(a_0, \dots, a_n) = \left[\sum_{i=0}^n \sum_{j=0}^n \frac{a_i a_j}{1+i+j} \right] \left[\sum_{i=0}^n \sum_{j=0}^n \frac{a_i a_j (-1)^{i+j}}{1+i+j} \right]^{-1}. \quad (10.65)$$

The supercardioid name is given to the differential system that has the maximum front-to-rear power ratio. In equation form, the front-to-rear power ratio can be written as

$$\begin{aligned} F(a_0, \dots, a_n) &= \left[\sum_{i=0}^n \sum_{j=0}^n \frac{a_i a_j}{1+i+j} \right] \left[\sum_{i=0}^n \sum_{j=0}^n \frac{(-1)^{i+j} a_i a_j}{1+i+j} \right]^{-1} \\ &= \frac{\mathbf{a}^T \mathbf{B} \mathbf{a}}{\mathbf{a}^T \mathbf{H} \mathbf{a}}, \end{aligned} \quad (10.66)$$

where \mathbf{H} is a Hankel matrix given by

$$H_{i,j} = \frac{(-1)^{i+j}}{1+i+j} \quad (10.67)$$

and

$$\mathbf{a}^T = \{a_0, a_1, \dots, a_n\}. \quad (10.68)$$

\mathbf{B} is a special form of a Hankel matrix designated as a Hilbert matrix and is given by

$$B_{i,j} = \frac{1}{1+i+j}. \quad (10.69)$$

Table 10.2 Table of maximum F ratio and corresponding eigenvector for differential arrays from first to fourth-order for spherically isotropic noise fields.

microphone order	maximum eigenvalue	corresponding eigenvector
1	$7+4\sqrt{3}$	$[\frac{1}{1+\sqrt{3}} \frac{1}{1+\sqrt{3}}]$
2	$127+48\sqrt{7}$	$[\frac{1}{2(3+\sqrt{7})} \frac{\sqrt{7}}{3+\sqrt{7}} \frac{5}{2(3+\sqrt{7})}]$
3	≈ 5875	$\approx [0.0184 \ 0.2004 \ 0.4750 \ 0.3061]$
4	≈ 151695	$[0.0036 \ 0.0670 \ 0.2870 \ 0.4318 \ 0.2107]$

From (10.66) we can see that, as was the case for the maximum directional gain, the front-to-back ratio can be represented as Rayleigh quotient of two hermitian forms. The maximum of the Rayleigh quotient is reached at a value equal to the largest eigenvalue of the equivalent generalized eigenvalue problem,

$$\mathbf{B}\mathbf{x} = \lambda\mathbf{H}\mathbf{x} \tag{10.70}$$

where λ is the eigenvalue and \mathbf{x} is the corresponding eigenvector. Thus, as in the case of maximizing the directional gain Q , the maximization of the front-to-back ratio is a general eigenvalue problem with F as the largest eigenvalue. The matrices \mathbf{H} and \mathbf{B} are real Hankel matrices and are positive definite. The resulting eigenvalues are therefore positive real numbers and the eigenvectors are real. Table 10.2 summarizes the results for the maximum front-to-back ratios for differential arrays up to fourth-order.

As with the directivity index, the front-to-back ratio is a very useful measure in quantifying the directional properties of electroacoustic transducers.

The utility of the front-to-back ratio F measure in teleconferencing is clear if we consider the following scenario. In a typical teleconference, people sit along one side of a table facing a video screen that is generally acoustically reflective. The rear and sides of the room are usually absorptive. Maximizing the front-to-back rejection ratio will therefore minimize reflections from the front wall and video screen, as well as minimize the response to a wide distribution of loudspeakers used for transmitting the remote site audio to the room. The above example is somewhat contrived and the actual optimal microphone array will depend on the source and receiver locations and the room acoustics. For the particular case above, however, the ratio F yields a better measure of microphone performance than the directivity index.

4.4 MINIMUM PEAK DIRECTIONAL RESPONSE

Another approach that might be of interest, is to design differential arrays to have an absolute maximum sidelobe response. This specification would allow the designer to guarantee that the differential array response would not exceed a defined level, over a given angular range, where suppression of acoustic signals is desired.

The first suggestion of an equi-sidelobe *differential* array design was in a "comment" publication by V. I. Korenbaum [9], who only discussed a restricted class of n^{th} -order microphones that have the following form:

$$E_{N_n}(\theta) = [\alpha_1 + (1 - \alpha_1) \cos \theta] \cos^{n-1} \theta. \quad (10.71)$$

The restricted class defined by (10.71) essentially assumes that an n^{th} -order differential microphone is the combination of an $(n - 1)^{\text{th}}$ -order dipole pattern and a general first-order pattern. The major reason for considering this restricted class is obvious; the algebra becomes very simple. Since we are dealing with systems of order less than or equal to three, we do not need to restrict ourselves to the class defined by (10.71).

A more general design of equi-sidelobe differential arrays can be obtained by using standard Dolph-Chebyshev design techniques [6]. With this method we can easily realize any order differential microphone that we desire. The roots of the Dolph-Chebyshev system are easily obtained. Knowledge of the roots simplifies formulation of the canonic equations that describe the n^{th} order microphones as products of first-order differential elements.

We begin our analysis with the Chebyshev polynomials

$$T_n(x) = \begin{cases} \cos(n \cos^{-1} x), & -1 < x < 1 \\ \cosh(n \cosh^{-1} x), & 1 \leq |x| \end{cases} \quad (10.72)$$

The Chebyshev polynomial of order n has n real roots for arguments between -1 and 1 , and grows proportional to x^n for arguments with a magnitude greater than 1 . The design of the n^{th} -order Chebyshev array requires a transformation of the variable x in (10.72). If we substitute $x = b + a \cos \theta$ in (10.72), then we can form a desired n^{th} -order directional response that follows the Chebyshev polynomial over any range. At $\theta = 0^\circ$, $x = x_o \equiv a + b$, and the value of the Chebyshev polynomial is $T_n(x_o) \geq 1$. Setting this value to the desired mainlobe to sidelobe ratio, say S , we have

$$S = T_n(x_o) = \cosh(n \cosh^{-1} x_o). \quad (10.73)$$

Equivalently,

$$x_o = a + b = \cosh\left(\frac{1}{n} \cosh^{-1} S\right). \quad (10.74)$$

The sidelobe at $\theta = 180^\circ$ corresponds to $x = b - a = -1$. Therefore

$$\begin{aligned} a &= \frac{x_o + 1}{2} \\ b &= \frac{x_o - 1}{2}. \end{aligned} \tag{10.75}$$

Since the zeros of the Chebyshev polynomial are readily calculable, the null locations are easily found. From the definition of the Chebyshev polynomial given in (10.72), the zeros occur at

$$x_m = \cos \left[\frac{(2m - 1)\pi}{2n} \right], \quad m = 1, \dots, n. \tag{10.76}$$

The nulls are therefore at angles

$$\theta_m = \cos^{-1} \left(\frac{2x_m - x_o + 1}{x_o + 1} \right). \tag{10.77}$$

4.5 BEAMWIDTH

Another useful measure of the array performance is the beamwidth. The beamwidth can be defined in many ways. It can refer to the angle enclosed between the zeros of a directional response, the 3 dB points, or the 6 dB points. We will use the 3 dB beamwidth definition in this chapter. For the first-order microphone response [(10.17)], the 3 dB beamwidth is simply

$$\theta_{B_1} = 2 \cos^{-1} \left(\frac{-2a_0 + \sqrt{2}(a_0 + a_1)}{2a_1} \right). \tag{10.78}$$

For the second-order system, the algebra is somewhat more difficult but still straightforward. The result from (10.28) is

$$\theta_{B_2} = 2 \cos^{-1} \left(\frac{-a_1 + \sqrt{a_1^2 + 2\sqrt{2}[a_2^2 + a_1a_2 + (1 - \sqrt{2})a_0a_2]}}{2a_2} \right), \tag{10.79}$$

where it is assumed that $a_2 \neq 0$. If $a_2 = 0$, the microphone degenerates into a first order array and the beamwidth can be calculated by (10.78).

Similarly, the beamwidth for a third-order array can be found although the algebraic form is extremely lengthy and, as such, has not been included here.

5. DESIGN EXAMPLES

For differential microphones with interelement spacing much less than the acoustic wavelength, the maximum directivity index is attained when all of the

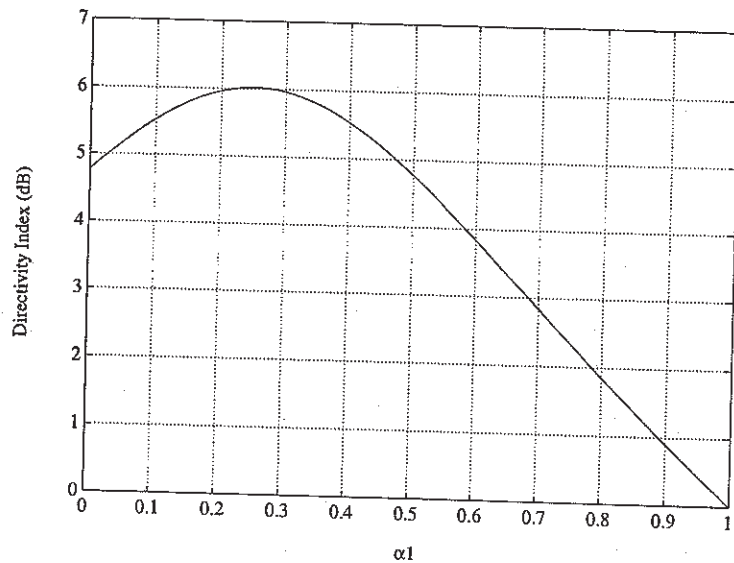


Figure 10.6 Directivity index of first-order microphone versus the first-order differential parameter α_1 .

microphones are situated collinearly. For this case, the maximum directivity index is $20 \log_{10}(n + 1)$ where n is the order of the microphone [13]. For first, second, and third-order microphones, the maximum directivity indices are, 6.0, 9.5, and 12.0 dB respectively. Derivations of the specific results for $n \leq 3$ are given in the following sections.

As indicated in (10.25), there are an infinite number of possible designs for n^{th} -order differential arrays. Presently, the most common first-order microphones are: dipole, cardioid, hypercardioid, and supercardioid. The extension to higher orders is straightforward and is developed in later sections. Most of the arrays that are described in this chapter have directional characteristics that are optimal in some way; namely, the arrays are optimal with respect to one of the performance measures previously discussed: directivity index, front-to-back ratio, sidelobe threshold, and beamwidth. A summary of the results for first, second, and third-order microphones is given in Table 10.3.

5.1 FIRST-ORDER DESIGNS

Before we discuss actual first-order differential designs, we first examine the effects of the parameter α_1 on the directivity index DI , the front-to-back ratio F , and the beamwidth of the microphone. We have defined $\alpha_1 = a_0$ and $a_1 = 1 - \alpha_1$. Figure 10.6 shows the directivity index of a first-order system for values of α_1 between 0 and 1.

Table 10.3 Table of first-order differential, second-order differential, and third-order differential designs.

microphone type	DI (dB)	F (dB)	3dB Beamwidth	Null(s) (degrees)
First-order designs				
dipole	4.8	0.0	90°	90
cardioid	4.8	8.5	131°	180
hypercardioid	6.0	8.5	105°	109
supercardioid	5.7	11.4	115°	125
Second-order designs				
dipole	7.0	0.0	65°	90
cardioid	7.0	14.9	94°	180
OSW cardioid	8.8	14.9	76°	90, 180
hypercardioid	9.5	8.5	66°	73, 134
supercardioid	8.3	24.0	80°	104, 144
Korenbaum	8.9	17.6	76°	90, 146
-15 dB sidelobe	9.4	10.7	70°	78, 142
-30 dB sidelobe	8.1	18.5	84°	109, 152
min. rear peak	8.5	22.4	80°	98, 149
Third-order designs				
dipole	8.5	0.0	54°	90
cardioid	8.5	21.0	78°	180
OSW cardioid	10.7	18.5	60°	90, 180
hypercardioid	12.0	11.2	48°	55, 100, 145
supercardioid	9.9	37.7	66°	97, 122, 153
-20 dB sidelobe	11.8	14.8	52°	62, 102, 153
-30 dB sidelobe	10.8	25.2	60°	79, 111, 156

ential pa-

ectivity
for first,
are, 6.0,
≤ 3 are

igns for
micro-
tension
Most of
ics that
to one
ront-to-
ults for

xamine
o-back
a₀ and
tem for

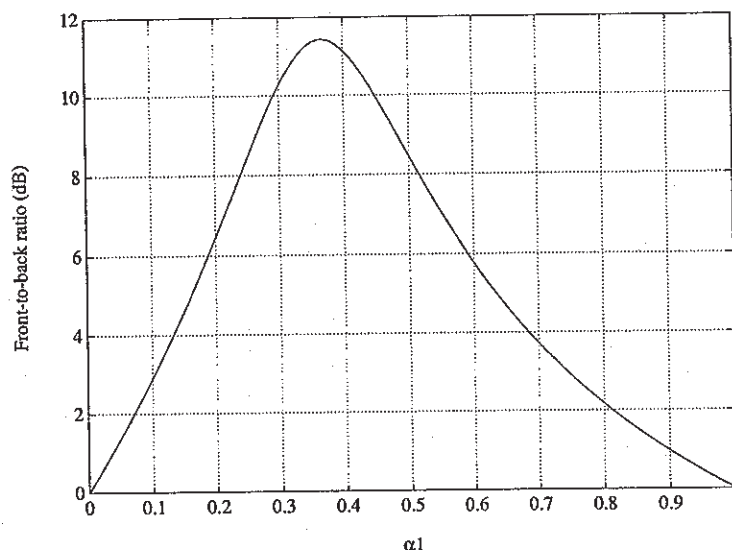


Figure 10.7 Front-to-back ratio of first-order microphone versus the first-order differential parameter α_1 .

The first-order differential microphone that corresponds to the maximum in Fig. 10.6 is given the name *hypercardioid*. When $\alpha_1 = 0$, the first-order differential system is a dipole. At $\alpha_1 = 1$, the microphone is an omnidirectional microphone with 0 dB directivity index. Figure 10.7 shows the dependence of the front-to-back ratio F on α_1 .

The maximum F value corresponds to the *supercardioid* design. Figure 10.8 shows the 3 dB beamwidth of the first-order differential microphone as a function of α_1 .

When $\alpha_1 \approx 0.7$, the 3 dB down point is approximately at 180° . Higher values of α_1 correspond to designs that are increasingly omnidirectional. Figure 10.8 indicates that the first-order differential microphone with the smallest beamwidth is the dipole microphone with a 3 dB beamwidth of 90° .

5.1.1 Dipole. The dipole microphone is basically an acoustic particle-velocity microphone. The construction was described earlier; the dipole is normally a diaphragm that is open on both sides to the acoustic field. In (10.17), the dipole microphone corresponds the simple case where $a_0 = 0$, $a_1 = 1$,

$$E_{D_1}(\theta) = \cos \theta. \quad (10.80)$$

In Fig. 10.9(a), a polar plot of the magnitude of (10.80) shows the classic cosine pattern for the microphone.

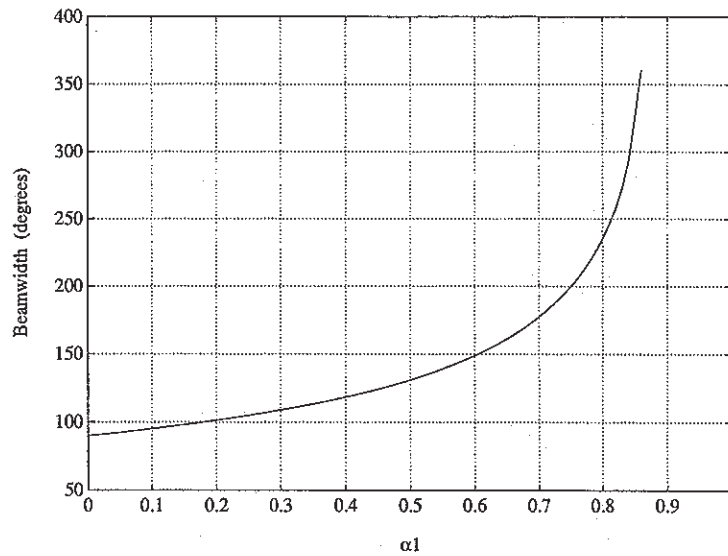


Figure 10.8 3 dB beamwidth of first-order microphone versus the first-order differential parameter α_1 .

The fact that the output phase reverses in either direction is of no concern to us here. The directivity index is 4.8 dB and the 3 dB beamwidth for the dipole microphone is 90° . The zero in the response is at $\theta = 90^\circ$. One potential problem, however, is that it is bidirectional; in other words, the pattern is symmetric about the axis tangential to the diaphragm or normal to the two zero-order microphone axis. As a result the front-to-back ratio is equal to 0 dB.

5.1.2 Cardioid. As shown earlier, all first-order patterns correspond to the "limaçon of Pascal" algebraic form. The special case of $\alpha_1 = 1/2$ is the cardioid pattern. The pattern is described by

$$E_{C_1}(\theta) = \frac{1 + \cos \theta}{2} \tag{10.81}$$

which is plotted in Fig. 10.9(b). Although the cardioid microphone is not optimal in directional gain or front-to-back ratio, it is the most commonly manufactured differential microphone. The cardioid directivity index is 4.8 dB, the same as that of the dipole microphone and the 3 dB beamwidth is 131° . The zero in the response is located at $\theta = 180^\circ$. The front-to-back ratio is 8.5 dB.

5.1.3 Hypercardioid. The hypercardioid microphone has the distinction of having the highest directivity index of any first-order microphone. The

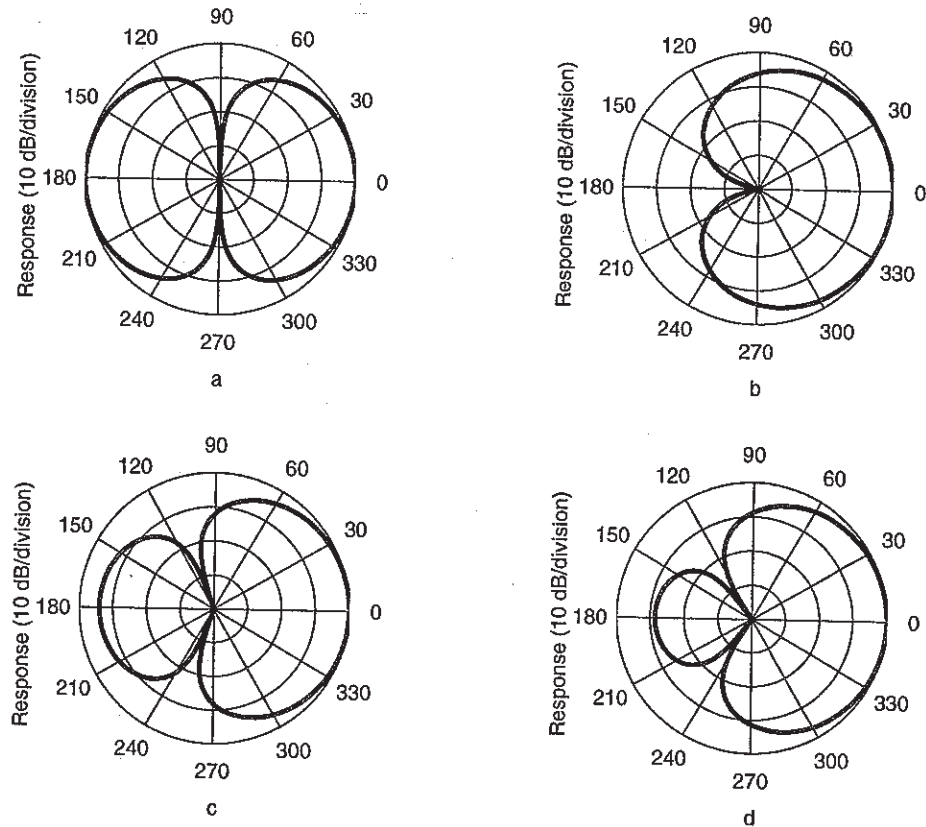


Figure 10.9 Various first-order directional responses, (a) dipole, (b) cardioid, (c) hypercardioid, (d) supercardioid.

derivation, which has apparently not been presented in the literature, is not difficult and was included in Section 4.2. The hypercardioid response can be written as

$$E_{HC_1}(\theta) = \frac{1 + 3 \cos \theta}{4}. \quad (10.82)$$

Figure 10.9(c) is a polar plot of the absolute value of (10.82). The 3 dB beamwidth is equal to 105° and the zero is at 109° . The directivity index is 6 dB or $10 \log_{10}(4)$, the maximum directivity index for a first-order system. The front-to-back ratio is equal to 8.5 dB.

5.1.4 Supercardioid. The name *supercardioid* is commonly used for the first-order differential design which maximizes the front-to-back received power; the term was probably coined by Shure engineers in the early 1940's, although the author could not find direct evidence of this. The first reference to the supercardioid design appears in a 1941 paper by Marshall and Harry [11].

The supercardioid is of interest since of all first-order designs it has the highest front-to-back power rejection for isotropic noise. The derivation of this result is contained in Section 4.3. The directional response can be written as

$$E_{SC_1}(\theta) = \frac{\sqrt{3} - 1 + (3 - \sqrt{3}) \cos \theta}{2} \tag{10.83}$$

Figure 10.9(d) is a plot of the magnitude of (10.83). The directivity index for the supercardioid is 5.7 dB and the 3 dB beamwidth is 115°. The zero in the response is located at 125°. The front-to-back ratio is equal to 11.4 dB.

5.2 SECOND-ORDER DESIGNS

As with first-order systems, there are an unlimited number of second-order designs. Since second-order microphones are not readily available on the market today, there are no "common" designs. Two designs that have been suggested are the second-order cardioid and the second-order hypercardioid [12, 15]. Another group of proposed differential microphones is a restricted class of equi-sidelobe designs for arbitrary order n [9]. The following section presents some of these designs as well as a non-restricted equi-sidelobe design and a variety of second-order differential array designs based on common first-order microphones. The general second-order form as given in (10.28) has three parameters, a_0 , a_1 , and a_2 . Equivalently, the second-order differential is the product of two first-order differential forms, as shown in (10.29).

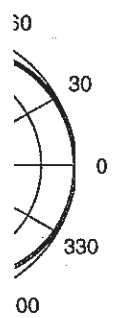
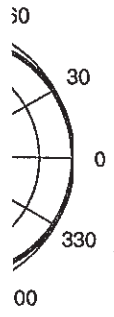
The contours in Fig. 10.10 and Fig. 10.11 depict the dependence of DI and F on the parameters α_1 and α_2 from (10.29). Both figures are plotted for values of α_1 and α_2 between -1 and $+1$. Figure 10.10 has a DI maximum value of 9.5 dB and the interval between the contours is 0.5 dB. Figure 10.11 has a maximum value of 24.0 dB; the contours are in 1 dB steps.

5.2.1 Second-Order Dipole. By pattern multiplication, the second-order dipole directional response is the product of two first-order dipoles which have $\cos \theta$ response patterns given by

$$E_{D_2}(\theta) = \cos^2 \theta. \tag{10.84}$$

Figure 10.12(a) shows the polar magnitude response for this array. The directivity index is 7.0 dB, and by symmetry the front-to-back ratio is 0 dB. The 3 dB beamwidth is 65°.

5.2.2 Second-Order Cardioid. In general the term second-order cardioid implies that either first-order term in the second-order expression given in (10.29), can be a cardioid. However, we first adhere to the specification that a second-order cardioid corresponds to the case where both first-order terms are



ypercardioid,

ture, is not
onse can be

(10.82)

The 3 dB
ivity index
der system.

ly used for
ck received
rly 1940's,
eference to
Harry [11].

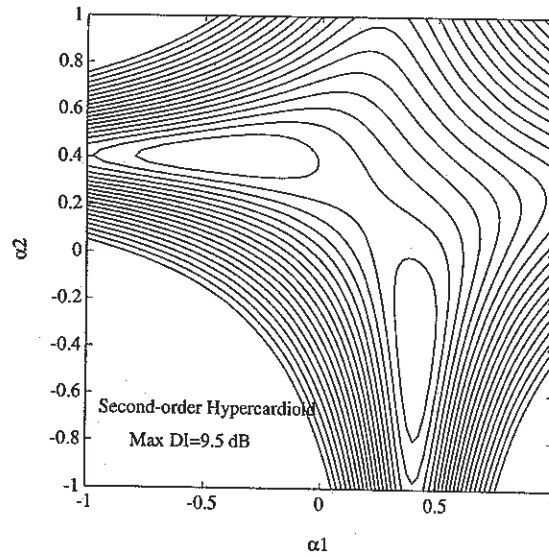


Figure 10.10 Contour plot of the directivity index DI in dB for second-order array versus α_1 and α_2 . The contours are in 0.5 dB intervals.

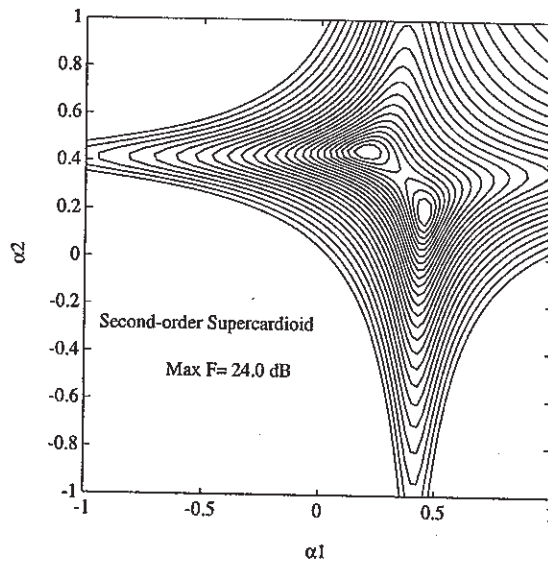


Figure 10.11 Contour plot of the front-to-back ratio in dB for second-order arrays versus α_1 and α_2 . The contours are in 1 dB increments.

of the cardioid form. In equation form,

$$E_{C_2}(\theta) = \frac{(1 + \cos \theta)^2}{4} \tag{10.85}$$

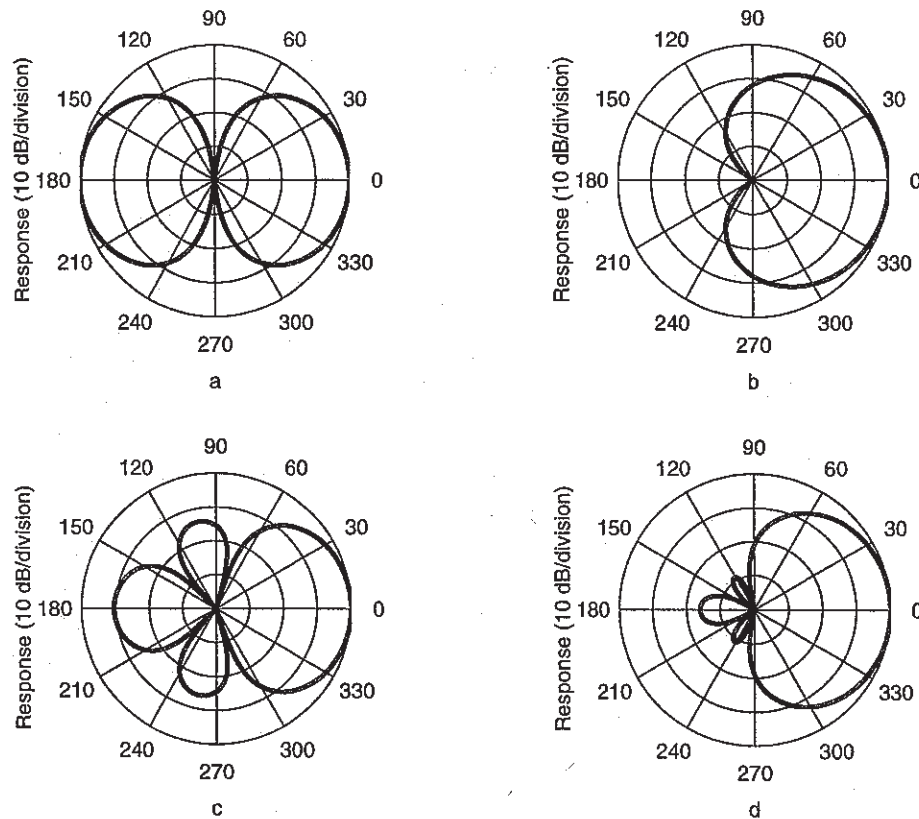


Figure 10.12 Various second-order directional responses, (a) dipole, (b) cardioid, (c) hypercardioid, (d) supercardioid.

In this case $\alpha_1 = \alpha_2 = 0.5$. The directivity index is 7.0 dB and the two zeros both fall at $\theta = 180^\circ$. The front-to-back ratio is equal to 14.9 dB.

Returning to the generality mentioned above, we now consider a second-order cardioid formed from a cardioid and a general first-order response. second-order cardioid design can be easily seen The equation for this second-order differential cardioid is

$$E_{FC_2}(\alpha_1, \theta) = \frac{[\alpha_1 + (1 - \alpha_1) \cos \theta][1 + \cos \theta]}{2} \tag{10.86}$$

Olson [12] and Sessler and West [15] presented results for the specific case of $\alpha_1=0$ in (10.86). Figure 10.13 is a plot of the magnitude of the response for this particular realization. The 3 dB beamwidth of the microphone is 76° . The directivity index is 8.8 dB, the nulls are at 90° and 180° , and the front-to-back ratio is equal to 14.9 dB.

(10.85)

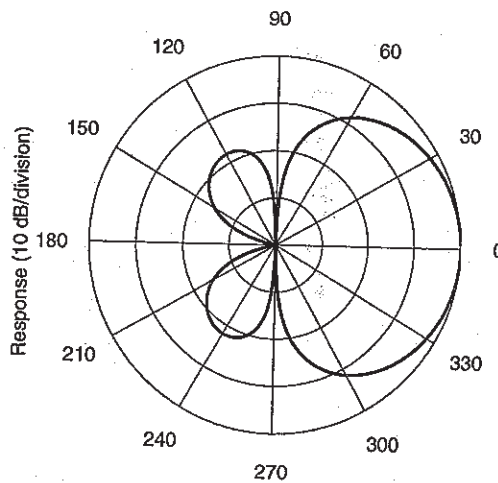


Figure 10.13 Second-order Olson-Sessler-West cardioid directional response.

5.2.3 Second-Order Hypercardioid. The second-order hypercardioid has the highest directivity index of a second-order system; its directivity index is 9.5 dB. The derivation of the directivity pattern and the parameters that determine the second-order hypercardioid are contained in Section 4.2. The results are:

$$\alpha_1 = \pm \frac{1}{\sqrt{6}} \approx \pm 0.41, \quad (10.87)$$

$$\alpha_2 = \mp \frac{1}{\sqrt{6}} \approx \mp 0.41. \quad (10.88)$$

These values correspond to the peaks in Fig. 10.10. The null locations for the second-order hypercardioid are at 73° and 134° . The front-to-back ratio is 8.5 dB, the same for the first-order differential cardioid and first-order differential hypercardioid. A polar response is given in Fig. 10.12(c).

5.2.4 Second-Order Supercardioid. The term second-order supercardioid designates an optimal design for the second-order differential microphone with respect to the front-to-back received power ratio. The derivation for the supercardioid microphone was given in Section 4.3. The results (repeated here) are:

$$\alpha_1 = \frac{\sqrt{7} - 2 \pm \sqrt{8 - 3\sqrt{7}}}{2} \approx 0.45, 0.20, \quad (10.89)$$

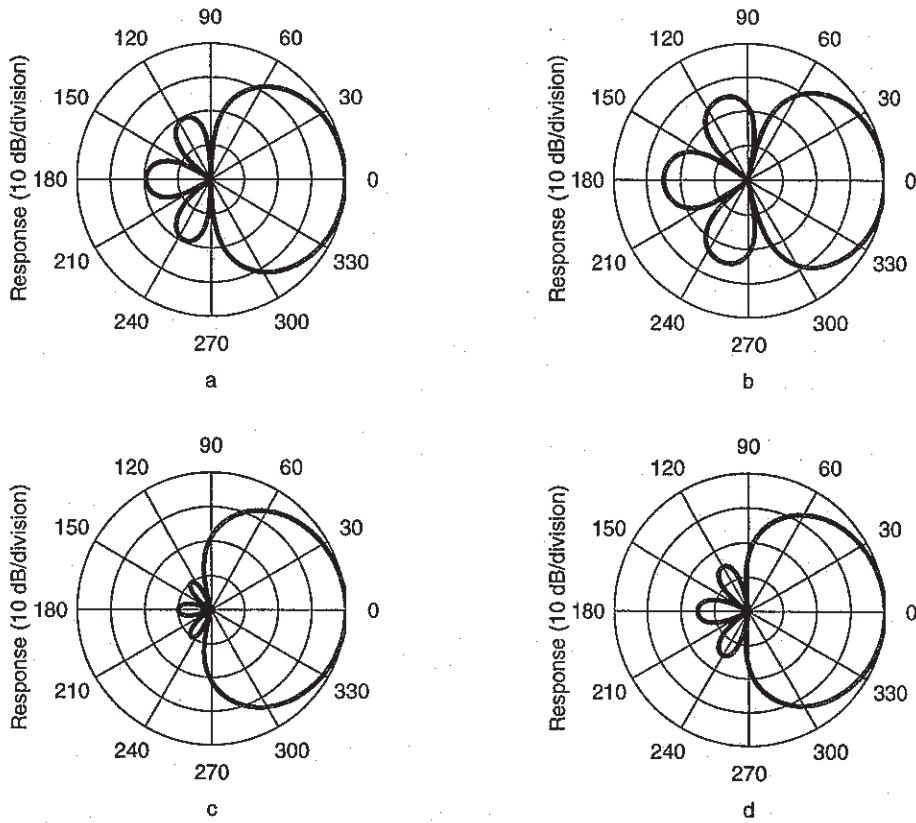


Figure 10.14 Various second-order equi-sidelobe designs, (a) Korenbaum design, (b) -15 dB sidelobes, (c) -30 dB sidelobes, (d) minimum rear half-plane peak response.

$$\alpha_2 = \frac{\sqrt{7} - 2 \mp \sqrt{8 - 3\sqrt{7}}}{2} \approx 0.20, 0.45. \quad (10.90)$$

These values correspond to the peaks in Figure 10.11. Figure 10.12(d) is a plot of the magnitude of the directional response. The directivity index is equal to 8.3 dB, the nulls are located at 104° and 144°, and the front-to-back ratio is 24.0 dB.

5.2.5 Equi-Sidelobe Second-Order Differential. Since a second-order differential microphone has two zeros in its response it is possible to design a second-order differential microphone such that the two lobes defined by these zeros are at the same level. Figure 10.14(a) shows the *only* second-order differential equi-sidelobe design possible using the form of (10.71). (The second-order differential cardioid as shown in Fig. 10.13 is not considered an equi-sidelobe design since the two lobes in the figure are actually the same lobe due to the symmetry of the polar pattern.) The directivity index of this *Koren-*

baum second-order differential array is 8.9 dB. The beamwidth is 76° and the front-to-back ratio is 17.6 dB.

We begin our analysis of second-order Chebyshev differential arrays begins by comparing terms of the Chebyshev polynomial and the second-order array response function. The Chebyshev polynomial of order 2 is

$$\begin{aligned} T_2(x) &= 2x^2 - 1 \\ &= 2b^2 - 1 + 4ab \cos \theta + 2a^2 \cos^2 \theta. \end{aligned} \quad (10.91)$$

Comparing like terms of (10.91) and (10.28) yields:

$$\begin{aligned} a_0 &= \frac{2b^2 - 1}{S} \\ a_1 &= \frac{4ab}{S} \\ a_2 &= \frac{2a^2}{S}, \end{aligned} \quad (10.92)$$

where S is again the sidelobe threshold.

By substituting the results of (10.75) into (10.92), we can determine the necessary coefficients for the desired equi-sidelobe second-order differential microphone:

$$\begin{aligned} a_0 &= \frac{x_o^2 - 2x_o - 1}{2S} \\ a_1 &= \frac{x_o^2 - 1}{S} \\ a_2 &= \frac{(x_o + 1)^2}{2S}, \end{aligned} \quad (10.93)$$

where

$$x_o = \cosh \left(\frac{1}{2} \cosh^{-1} S \right). \quad (10.94)$$

Thus for the second-order differential microphone,

$$\theta_{1,2} = \cos^{-1} \left(\frac{1 - x_o \pm \sqrt{2}}{1 + x_o} \right). \quad (10.95)$$

The zero locations given in (10.95) can be used along with (10.32) and (10.33) to determine the canonic first-order differential parameters α_1 and α_2 . Figures 10.14(b) and 10.14(c) show the resulting second-order designs for -15 dB and -30 dB sidelobes respectively. The directivity indices for the two designs

are respectively 9.4 dB and 8.1 dB. The null locations for the -15 dB sidelobes design are at 78° and 142°. By allowing a higher sidelobe level than the Korenbaum design (for $x_o = 1 + \sqrt{2}$, with $\theta_1 = 90^\circ$), a higher directivity index can be achieved. In fact, the directivity index monotonically increases until the sidelobe levels exceed -13 dB; at this point the directivity index reaches its maximum at 9.5 dB, almost the maximum directivity index for a second-order differential microphone. For sidelobe levels less than -20.6 dB (Korenbaum design), both nulls are in the rear half-plane of the second-order microphone; the null locations for the -30 dB sidelobes design are at 109 and 152 degrees. Equi-sidelobe second-order directional patterns is always contain a lobe peak at $\theta = 180^\circ$.

An interesting design that arises from the preceding development is a second-order differential microphone that minimizes the *peak* rear half-space response. This design corresponds to the case where the front-lobe response level at $\theta = 90^\circ$ is equal to the equi-sidelobe level (for $x_o = 3$). Figure 10.14(d) is a directional plot of this realization. The canonic first-order differential parameters for this equi-sidelobe design are:

$$\begin{aligned} \alpha_1 &= \frac{5 \pm 2\sqrt{2}}{17} \\ \alpha_2 &= \frac{5 \mp 2\sqrt{2}}{17} \end{aligned} \tag{10.96}$$

The directivity index is 8.5 dB. The nulls are located at 149° and 98°, and the front-to-back ratio is 22.4 dB.

Two other design possibilities can be obtained by determining the equi-sidelobe second-order design that maximizes either the directivity index DI or the front-to-back ratio F . Figure 10.15 is a plot of the directivity and front-to-back indices as a function of sidelobe level. As mentioned earlier, a -13 dB sidelobe level maximizes the directivity index at 9.5 dB. A sidelobe level of -27.5 dB maximizes the front-to-back ratio. Plots of these two designs are shown in Fig. 10.16. Of course, an arbitrary combination of DI and F could also be maximized for some given optimality criterion if desired.

5.2.6 Maximum Second-Order Differential DI and F Using Common First-Order Differential Microphones.

Another typical approach to the design of second-order differential microphones involves the combinations of the outputs of two first-order differential microphones. Specifically, the combination is a subtraction of the first-order differential outputs after one is passed through a delay element. If the first-order differential microphone can be designed to have any desired canonic parameter α_1 , then *any* second-order differential array can be designed. More commonly, however, the designer will have to work with off the shelf first-order differential microphones, such as, the

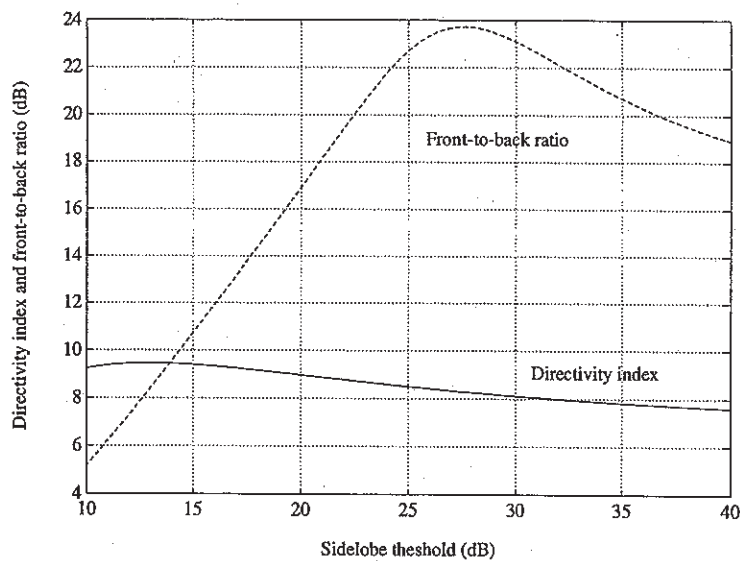


Figure 10.15 Directivity index (solid) and front-to-back ratio (dotted) for equi-sidelobe second-order array designs versus sidelobe level.

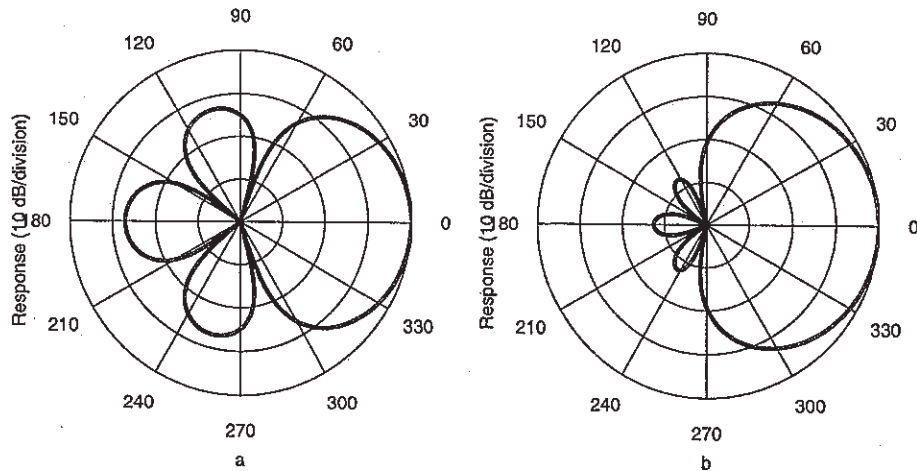


Figure 10.16 Directional responses for equi-sidelobe second-order differential arrays for, (a) maximum directivity index, and, (b) maximum front-to-back ratio.

standard first-order differential designs discussed in Section 3.1. If we constrain the second-order differential design to these typical first-order differential microphones, then we will not be able to reach the maximum directivity index and front-to-back ratio that is possible with the more general second-order differential array designed previously. The following equations show how to

Figure
tial m

impl
power
G

when
micro
by n
of th
the r

A p
max
A

α_1

A p
A
are

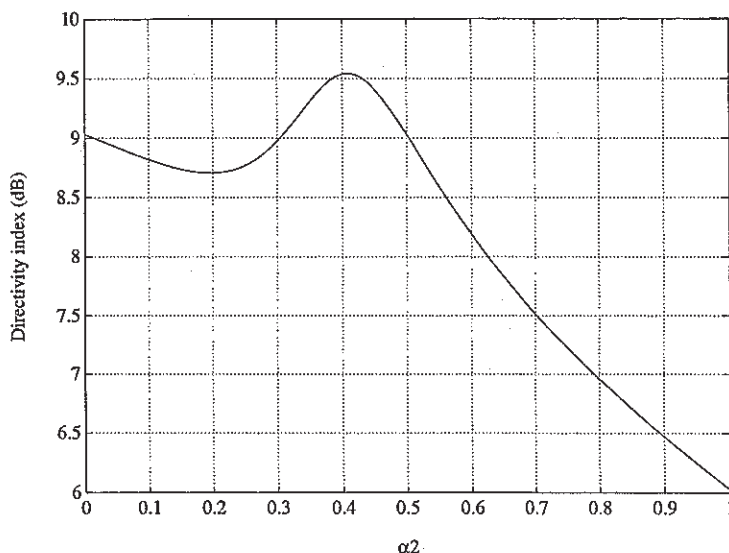


Figure 10.17 Maximum second-order differential directivity index DI for first-order differential microphones defined by (10.97).

implement an optimal design with respect to directivity index and front-to-back power rejection.

Given a first-order differential microphone with the directivity function,

$$E_{N_1}(\alpha_2, \theta) = \alpha_2 + (1 - \alpha_2) \cos \theta, \tag{10.97}$$

where α_2 is a constant, we would like to know how to combine two of these microphones so that the directivity index is maximized. The maximum is found by multiplying (10.97) by a general first-order response, integrating the square of this product from $\theta = 0$ to π , taking derivative with respect to α_1 , and setting the resulting derivative to zero. The result is

$$\alpha_1 = \frac{3}{8} - \frac{5\alpha_2}{8(2 - 9\alpha_2 + 12\alpha_2^2)}. \tag{10.98}$$

A plot of the directivity index for $0 \leq \alpha_2 \leq 1$ is shown in Fig. 10.17. A maximum value of 9.5 dB occurs when $-\alpha_1 = \alpha_2 \approx 0.41$.

A similar calculation for the maximum front-to-back power response yields

$$\alpha_1 = \frac{\sqrt{8\alpha_2^4 + 8\alpha_2^3 + 8\alpha_2^2 - 12\alpha_2 + 3}\sqrt{12\alpha_2^4 + 6\alpha_2^3 + 17\alpha_2^2 - 20\alpha_2 + 5 - 8\alpha_2^3 - 12\alpha_2^2 + 13\alpha_2 - 3}}{24\alpha_2^4 - 6\alpha_2 + 2}. \tag{10.99}$$

A plot of the front-to-back ratio for $0 \leq \alpha_2 \leq 1$ is shown in Fig. 10.18.

A maximum value of 24.0 dB occurs when $\alpha_2 \approx 0.45$ and $\alpha_1 \approx 0.20$, which are the values of the second-order supercardioid. By symmetry, the values of

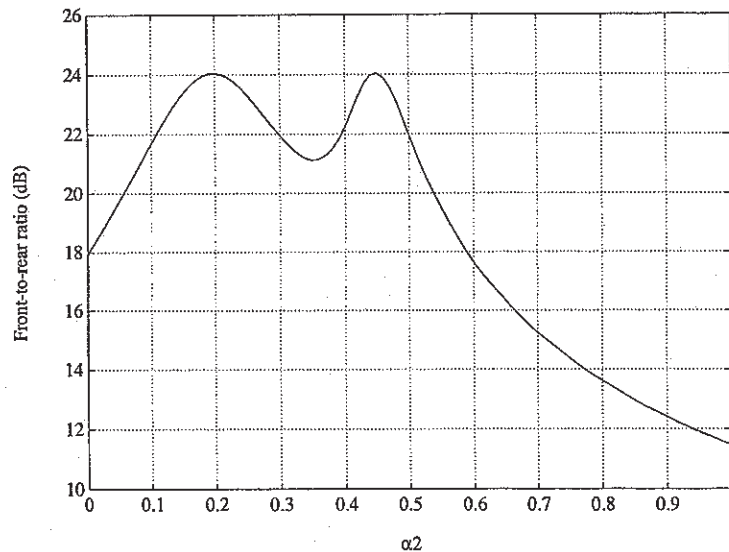


Figure 10.18 Maximum second-order differential front-to-back ratio for first-order differential microphones defined by (10.97).

α_1 and α_2 can obviously be interchanged. The double peak at $F = 24.0$ dB in Figure 10.18 is a direct result of this symmetry.

5.3 THIRD-ORDER DESIGNS

Very little can be found in the open literature on the construction and design of third-order differential microphones. The earliest paper in which an actual device was designed and constructed was authored by B. R. Beavers and R. Brown in 1970 [2]. This lack of any papers is not unreasonable given both the extreme precision that is necessary to realize a third-order array and the serious signal-to-noise problems. Recent advances in low noise microphones and electronics, however, support the feasibility of third-order microphone construction. With this in mind, the following section describes several possible design implementations. The mathematics that govern the directional response were given in (10.34) and (10.35).

5.3.1 Third-Order Differential Dipole. By the pattern multiplication the third-order dipole directional response is given by

$$E_{D_3}(\theta) = \cos^3 \theta. \tag{10.100}$$

Figure 10.19(a) shows the magnitude response for this array.

The directivity index is 8.5 dB, the front-to-back ratio is 0 dB and the 3 dB beamwidth is 54° .

Response (10 dB/division)

Figure
dioid,

5.3.2
that th
third-
sugg
straig
we h

Figur
all fa
21.0
A
tern
diffe
desig

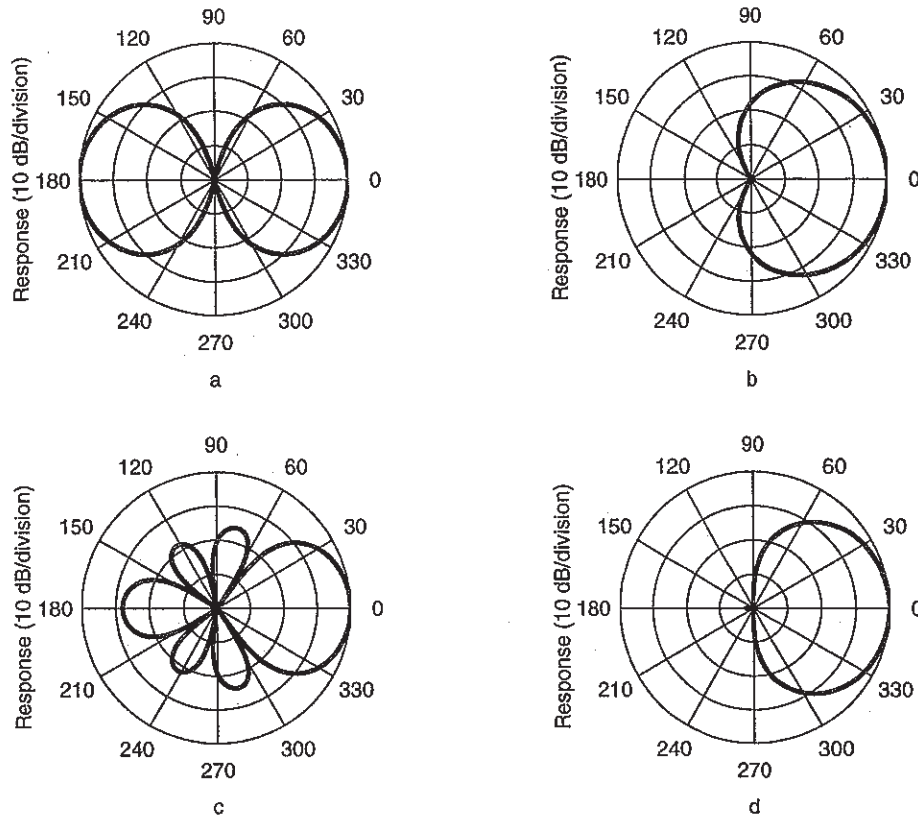


Figure 10.19 Various third-order directional responses, (a) dipole, (b) cardioid, (c) hypercardioid, (d) supercardioid.

5.3.2 Third-Order Differential Cardioid. In Section 3.2.2 we noted that the terminology of cardioids is ambiguous for second-order arrays. For the third-order, this ambiguity is even more pervasive. Nevertheless, we begin by suggesting the most obvious array possibility. If we form the cardioid by the straightforward pattern multiplication of three first-order differential cardioids we have

$$E_{c3} = \frac{(1 + \cos \theta)^3}{8} \tag{10.101}$$

Figure 10.19(b) shows the directional response for this array. The three nulls all fall at 180°. The directivity index is 8.5 dB and the front-to-back ratio is 21.0 dB.

Another possible design for the third-order cardioid corresponds to the pattern multiplication of a first-order differential cardioid with a second-order differential bidirectional pattern. The third-order differential OSW cardioid design implies that $\alpha_1 = 1$ and $\alpha_2 = \alpha_3 = 0$ in (10.35). Figure 10.20 shows

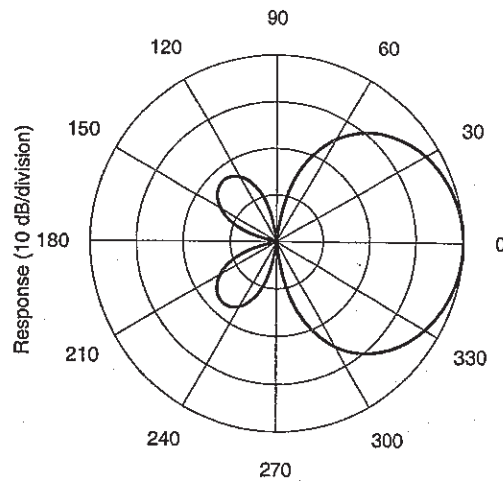


Figure 10.20 Third-order Olson-Sessler-West cardioid directional response.

the directional response of this third-order differential microphone. The directivity index is 10.7 dB and the front-to-back ratio is 18.5 dB. The nulls fall at $\theta = 180^\circ$ and at $\theta = 90^\circ$, the latter of which is a second-order zero.

5.3.3 Third-Order Differential Hypercardioid. The derivation of the third-order differential hypercardioid was given in Section 4.2. The results for the coefficients in (10.34) are:

$$\begin{aligned} a_0 &= -3/32 \\ a_1 &= -15/32 \\ a_2 &= 15/32 \\ a_3 &= 35/32. \end{aligned} \quad (10.102)$$

After solving for the roots of (10.34) with the coefficients given in (10.102), we can obtain the coefficients of the canonic representation given in (10.35), namely

$$\begin{aligned} \alpha_1 &= 1/2 \left[\sqrt{5} \cos(\phi/3) - 1/2 \right] \approx 0.45 \\ \alpha_2 &= 1/2 \left[\sqrt{5} \cos(\phi/3 + 2\pi/3) - 1/2 \right] \approx 0.15 \\ \alpha_3 &= 1/2 \left[\sqrt{5} \cos(\phi/3 + 4\pi/3) - 1/2 \right] \approx -1.35, \end{aligned} \quad (10.103)$$

where

$$\phi = \arccos(-2/\sqrt{5}). \quad (10.104)$$

Figure 10.19(c) shows the directional response of the third-order differential hypercardioid. The directivity index of the third-order differential hypercardioid is the maximum for all third-order designs: 12.0 dB. The front-to-back ratio is 11.2 dB and the three nulls are located at $\theta = 55^\circ, 100^\circ,$ and 145° .

5.3.4 Third-Order Differential Supercardioid. The third-order supercardioid is the third-order differential array with the maximum front-to-back power ratio. The derivation of this array was given in Section 4.3. The requisite coefficients a_i are:

$$\begin{aligned}
 a_0 &= \frac{\sqrt{2}\sqrt{21 - \sqrt{21}} - \sqrt{21} - 1}{8} \approx 0.018 \\
 a_1 &= \frac{21 + 9\sqrt{21} - \sqrt{2}(6 + \sqrt{21})\sqrt{21 - \sqrt{21}}}{8} \approx 0.200 \\
 a_2 &= \frac{3[\sqrt{2}(4 + \sqrt{21})\sqrt{21 - \sqrt{21}} - 25 - 5\sqrt{21}]}{8} \approx 0.475 \\
 a_3 &= \frac{63 + 7\sqrt{21} - \sqrt{2}(7 + 2\sqrt{21})\sqrt{21 - \sqrt{21}}}{8} \approx 0.306. \quad (10.105)
 \end{aligned}$$

Figure 10.19(d) is a directivity plot of the resulting supercardioid microphone. The directivity index is 9.9 dB and the front-to-back ratio is 37.7 dB. The nulls are located at $97^\circ, 122^\circ,$ and 153° . The third-order supercardioid has almost no sensitivity to the rear half-plane. For situations where the user desires information from only one half-plane, the third-order supercardioid microphone performs optimally. Finding the roots of (10.34) with the coefficients given by (10.105) yields the parameters of the canonic expression given in (10.35). The results are:

$$\begin{aligned}
 \alpha_1 &\approx .113 \\
 \alpha_2 &\approx .473 \\
 \alpha_3 &\approx .346. \quad (10.106)
 \end{aligned}$$

5.3.5 Equi-Sidelobe Third-Order Differential. Finally, we discuss the design of equi-sidelobe third-order differential arrays. Like the design of equi-sidelobe second-order differential microphones, the design of third-order equi-sidelobe arrays relies on the use of Chebyshev polynomials and the Dolph-Chebyshev antenna synthesis technique. The basic technique was discussed earlier in Section 2.3. For the third-order microphone, $n=3,$ and the Chebyshev polynomial is

$$T_3(x) = 4x^3 - 3x. \quad (10.107)$$

Using the transformation $x = b + a \cos \theta$ and comparing terms with (10.34) we have

$$\begin{aligned} a_0 &= \frac{b(4b^2 - 3)}{S} \\ a_1 &= \frac{3a(4b^2 - 1)}{S} \\ a_2 &= \frac{12a^2b}{S} \\ a_3 &= \frac{4a^3}{S}. \end{aligned} \tag{10.108}$$

Combining (10.73), (10.74), (10.75), and (10.108) yields the coefficients describing the equi-sidelobe third-order differential. These results are:

$$\begin{aligned} a_0 &= \frac{x_o^3 - 3x_o^2 + 2}{2S} \\ a_1 &= \frac{3x_o(x_o + 1)(x_o - 2)}{2S} \\ a_2 &= \frac{3(x_o - 1)(x_o + 1)^2}{2S} \\ a_3 &= \frac{(x_o + 1)^3}{2S}. \end{aligned} \tag{10.109}$$

Figures 10.21(a) and 10.21(b) show the resulting patterns for -20 dB and -30 dB sidelobe levels.

From (10.77), the nulls for the -20 dB sidelobe levels are at 62° , 102° , and 153° . The nulls for the -30 dB sidelobe design are at 79° , 111° , and 156° . The directivity indices are 11.8 dB and 10.8 dB, respectively. The front-to-back ratio for the -20 dB design is 14.8 dB and for the -30 dB design is 25.2 dB.

Finally, we examine the directivity index and the front-to-back ratio for the equi-sidelobe third-order array as a function of sidelobe level. Figure 10.22 shows these two quantities for equi-sidelobe levels from -10 dB to -60 dB.

The directivity reaches its maximum at 12.0 dB for a sidelobe level of -16 dB. The -16 dB equi-sidelobe design plotted in Fig. 10.23(a), approaches the optimal third-order differential hypercardioid of Fig. 10.19(c).

The front-to-back ratio reaches a maximum of 37.3 dB at a sidelobe level of -42.5 dB; the response is plotted in Fig. 10.23(b). For sidelobe levels less than -42.5 dB, the mainlobe moves into the rear half-plane. For sidelobe levels greater than -42.5 dB, the zero locations move towards $\theta = 0^\circ$ and as a result the beamwidth decreases.

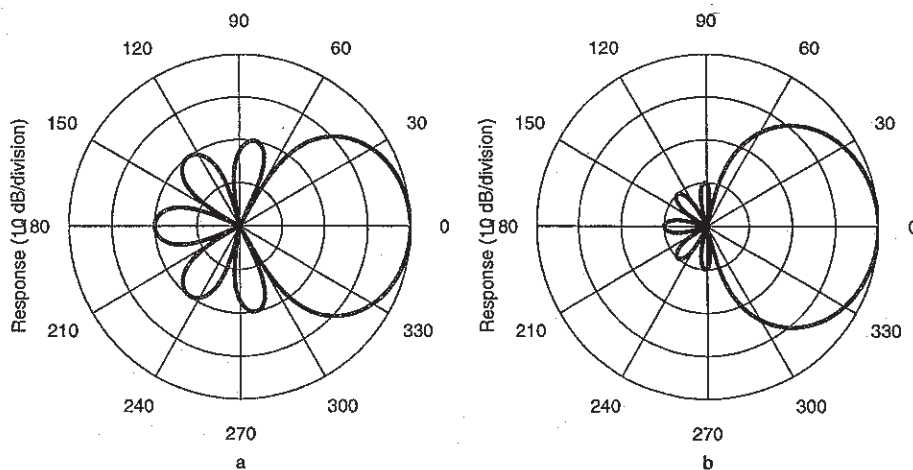


Figure 10.21 Equi-sidelobe third-order differential microphone for (a) -20 dB and (b) -30 dB sidelobes.

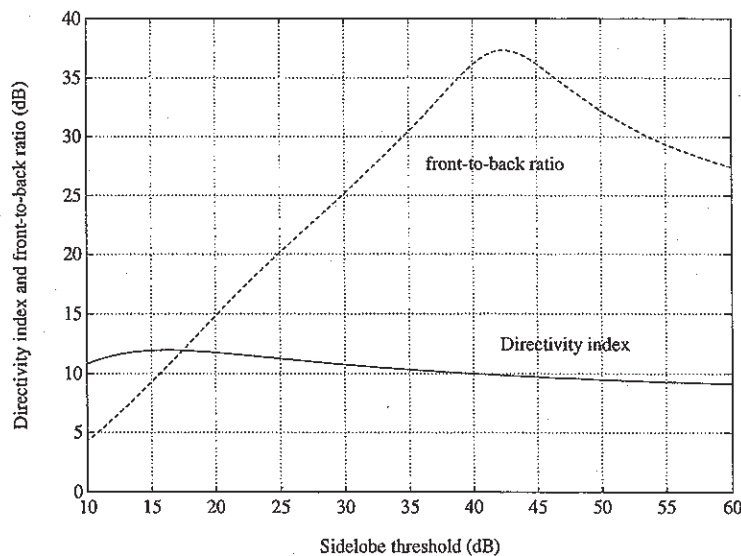


Figure 10.22 Directivity index and front-to-back ratio for equi-sidelobe third-order differential array designs versus sidelobe level.

5.4 HIGHER-ORDER DESIGNS

Due to sensitivity to electronic noise and microphone matching requirements, differential array designs higher than third-order are not practically realizable. These arrays will probably never be implemented on anything other than in a computer simulation. In fact, the design of higher-order supercardioid and

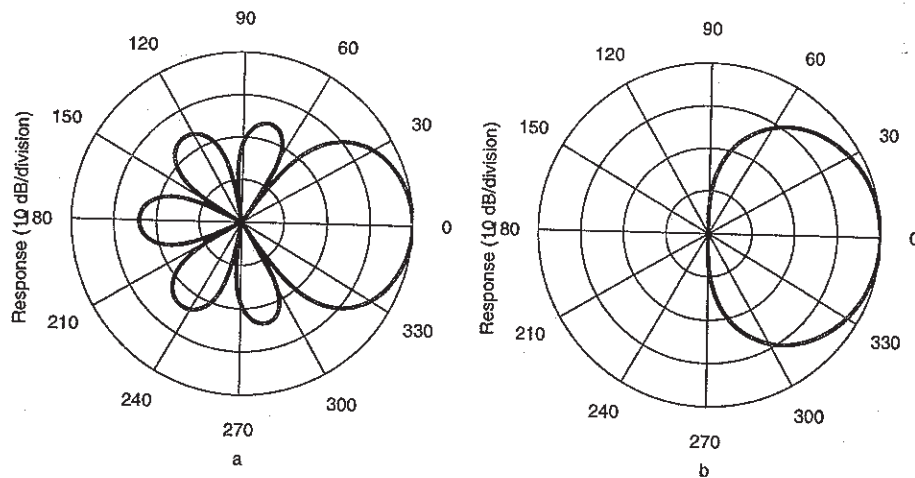


Figure 10.23 Directivity responses for equi-sidelobe third-order differential arrays for (a) maximum directivity index and (b) maximum front-to-back ratio.

hypercardioid differential arrays using the techniques discussed in Sections 4.2 and 4.3, can become difficult on present computers.

6. OPTIMAL ARRAYS FOR CYLINDRICALLY ISOTROPIC FIELDS

Although the standard to model for reverberant acoustic fields has been the “diffuse” field model (spherically isotropic noise), another noise field that is appropriate for room acoustics is cylindrical noise. In many rooms, where carpet and ceiling tiles are used, the main surfaces of absorption are the ceiling and the floor. As a result, a noise field model that has the noise propagating in the axial plane may be more appropriate. This type of noise field is better modeled as a cylindrically distributed noise field and the optimization of directional gain in this type of field is therefore of interest. The following sections deal with the design of differential arrays in a cylindrical noise field.

6.1 MAXIMUM GAIN FOR OMNIDIRECTIONAL MICROPHONES

For a cylindrically isotropic field we have plane waves arriving with equal probability from any angle ϕ and wave vector directions that lie in the ϕ plane. The cylindrical directivity factor in this field is defined as

$$Q_C(\omega, \phi_0) = \frac{|E(\omega, \phi_0)|^2}{\frac{1}{2\pi} \int_0^{2\pi} |E(\omega, \phi)|^2 u(\omega, \phi) d\phi} \quad (10.110)$$

Again, the general weighting function u allows for the possibility of a nonuniform distribution of noise power and microphone directivity. For the case that we are presently interested in

$$u(\omega, \phi) = 1. \tag{10.111}$$

Following the development in the last section, we expand the directional response of N closely-spaced elements in a series of orthogonal functions. For cylindrical fields we can use the normal expansion in the ϕ dimension:

$$E(\phi) = \sum_{m=0}^{N-1} h_m \cos[m(\phi - \phi_z)]. \tag{10.112}$$

The normalization of these cosine functions is simply [1]:

$$\begin{aligned} N_m &= \int_0^{2\pi} \cos^2(m\phi) d\phi \\ &= \frac{2\pi}{\epsilon_m}. \end{aligned} \tag{10.113}$$

The directivity factor can therefore be written as

$$Q_C(\phi_o) = \frac{\left[\sum_{m=0}^{N-1} h_m \cos(m(\phi_o - \phi_z)) \right]^2}{\frac{1}{2\pi} \sum_{m=0}^{N-1} h_m^2 N_m}. \tag{10.114}$$

The maximum is found by equating the derivative of this equation for Q_C with respect to the h_m weights to zero. The result is

$$Q_{Cmax}(\phi_o) = \sum_{m=0}^{N-1} \frac{\cos^2[m(\phi_o - \phi_z)]}{N_m}. \tag{10.115}$$

The equation for Q_C maximizes when $\phi_o = \phi_z$. Therefore

$$\begin{aligned} Q_{Cmax} &= \sum_{m=0}^{N-1} \epsilon_m \\ &= 2N - 1. \end{aligned} \tag{10.116}$$

The above result indicates that the maximum directional gain of N closely-spaced omnidirectional microphones in a cylindrically correlated sound field is $2N - 1$. This result is apparently known in the microphone array processing community [5], but apparently there is no general proof that has been published. One obvious conclusion that can be drawn from the above result is that the rate of increase in directional gain as a function of the number of microphones is much slower in a cylindrically isotropic field than a spherically isotropic field. A plot comparing the maximum gain for microphone arrays up to $N = 10$ for both types of isotropic fields is shown in Fig. 10.24.

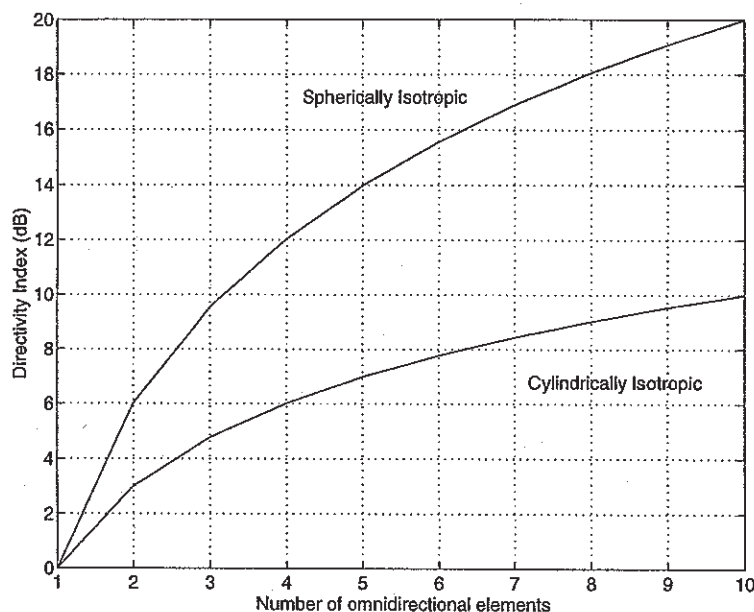


Figure 10.24 Maximum gain of an array of N omnidirectional microphones for spherical and cylindrical isotropic noise fields.

6.2 OPTIMAL WEIGHTS FOR MAXIMUM DIRECTIONAL GAIN

It was shown previously that the directivity pattern for a N^{th} -order differential array can in general be written as

$$E(\theta) = a_0 + a_1 \cos \theta + a_2 \cos^2 \theta + \dots + a_{N-1} \cos^{N-1} \theta, \quad (10.117)$$

where the coefficients a_i are general weighting scalars. The directivity factor, Q_C , from (10.38) is

$$Q_C(a_0, \dots, a_{N-1}) = \frac{\mathbf{a}^T \mathbf{B} \mathbf{a}}{\mathbf{a}^T \mathbf{H} \mathbf{a}}, \quad (10.118)$$

where the subscript C indicate a cylindrical field and \mathbf{H} is a Hankel matrix given by

$$H_{i,j} = \begin{cases} \frac{(i+j-1)!!}{(i+j)!!} & \text{if } i+j \text{ even,} \\ 0 & \text{otherwise,} \end{cases}$$

where

$$\mathbf{a}^T = \{a_0, a_1, \dots, a_n\}, \quad (10.119)$$

Table 10
from fir

micro
order

1

2

3

4

and

The
even
the n
equiv

when
tor.
coef
prod
Thu

Tabl
fere
gain
Fig.

6.3

7
the

Table 10.4 Table of maximum eigenvalue and corresponding eigenvector for differential arrays from first to fourth-order, for cylindrically isotropic noise fields.

microphone order	maximum eigenvalue	corresponding eigenvector
1	3	[1/3 1/2]
2	5	[-1/5 2/5 4/5]
3	7	[-1/7 -4/7 4/7 8/7]
4	9	[1/9 -4/9 -4/3 8/9 16/9]

$$\mathbf{B} = \mathbf{b}\mathbf{b}^T, \tag{10.120}$$

and

$$\mathbf{b}^T = \overbrace{\{1, 1, \dots, 1\}}^{n+1}. \tag{10.121}$$

The double factorial function is defined as [1]: $(2n)!! = 2 \cdot 4 \dots \cdot (2n)$ for n even and $(2n + 1)!! = 1 \cdot 3 \cdot \dots \cdot (2n + 1)$ for n odd. As was stated previously, the maximum directivity factor Q_C is equal to the maximum eigenvalue of the equivalent generalized eigenvalue problem:

$$\mathbf{B}\mathbf{x} = \lambda\mathbf{H}\mathbf{x}. \tag{10.122}$$

where, λ is the general eigenvalue and \mathbf{x} is the corresponding general eigenvector. The eigenvector corresponding to the largest eigenvalue will contain the coefficients a_i which maximize the directivity factor Q_C . Since \mathbf{B} is a dyadic product there is only one eigenvector $\mathbf{x} = \mathbf{H}^{-1}\mathbf{b}$ with the eigenvalue $\mathbf{b}^T\mathbf{H}^{-1}\mathbf{b}$. Thus,

$$\max_a Q_C = \lambda_m = \mathbf{b}^T\mathbf{H}^{-1}\mathbf{b}. \tag{10.123}$$

Table 10.4 gives the optimum values for array gain in isotropic noise for differential orders up to and including fourth-order. A plot of the highest array gain directivity patterns for differential orders up to fourth-order is given in Fig. 10.25.

6.3 SOLUTION FOR OPTIMAL WEIGHTS FOR MAXIMUM FRONT-TO-BACK RATIO FOR CYLINDRICAL NOISE

The front-to-back ratio F is defined as the ratio of the power of the output of the array to signals propagating from the front-half plane to the output power for

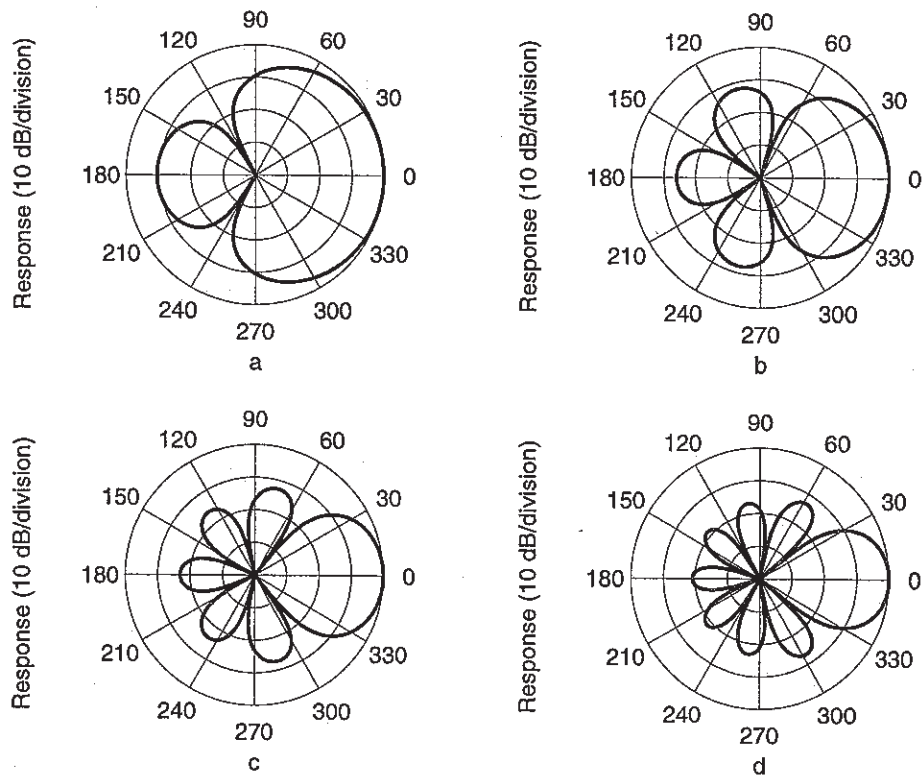


Figure 10.25 Optimum directivity patterns for differential arrays in a cylindrically isotropic noise field for (a) first, (b) second, (c) third, and (d) fourth-order

signals arriving from the rear-half plane. The ratio for cylindrically isotropic fields is mathematically defined as

$$F_C = \frac{\int_0^{\pi/2} |E(\phi)|^2 d\phi}{\int_{\pi/2}^{\pi} |E(\phi)|^2 d\phi} \quad (10.124)$$

Using the differential pattern expansion from (10.117), we can write

$$F_C = \frac{\mathbf{a}^T \mathbf{B} \mathbf{a}}{\mathbf{a}^T \mathbf{H} \mathbf{a}},$$

where

$$B_{ij} = \frac{\Gamma(\frac{1+i+j}{2})}{\Gamma(\frac{2+i+j}{2})}$$

and

$$H_{ij} = (-1)^{i+j} \frac{\Gamma(\frac{1+i+j}{2})}{\Gamma(\frac{2+i+j}{2})}, \quad (10.125)$$

Table 10.5 Table of maximum eigenvalue corresponding to the maximum front-to-back ratio and corresponding eigenvector for differential arrays from first to fourth-order, for cylindrically isotropic noise fields.

microphone order	maximum eigenvalue	corresponding eigenvector
1	$7+4\sqrt{3}$	$[\sqrt{2}-1 \ 2-\sqrt{2}]$
2	$\frac{9\pi^2+12\sqrt{22}\pi+88}{9\pi^2-88}$	$\approx [0.103 \ 0.484 \ 0.413]$
3	≈ 11556	$\approx [0.002 \ 0.217 \ 0.475 \ 0.286]$
4	≈ 336035	$\approx [0.00430 \ 0.07429 \ 0.29914 \ 0.42521 \ 0.19705]$

where Γ is the Gamma function [1]. From (10.125) we can see that the front-to-back ratio is a Rayleigh quotient. The maximum of the Rayleigh quotient is reached at a value equal to the largest eigenvalue of the equivalent generalized eigenvalue problem

$$\mathbf{B}\mathbf{x} = \lambda\mathbf{H}\mathbf{x}, \tag{10.126}$$

where λ is the eigenvalue and \mathbf{x} is the corresponding eigenvector. Thus, the maximization of the front-to-back ratio is again a general eigenvalue problem with F_C as the largest eigenvalue. As before, the corresponding eigenvector will contain the coefficients a_i , which maximize the front-to-back ratio F_C ,

$$\max_a F_C = \max_k \lambda_k = \frac{\mathbf{a}_k^T \mathbf{B} \mathbf{a}_k}{\mathbf{a}_k^T \mathbf{H} \mathbf{a}_k}, \tag{10.127}$$

where the subscript k refers to the k^{th} eigenvalue or eigenvector. The matrices \mathbf{H} and \mathbf{B} are real Hankel matrices and are positive definite. The resulting eigenvalues are positive real numbers and the eigenvectors are real.

Table 10.5 contains the maximum front-to-back power ratios (given by the maximum eigenvalue). The maximum eigenvalue for the third and fourth-order cases result in very complex algebraic expressions. Therefore only the numeric results are given. A plot showing the highest front-to-back power ratio directivity patterns given by the optimum weightings (corresponding to the eigenvectors given in Table 10.5 are displayed in Fig. 10.26). One observation that can be made by comparing the cylindrical noise results with the spherical noise results is that the patterns are fairly similar although there are differences. The differences are due to the omission of the sine term in the denominator of

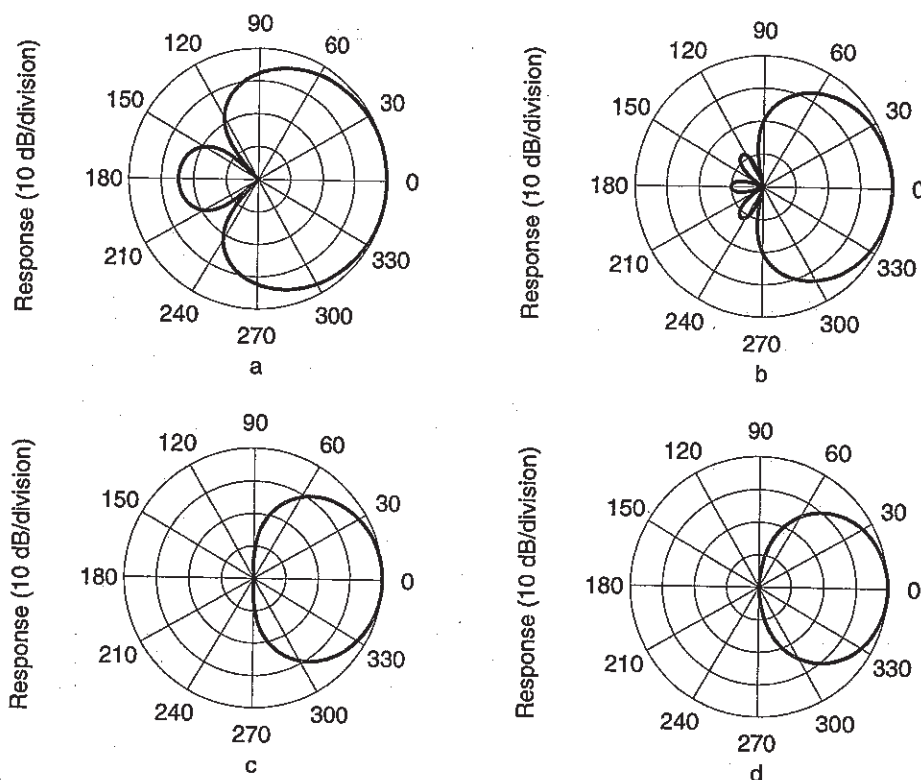


Figure 10.26 Directivity patterns for maximum front-to-back power ratio for differential arrays in a cylindrically isotropic noise field for (a) first, (b) second, (c) third, and (d) fourth-order

(10.36). The optimal patterns for cylindrically isotropic fields keep their side-lobes smaller in the rear-half of the microphone since this area is not weighted down by the sine term. Table 10.6 also summarizes the above results relative to the results for the spherically isotropic condition. Table 10.6 also contains the 3 dB beamwidth and the position of the pattern nulls. By knowing the null positions, these designs can be easily realized by combining first-order sections in a nulling tree architecture.

The results summarized in Table 10.6 also show that there is relatively small difference between the optimal designs of differential arrays for the spherically and cylindrically isotropic noise fields. Typically the differences between the optimum directional gains from either the cylindrical or spherical isotropy assumption results in less than a few tenths of a dB; most probably an insignificant amount. The most significant detail to notice is that the rate of increase in the directional gain versus differential array order is much smaller for cylindrically isotropic fields. This conclusion was also proven earlier and shown in Fig. 10.24.

Table 10.6 Table of maximum directional gain and front-to-back power ratio for differential arrays from first to fourth-order, for cylindrically and spherically isotropic noise fields.

Mic. order	DI_C (dB) cyl	F_C (dB) cyl	DI (dB) sph	F (dB) sph	Beam width degs	Null(s) degs
Maximum gain for cylindrical noise						
1 st	4.8	10.9	5.9	11.1	112°	120
2 nd	7.0	10.9	9.4	7.5	65°	72,144
3 rd	8.5	13.9	11.8	10.3	46°	51,103,154
4 th	9.5	13.9	13.7	8.9	36°	80,120,160
Maximum gain for spherical noise						
1 st	4.6	7.4	6.0	8.5	105°	109
2 nd	6.9	9.7	9.5	8.5	65°	73,134
3 rd	8.3	12.4	12.0	11.2	48°	55,100,145
4 th	9.4	13.8	14.0	11.2	38°	44,80,117,152
Maximum front-to-back ratio for cylindrical noise						
1 st	4.6	12.8	5.4	10.9	120°	135
2 nd	6.3	26.3	8.2	23.4	81°	106,153
3 rd	7.2	40.6	9.8	37.0	66°	98,125,161
4 th	7.8	55.3	10.9	51.1	57°	95,112,137,165
Maximum front-to-back ratio for spherical noise						
1 st	4.8	12.0	5.7	11.4	115°	125
2 nd	6.4	25.1	8.3	24.0	80°	104,144
3 rd	7.2	39.2	9.9	37.7	65°	97,122,154
4 th	7.8	53.6	11.0	51.8	57°	94,111,133,159

7. SENSITIVITY TO MICROPHONE MISMATCH AND NOISE

There is a significant amount of literature on the sensitivity of superdirectional microphone array design to interelement errors in position, amplitude, and phase [7, 10, 5]. Since the array designs discussed in this chapter have interelement spacings which are much less than the acoustic wavelength, differential arrays are indeed superdirectional arrays. Early work in superdirectional for *supergain* arrays involved over-steering a Dolph-Chebyshev array past endfire. When the effective interelement spacing becomes much less than the acoustic wavelength, the amplitude weighting of the elements oscillate between plus and minus, resulting in pattern differencing or differential operation. Curiously though, the papers in the field of superdirectional arrays never point out that at small spacings the array can be designed as a differential system as given by (10.25). The usual comment in the literature is that the design of superdirectional arrays requires amplitude weighting that is highly frequency dependent. For the application of the designs that we are discussing, namely differential systems where the wavelength is much larger than the array size, the amplitude weighting is constant with frequency as long as we do not consider the necessary time delay as part of the weighting coefficient. The only frequency correction necessary is the compensation of the output of the microphone for the ω^n high-pass characteristic of the n^{th} order system.

One quantity which characterizes the sensitivity of the array to random amplitude and position errors is the sensitivity function introduced by Gilbert and Morgan [7]. The sensitivity function modified by adding a delay parameter τ is

$$K = \frac{\sum_{m=1}^n |b_m|^2}{|\sum_{m=1}^n b_m e^{-jk(r_m + c\tau_m)}|^2}, \quad (10.128)$$

where, r_m is the distance from the origin to microphone m , b_m are the amplitude shading coefficients of a linear array, and τ_m is the delay associated with microphone m . For the differential microphones discussed, the sensitivity function reduces to

$$K = \frac{n+1}{[\prod_{m=1}^n 2 \sin(k(d + c\tau_m)/2)]^2}, \quad (10.129)$$

where d is the microphone spacing. For values of $kd \ll 1$, (10.129) can be further reduced to

$$K \approx \frac{n+1}{[\prod_{m=1}^n k(d + c\tau_m)]^2}. \quad (10.130)$$

For the n^{th} -order dipole case, (10.130) reduces to

$$K_D \approx \frac{n + 1}{(kd)^{2n}} \tag{10.131}$$

The ramifications of (10.131) are intuitively appealing. The equation merely indicates that the sensitivity to noise and array errors for n^{th} -order differential arrays is inversely proportional to the frequency response of the array.

The response of an array to perturbations of amplitude, phase, and position can be expressed as a function of a common error term δ^2 . The validity to combining these terms into one quantity hinges on the assumption that these errors are small compared to the desired values. The reader is referred to the article by Gilbert and Morgan for specific details [7].

The error perturbation power response pattern is dependent on the error term δ^2 , the actual desired beam pattern, and the sensitivity factor K . The response is given by

$$E_{N_{np}}(\theta) = E_{N_n}(\theta) + K \delta^2 \tag{10.132}$$

Typically δ is very small, and can be controlled by careful design. However, even with careful control, we can only hope for 1% tolerances in amplitude and position. Therefore, even under the best of circumstances we will have trouble realizing a differential array if the value of K approaches or exceeds 10,000 (40 dB). A plot of the value of K for various first-order microphones as a function of the dimensionless parameter kd , is shown in Figure 10.27(a). We note here that of all of the microphone designs discussed, the hypercardioid is the design that has the lowest K factor. This is in direct contradiction to most superdirectional array designs that can be found in the literature [5].

Typically, the higher the directional supergain, the higher the value of K . The reason for the apparent contradiction in Fig. 10.27(a) is that the overall gain of the hypercardioid is higher than the other microphones shown since it uses the highest delay. Other first-order designs with lower values of K are possible, but these do not exhibit the desired optimum directional patterns. Figure 10.27(b) shows the sensitivity function for first, second, and third-order dipoles. As is obvious, a higher differential array order results in a much larger sensitivity. Also, as the phase delay (d/c) between the elements is increased, the upper frequency limit of the usable bandwidth is reduced; in Figures 24a and 24b, it is clear that as the spacing or the frequency is reduced, the sensitivity increases exponentially.

Another problem that is directly related to the sensitivity factor K is the susceptibility of the differential system to microphone and electronic preamplifier noise. If the noise is approximately independent between microphones, the SNR loss will be proportional to the sensitivity factor K . At low frequencies

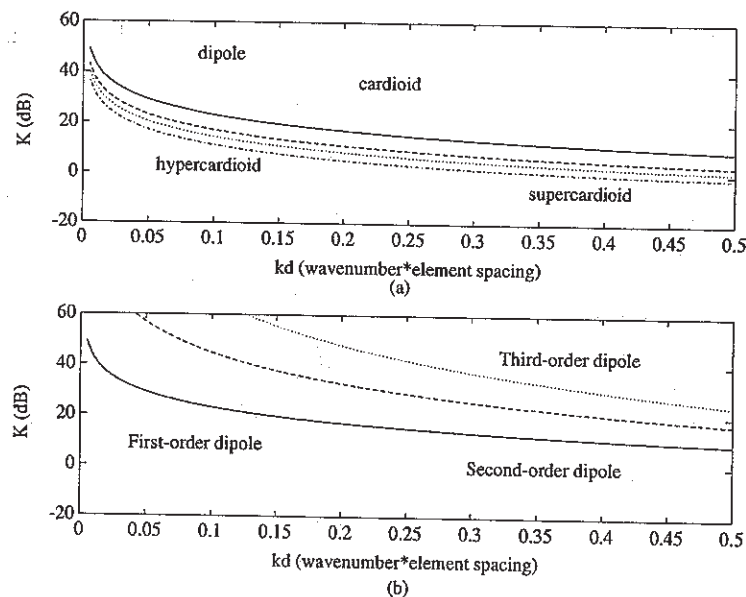


Figure 10.27 Sensitivity as a function of wavelength element-spacing product for, (a) various first-order differential microphones, and, (b) first, second, and third-order dipoles.

and small spacings, the signal to noise ratio can easily become less than 0 dB and that is of course not a very useful design.

As an example, we consider the case of a first-order dipole array with an effective dipole spacing of 1 cm. Assume that the self-noise of the microphone is equal to an equivalent sound pressure level of 35 dB re $20\mu\text{Pa}$, which is typical for available first-order differential microphones. Now, we place this first-order differential dipole at 1 meter from a source that generates 65 dB at 500 Hz at 1 meter (typical of speech levels). The resulting first-order differential microphone output SNR from Fig. 10.27(b), is only 9 dB. For a second-order array with equivalent spacing the SNR would be -12 dB, and for a third-order array, -33 dB. Although this example makes differential arrays higher than first-order look hopeless, there are design solutions that can improve the situation.

In the design of second-order arrays, West, Sessler, and Kubli [15] used baffles around first-order dipoles to increase the second-order differential signal-to-noise. The diffraction caused by the baffle effectively increases the dipole distance d , by a factor that is proportional to the baffle radius. The diffraction is angle and frequency dependent and, if used properly, can be exploited to offer superior performance to an equivalent dipole composed of two zero-order (omnidirectional) microphones. The use of the baffles discussed in reference [15] resulted in an effective increase in the SNR by approximately 10 dB.

The benefit of the baffles used by West, Sessler, and Kubli, becomes clear by examining (10.131) and noting the aforementioned increase in the effective dipole distance.

Another possible technique to improve both the signal-to-noise ratio and reduce the sensitivity to microphone amplitude and phase mismatch, is to split the design into multiple arrays, each covering a specific frequency range. In the design of a differential array, the spacing must be kept small compared to the acoustic wavelength. Since the acoustic wavelength is inversely proportional to the frequency, the desired upper frequency cutoff for an array sets the array microphone spacing requirements. If we divide the differential array into frequency subbands, then the ratio of upper frequency to lower frequency cutoff can be reduced and the spacing for each subband can be made much larger than the spacing for a full-band differential array. The increase in signal-to-noise ratio is proportional to the relative increase in spacing allowed by the use of the subband approach. If the desired frequency range is equally divided into m subbands, the lowest subband SNR increase will be proportional to $20 \log_{10}(m)$. The increase in SNR for each increasing frequency subband will diminish until the highest subband which will have the same SNR as the full-band system. The subband solution does have some cost: the number of array elements must also increase. The increase is at least m , and by reuse of the array elements in the subband arrays, can be controlled to be less than nm , where n is the differential array order.

Finally, another approach to control microphone self-noise would be to construct many differential arrays that are very close in position to each other. By combining the outputs of many arrays with uncorrelated self-noise, the SNR can be effectively enhanced by $10 \log_{10}(u)$, where u is the number of individual differential arrays.

8. CONCLUSIONS

Very little work regarding the analytical development of optimal differential microphones can be found in the literature. The purpose of the work presented in this chapter is to provide a basis for the design of differential microphone array systems. Systems with differential orders greater than three require microphones and calibration with tolerances and noise levels not yet currently available. Also, higher order systems are somewhat impractical in that the relative gain in directivity is small [$O(\log_{10}(n))$] as the order n of the microphone increases. Primarily though, differential microphone array designs are limited by the sensitivity to microphone mismatch and self-noise. One feasible design solution is to split the system into frequency bands and change the spacing as a function of frequency, thereby maintaining an approximately constant signal-to-noise ratio over the desired operating frequency range.

The results presented in this chapter have shown some novel optimal designs for second and third-order systems. Table 10.3 summarizes most of the results.

One possible critical issue that has not been discussed in this chapter is the sensitivity of these differential systems to non-propagating acoustic high-wavenumber noise. These forms of noise occur in turbulent flow and in the near-field of sources undergoing subsonic bending waves below the critical frequency. The problem of high-wavenumber noise can be counteracted by combining multiple differential arrays that are themselves part of a conventional delay-sum beamformer. The synergy here is that the conventional beamformer acts like a spatial lowpass filter, which can greatly reduce the high-wavenumber spatial reception by the differential elements. Another advantage of a hybrid combination of differential elements and a classical delay-sum beamformer is the increase in signal-to-noise ratio achieved by the addition of many independent elements. If the element noise is uncorrelated between differential elements in a classic uniformly weighted array, the gain in signal-to-noise will be $10 \log_{10}(N)$, where N is the total number of array elements. The incorporation of differential sub-arrays as elements in a classic delay-sum beamformer has yet another advantage: the differential elements put a lower bound on the frequency dependent directivity index of the classic beamformer.

References

- [1] M. Abramowitz and I. A. Stegun, *Handbook of Mathematical Functions*. Dover, New York, 1965.
- [2] B. R. Beavers and R. Brown, "Third-order gradient microphone for speech reception," *J. Audio Eng. Soc.*, vol. 16, pp. 636-640, 1970.
- [3] D. K. Cheng, "Optimization techniques for antenna arrays," *Proc. IEEE*, vol. 59, pp. 1664-1674, Dec. 1971.
- [4] L. J. Chu, "Physical limitations of omni-directional antennas," *J. Applied Physics*, vol. 19, pp. 1163-1175, 1948.
- [5] H. Cox, R. Zeskind, and T. Kooij, "Practical supergain," *IEEE Trans. Acoust., Speech, Signal Processing*, vol. ASSP-34, pp. 393-398, June 1986.
- [6] C. L. Dolph, "A current distribution for broadside arrays which optimizes the relationship between beamwidth and sidelobe level," *Proc. IRE*, pp. 335-348, June 1946.
- [7] E. N. Gilbert and S. P. Morgan, "Optimum design of directive antenna array subject to random variations," *Bell Syst. Tech. J.*, vol. 34, pp. 637-663, 1955.
- [8] R. F. Harrington, "On the gain and beamwidth of directional antennas," *IRE Trans. Anten. and Prop.*, pp. 219-223, 1958.
- [9] V. I. Korenbaum, "Comments on unidirectional, second-order gradient microphones," *J. Acoust. Soc. Am.*, 1992.
- [10] Y. T. Lo, S. W. Lee, and Q. H. Lee, "Optimization of directivity and signal-to-noise ratio of an arbitrary antenna array," *Proc. IEEE*, vol. 54, pp. 1033-1045, 1966.
- [11] R. N. Marshall and W. R. Harry, "A new microphone providing uniform directivity over an extended frequency range," *J. Acoust. Soc. Am.*, vol. 12, pp. 481-497, 1941.

[12]

[13]

[14]

[15]

[16]

[17]

[18]

- [12] H. F. Olson, *Acoustical Engineering*. D. Van Nostrand Company, Inc., Princeton, NJ, 1957.
- [13] A. T. Parsons, "Maximum directivity proof of three-dimensional arrays," *J. Acoust. Soc. Amer.*, vol. 82, pp. 179-182, 1987.
- [14] M. R. Schroeder, "The effects of frequency and space averaging on the transmission responses of multimode media," *J. Acoust. Soc. Am.*, vol. 49, pp. 277-283, 1971.
- [15] G. M. Sessler and J. E. West, "Second-order gradient unidirectional microphone utilizing an electret microphone," *J. Acoust. Soc. Am.*, vol. 58, pp. 273-278, July 1975.
- [16] C. T. Tai, "The optimum directivity of uniformly spaced broadside arrays of dipoles," *IEEE Trans. Anten. and Prop.*, pp. 447-454, 1964.
- [17] A. I. Uzkov, "An approach to the problem of optimum directive antenna design," *Compt. Rend. Dokl. Acad. Sci. USSR*, vol. 53, pp. 35-38, 1946.
- [18] D. E. Weston, "Jacobi arrays and circle relationships," *J. Acoust. Soc. Amer.*, vol. 34, pp. 1182-1167, 1986.

Appendix: Directivity Factor and Room Acoustics

The relative sound pressure level (SPL) in a reverberant enclosure can be ideally modeled as the sum of the direct sound signal and a diffuse reverberant part. The ratio of these terms can be used to obtain a rough estimate of the signal-to-reverberation ratio. The relative sound-pressure level is

$$SPL_{rel} = 10 \log_{10} \left[\frac{Q}{4\pi r^2} + \frac{4}{R} \right], \quad (10.A.1)$$

where Q is the directivity factor, and R is the *room constant* equal to $S\bar{\alpha}/(1-\bar{\alpha})$, where S is equal to the room surface area and $\bar{\alpha}$ is equal to the average absorption coefficient. The term "critical distance" is given to the value of r for which the two terms of (10.A.1) are equal:

$$r_{critical} = \frac{1}{4} \sqrt{\frac{QR}{\pi}}. \quad (10.A.2)$$

If we use the simple reverberation equation of Sabine, $T_{60} \approx 0.16V/(S\bar{\alpha})$, where T_{60} is the -60 dB reverberation time and V is the volume in cubic meters, and if we assume that $\alpha \ll 1$ so that $R \approx S\bar{\alpha}$, then (10.A.2) can be written as

$$r_{critical} = \frac{1}{10} \sqrt{\frac{QV}{\pi T_{60}}}. \quad (10.A.3)$$

Equations (10.A.2) and (10.A.3) indicate that a higher value of the term Q corresponds to a larger critical distance; the higher values of Q correspond to an improved ratio of direct sound to reverberant sound at a given position. Equation (10.A.2) can also be interpreted in another way: if we define a new room constant R' such that $R' = QR$, then we have an equivalent situation of an omnidirectional transducer ($Q = 1$) in a more absorbent room, in other words a room with a larger $\bar{\alpha}$.

One caveat that should be mentioned here is that these expressions assume a *diffuse* sound field, where the term diffuse means that acoustic energy incident on a point in space, is equally probable from any direction. The diffuse assumption is valid only at frequencies where the room modal overlap is such that three modes fall into one modal bandwidth. The frequency where the modal density reaches this value depends on the room size and the absorption; this frequency is usually referred to as the *Schroeder cutoff frequency* [14]. It should be emphasized that the transition from non-diffuse to diffuse is of course not instantaneous. The original "Schroeder cutoff frequency" was formulated as twice the present value. The cutoff frequency is

$$f_c = C \sqrt{\frac{T_{60}}{V}}, \quad (10.A.4)$$

where

$$C \approx 2000 (m/s)^{3/2}. \tag{10.A.5}$$

Below the *diffuse* frequency limit, the sound field is dominated by individual modes propagating in discrete directions. At low frequencies, the axial modes dominate and the use of the above analysis breaks down. Since axial modes have the longest mean-free-path, the decay rate for these modes is much slower than for tangential and oblique modes. Compounding the problem is the fact that wall absorption decreases at lower frequencies. To account for the effects of individual modes, an optimal transducer design must necessarily depend on the position and orientation of the sensor in the room as well as the room acoustics.